ABSTRACT

HNO-Myoglobin Reactivity Examined by SVD and Global Analysis

Adrian Lawrence Zapata, Ph.D.

Mentor: Patrick J. Farmer, Ph.D.

Analyses of reactions involving HNO are inherently difficult as it must be generated in situ, and undergoes several concurrent and competitive reactions; thus its concentration flux is difficult to characterize. Global kinetic modeling, using singular value decomposition software, allows for investigation of complex time course spectra. Using this method, the determined rate for trapping of HNO by metmyoglobin, which produces NO-myoglobin, is found to be 2.7 x 10^5 $M^{-1}s^{-1}$ at pH 7.0 and 1.1 x 10^5 $M^{-1}s^{-1}$ at pH 9.4. The reaction of deoxymyoglobin with HNO generates the adduct HNO-myoglobin directly. It is followed by a secondary reaction of the adduct with HNO yielding NO-myoglobin; the determined bimolecular rate constants for these reactions are 3.48 x 10^5 $M^{-1}s^{-1}$ and 1.67 x 10^4 $M^{-1}s^{-1}$ respectively, both of which are independent of pH. The derived spectrum for HNO-myoglobin is characterized by a Soret absorbance maximum at 423 nm with an extinction coefficient of 1.66 x 10^5 $M^{-1}cm^{-1}$. The rate constant for unimolecular loss of HNO from HNO-myoglobin was determined by competitive trapping with CO at 8.9 x 10^{-5} s^{-1}, which produced a thermodynamic binding affinity of HNO to deoxymyoglobin of 3.9 x 10^{10} M^{-1}. Also in this report, sequential absorbance spectra are

used to analyze reactions of HNO with a mixture of met- and deoxy-Mb, (which have highly overlapping spectra) and also to model the flux of HNO over the course of the reaction. The determined trapping rate constants, 2.76 x 10^5 $M^{-1}s^{-1}$ for met-Mb and 3.74 x 10^5 $M^{-1}s^{-1}$ for deoxy-Mb, are qualitatively similar, thus little kinetic preference is predicted in physiological reactivity of HNO. Lastly, the study of a pH and O_2 dependent RNS is generated *in situ* by the reaction of HNO-Mb with O_2, which introduces the possibility of heme modifications and N-bound ferrous RNS adducts. These results suggest that the formation of HNO-ferrous adducts and their intermediates represent an important consideration in the biological action of HNO-releasing drugs.

HNO-Myoglobin Reactivity Examined by SVD and Global Analysis

by

Adrian Lawrence Zapata, B.S.

A Dissertation

Approved by the Department of Chemistry and Biochemistry

_____

Patrick J. Farmer, Ph.D., Chairperson

Submitted to the Graduate Faculty of
Baylor University in Partial Fulfillment of the
Requirements for the Degree
of

Doctor of Philosophy

Approved by the Dissertation Committee

_____

Patrick J. Farmer, Ph.D., Chairperson

_____

Caleb D. Martin, Ph.D.

_____

Sung Joon Kim, Ph.D.

_____

Mary Lynn Trawick, Ph.D.

_____

Joseph White, Ph.D.

Accepted by the Graduate School

December 2016

_____

J. Larry Lyon, Ph.D., Dean

Page bearing signatures is kept on file in the Graduate School.

Copyright © 2016 by Adrian Lawrence Zapata

All rights reserved

TABLE OF CONTENTS

LIST OF FIGURES

LIST OF SCHEMES

LIST OF TABLES

LIST OF ABBREVIATIONS

SVD- Singular Value Decomposition

Mb- Myoglobin

cGMP- cyclic guanosine monophosphate

cAMP- cyclic adenosine monophosphate

AS- Angeli's Salt or trioxodinitrate

PA- Piloty's Acid or benzenesulfohydroxamic acid

MSHA- N-methane sulfonylhydroxylamine

MLA- Marquardt-Levenberg algorithm

RKI- Runge-Kutta integration

ACKNOWLEDGMENTS

First I need to thank my awesome family. Thank you for raising my son as if he was your own child. Things happen and families get separated but our bond as Zapatas is unfailing and I am forever indebted for the love that you have shown me and Elias over the last 5 years.

I would also like to thank two of my biggest inspirations and chemistry heroes, Murugaeson "Ravi" Kumar and Elky Almaraz. Without you guys this would not have been possible. Thank you Ravi, for being an all-around research maven and a very good friend, I could not have done this without you. Thank you very much Elky, you were the most undervalued and underappreciated member of the group. I am the only person who may know that you gave your all and you worked hard to get stuff done because I was right there beside you working until 2:00 in the morning on holidays, and putting in 10 hour days on the weekends. You showed me how to be a proper graduate student and taught me how to be a scientist.

I would also like to thank my beautiful girlfriend. I love you to the moon and back. I can't wait to marry you one day. You have completed my life and I am forever grateful for your presence. God gave me you, and I will do my best to give you the world.

DEDICATION

To my handsome baby boy Elias Zapata,

I love you, and don't be in such a hurry to grow up.

CHAPTER ONE

Introduction

Prologue to NO/HNO

Nitric oxide or NO, is well known as a highly toxic and corrosive gas.[1,2] In years past, it was primarily known as a noxious byproduct of pollution from combustion processes and electrical discharges from lightning. NO is known to be extremely toxic to humans, forming nitrous acid in the lungs when over exposure occurs.[3] It was not until 1987 that NO was found to play an important role in physiology as the endothelium-derived relaxation factor in blood vessels.[4,5] This proved to be groundbreaking news, resulting in a whole new field of medical research that was awarded a Nobel prize awarded in 1998.

Recently, interest has shifted to the roles of its congeners NO^+ and NO^-. In inorganic chemistry NO is known as a "non-innocent ligand" due to its ability to interconvert between all three NO redox states, and the same seems to be true in its biological activity.[6] This dissertation focuses on the reactivity of the latter, NO^-, nitroxyl anion. The protonated form, HNO, goes by many names, such as: nitroxyl, nitrosyl hydride, and azanone.

The self-dimerization of HNO along with its reactivity to oxygen, thiols, and transition metals has resulted in the difficulty of the determination of nitroxyl's role in physiological processes.[7–10] Simply put, there is an ongoing controversy concerning the generation of HNO naturally by mammals.

Table 1.1. A List of the Biological Targets of NO. [13]

Biological Target	[NO]	Effect of NO Signaling
Aconitase (mitochondrial)	>50 nM	Citric acid cycle inhibition
IRE-BP (cytosolic aconitase)	nM	Iron homeostasis
6-phospogluconate	>50 nM	Entner-Doudoroff pathway inhibition
Dihydroxy acid dehydroatase	nM	Branched chain amino acid deficiency
Iron-sulfur enzymes	nM	Formation of toxic iron-dinitrosyl complexes
Cytochrome oxidase	nM	Respiratory inhibition
Catalase	nM	H_2O_2 damage
Cytochrome P450 family	nM	Metabolism of hormones, lipid second messengers, and so forth, heme release and damage
Ribonuclleotide reductase (diiron)	nM - μM	Inhibition of DNA synthesis
Heme oxygenase family	nM	Inhibition of toxic heme breakdown
Photosystem II	Undefined	Inhibition of photosynthesis
Nitrogenase	nM - μM	Inhibition of N_2 fixation
Hydrogenase	nM	Inhibition of N_2 fixation
O_2	μM	NO_2 damage
O_2^-	nM	Peroxynitrite damage
Guanylate cyclase	0.1-10 nM	cGMP kinase activation and smooth muscle relaxation
Transcription regulators (NorR, NsrR, DevS, ect.)	nM	NO defense gene expression
ACO (1-aminoacyl cyclopropane-1-carboxylic acid oxidase)	nM	Ethylene production and signaling in plants

Physiological Reactivity of Nitric Oxide/NO

NO has been implicated in a wide variety of physiologically relevant processes including bioenergetic transformations, immune response, and signaling.[11,12] Its diverse functionality suggests that numerous essential physiological targets can be directly affected by NO flux *in vivo*; mainly, due to its uncharged free radical status. Table 1.1[13] presents a list of NO targets within biological systems in nanomolar concentrations. Although NO has a myriad of functions in biological pathways; the focus will be on its relationship with the globin proteins.

Nitroxyl or HNO

Nitroxyl, a reduced and protonated form of nitric oxide (i.e., HNO) has been studied for over 100 years. Recent research has shown its pharmaceutical potential in treating heart disease.[14–16] However, HNO remains difficult to detect and study as a result of its short lifetime in aqueous solutions, which is due to rapid dimerization as detailed in Equation 1.1.[9]

(1.1) $2\ HNO \rightarrow [H_2N_2O_2] \rightarrow N_2O_{(g)} + H_2O$

(1.2) $HN_2O_3^- \leftrightarrows HNO + NO_2^-$ *pH 4 to 8*

(1.3) $RSO_2NHO^- \leftrightarrows RSO_2^- + HNO$ *pH 8 to 13*

As a result, HNO can be neither purchased nor stored. Instead, HNO must be generated from precursors *in situ*. Angeli's salt, AS, decomposes into HNO at a rate of 6.75×10^{-4} sec^{-1} within a pH range of 4 to 8, as is shown in Equation 1.2.[16] HNO, can be also be generated under alkaline conditions from phenylsulfohydroxamic acid (i.e., Piloty's acid) as detailed in Equation 1.3.[17] Piloty's acid is the second most common precursor, with a unimolecular decomposition rate constant of 3.47×10^{-4} sec^{-1}.[16] A representation of HNO forming reactions from the two precursors is illustrated below in Figure 1.1.

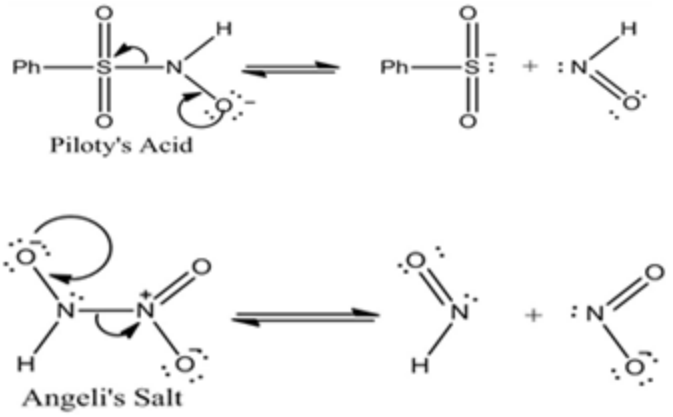

Figure 1.1. A shorthand depiction of the decomposition of HNO precursors: Piloty's acid (PA) and Angeli's salt (AS) respectively.[18]

Although HNO detection is extremely difficult, due to the large variance between precursor decomposition rate and dimerization rate, some methods do exist. Recently several groups have described HNO sensing methods, including electrochemicaldetection, fluorescent probes, and chemical trapping.[19–21] But there questions remain about selectivity. The most common method of HNO detection is by characterization of its dimerization product, N_2O, which can be monitored by gas chromatography in the headspace of a reaction.[22] Isotopic labeling can then be used to prove that the generated N_2O originated from the HNO source. Better characterization techniques are important in the study of the reactivity of nitroxyl, particulary in biological systems.

Since HNO is elusive in situ, our understanding of its fundamental characterizations have changed over the years. For example, the rate constant for its bimolecular dimerization has much debated, but a value of 8×10^6 $mol^{-1}s^{-1}$ is now widely accepted. The reduction potential of NO to a nitroxyl anion ($^3NO^-$) was theoretically predicted to be -0.35 V, which would suggest that nitroxyl generation is readily produced physiologically.[23] However subsequent theoretical calculations combined with physical measurements showed it to be -0.8 V (at 1 M vs. NHE), much less likely to be physiologically relevant.[24] Another dramatic correction was for the pKa of HNO

deprotonation, shown to be ca. 11.5, vastly more alkaline than the previous value of 4.7 obtained from pulse radiolysis experiments. Therefore, nitroxyl exists in aqueous solution almost exclusively in its protonated form, HNO.

Pharmaceutical Reactivity of HNO

HNO precursors have been considered for the treatment of disease. Nitroxyl has been shown to induce myocardial contractility,[25] aid in preconditioning against ischemia/reperfusion injury,[26] aid in the induction of apoptosis and suppression of tumor angiogenesis,[27] aid in the inhibition of alcohol metabolism, [28–30] and has also even been shown to have an analgesic effect in mouse models.[31]

The most promising clinical use of HNO is for the treatment of cardiovascular disease. Investigations by Paolocci *et al*. demonstrated positive effects of HNO on both healthy and failing hearts.[10, 25, 32] HNO generated from decomposition of Angeli's salt (AS) also demonstrated a direct positive inotropic outcome in rat cardiac muscle, leading to development of increased force and output.[33] Also, the positive endothelial effects of nitroxyl were resistant to the development of tolerance in rat isolated aorta.[34] The target and mechanism of these effects are under extensive investigation.

Physiological effects of Oxidative/Nitrosative Stress, Peroxynitrite

Both NO and HNO are considered to be reactive nitrogen species (RNS) akin to the more commonly known ROS (reactive oxygen species). Both ROS and RNS are small reactive species associated with oxidative stress and disease. The origin of most ROS is the superoxide anion ($\bullet O_2^-$) which can be produced by NADPH oxidase, cystolic xanthine oxidase, or the mitochondrial electron transport chain.[25,32] RNS is typically derived from nitric oxide, (NO) which is generated

enzymatically by nitric oxide synthases (NOS) and non-enzymatically by the breakdown of L-citrulline and L-arginine.[5,35]

Neither superoxide nor NO is particularly toxic *in vivo* because they are efficiently regulated to minimize their accumulation.[36] Superoxide is regulated by several Superoxide Dismutases (SOD), which are expressed as both intra- and extra-cellular enzymes. SOD permits superoxide to be converted into dioxygen and hydrogen peroxide, as detailed in Equation 1.4. Superoxide is decomposed enzymatically by catalases to form nontoxic dioxygen and water as demonstrated in Equations 1.5 and 1.6.

(1.4) M^{n+}-SOD + $\bullet O_2^-$ + $2H^+$ → $M^{(n+1)}$-SOD + H_2O_2

(1.5) H_2O_2 + Fe(III)- porphyrin → H_2O + O=Fe(IV)-porphyrin(.+)

(1.6) H_2O_2 + O=Fe(IV)- porphyrin (.+) → H_2O + Fe(III)- porphyrin + O_2

It is widely accepted that NO itself is the major source of RNS. I*n vivo* reactions have been observed between NO and ferrous globins, such as deoxy states of hemoglobin (Hb) and myoglobin (Mb), akin to its binding by ferrous soluble guanyl cyclase which initiates its vasodilatory activity. More importantly, the ferrous dioxygen adducts of Hb and Mb also react with excess NO to form relatively harmless nitrate, NO_3^-, and oxidized ferric heme protein (Equation 1.11), which is termed nitric oxide dioxygenase (NOD) reactivity.[37] Because NO diffuses rapidly through tissue and blood cells, the NOD

reactivity catalyzed by oxy-globins represents the major mechanism of RNS detoxification.[38]

History of NOD Reactivity

Doyle et al. initially observed NOD reactivity in a competitive reaction of deoxy-Hb with NO and O_2, which first characterized the formation of nitrate ions and met-Hb as end products of the reaction.[39] Doyle applied this trapping method to study the amount of NO that was generated

by nitrite oxidation of deoxy-Hb. He later used this NOD reactivity to trap the auto-oxidation of cobalt nitrosyls with oxy-Mb.[40] Similarly an intermediate was produced when Angeli's salt and dioxygen were reacted, but its characterization proved problematic.[41] At the time Doyle et al. did not realize the physiological implications of this reactivity because NO was viewed as a noxious gas. A decade later, similar reactivity was seem in meat curing, in which NO-Mb was oxidized by O_2 slowly generating nitrate and oxidized metmyoglobin.[42] Both sets of experiments demonstrated similar reactivities and products, but the individual steps of the reactions were ill defined.

Olson was the first to propose that the NOD reaction proceeded by the coupling of superoxide and NO to form a peroxynitrite adduct on the ferric heme of myoglobin, which in turn facilitated a rapid isomerization of the adduct to nitrate.[43] In the late 1990's, Gardner proposed the term NOD for this type of interaction in enzymes that were discovered in *E. coli* (flavohemoglobins), which detoxify high levels of nitric oxide.[37, 43] It was later proposed by Gardner that the mammalian myoglobin functions as an NOD, an

illustrated in Figure 1.2.[44–49]

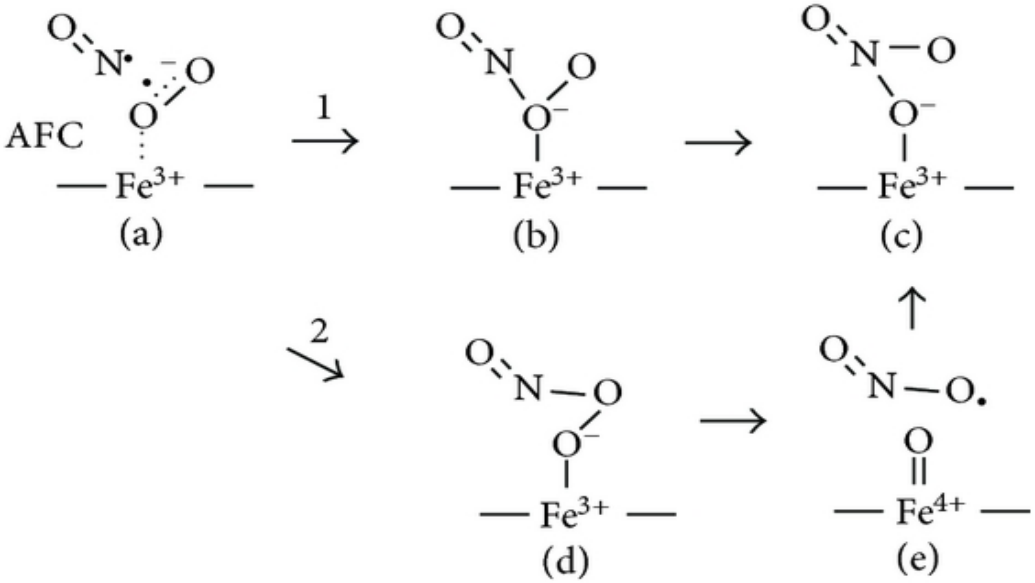

Figure 1.2. NOD reactivity[46]

Herold reported the first observation of an intermediate in NOD reactivity, seeing a transient absorbance in the heme q-band region under alkaline conditions.[50] The intermediate was suggested to be a ferric peroxynitrite complex, observed at high pH because of the alkaline pKa of peroxynitrite. This observation inspired several attempts to characterize this unusual species in both heme proteins and non-physiological porphyrin model complexes.[51,52]

A team led by Pierre Moennes-Loccoz used resonance Raman spectroscopy on samples that were generated using Herold's alkaline reaction conditions by rapid-freeze-quenching at millisecond timescales.[53] Analysis of the vibrational data obtained using $^{14/15}$N-isotopic labeling implied that the "green" intermediate was not that of peroxynitrite but of a nitrate ion bound to the ferric heme. Thus, the peroxynitrite intermediate decomposed too rapidly to observe. The intermediate observed was several steps behind the mechanistic series outlined in Figure 1.3, and was determined to be nitrate bound to a ferric heme. An authentic sample of this ferric nitrate complex cannot be made, as heme proteins have no affinity for binding nitrate. As in the previous report, intermediates could not be observed at neutral pH conditions, suggesting that the release of the Fe-bound nitrate was facilitated by protonation.

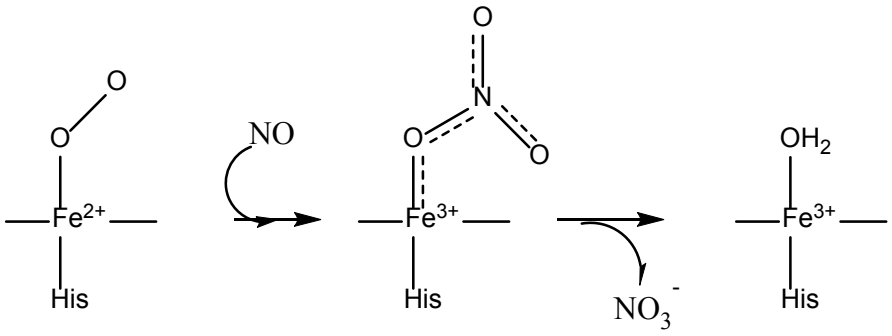

Figure 1.3. The proposed intermediate that was obtained by rapid freeze quenching and characterized by resonance Raman as an O-bound nitrate. [53]

In a follow-up study by Groves, ferric myoglobin was reacted with peroxynitrite which resulted in the formation of a transient ferryl-Mb adduct (Fe^{IV}=O) and nitrogen dioxide gas (NO_2).[54] These geminate species may then recombine to form nitrate as a major product in the so-called "rebound mechanism," or NO_2 may escape and cause nitrosation of myoglobin tyrosine residues. Ferryl heme intermediates are well known in several enzymatic systems, most notably in cytochromes P450 and peroxidases, but can also be generated in globin by reacting with peroxides or bleach.[55] The rebound mechanism proposed for the NOD was analogous to the previously proposed mechanism by Groves for the enzymatic cytochrome P450 reaction cycle.[55]

These mechanistic proposals were contradicted by a subsequent report by Pacheco *et al*. They studied the native NOD reactivity of oxy-Mb with NO using time resolved UV-vis with single value decomposition (SVD) methods and global kinetic modeling. Their analysis showed no evidence of a ferryl intermediate being formed on the millisecond timescale, as outlined in Figure 1.4.[56] Instead, they proposed that the NO reacts with O_2 and rapidly isomerizes to form the oxidized O bound nitrate adduct of ferric-Mb. Therefore, the chemical character of the observed intermediate and the reaction path followed in NOD reactivity are still unconfirmed. One goal of this dissertation is to approach this NOD reactivity from a new and unique direction.

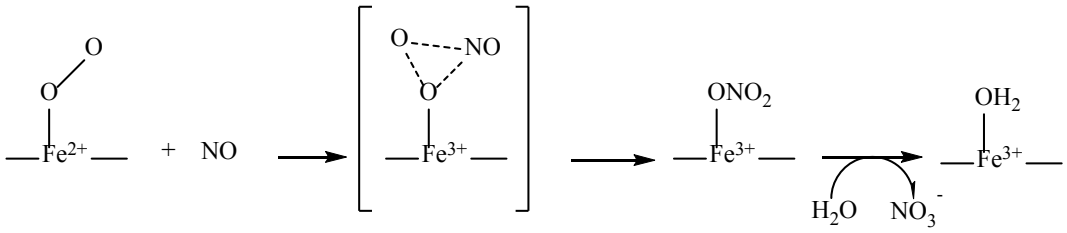

Figure 1.4. NOD reactivity showing that nitrate is formed as an isomerized product.[56]

HNO Research in the Farmer Lab

HNO and its reactions with metalloproteins have long been investigated by the Farmer research lab.[57] Lin was the first to generate a stable HNO adduct of ferrous myoglobin (HNO-Mb) by reduction of NO-Mb.[58,59] The same adduct can be formed by trapping of free HNO by deoxymyoglobin (deoxyMb or Mb-Fe^{II}),[60] or by treatment of metmyoglobin (met-Mb or Mb-Fe^{III}) with salts of nitrite and borohydride.[61] The HNO adducts of several hemoglobins have been characterized by ^{1}HNMR,[62] ^{1}H-^{15}N heteronuclear single quantum coherence (HSQC),[63] as well as resonance Raman, and X-ray absorption spectroscopy.[64] HNO is isoelectronic with O_2, which suggests it may serve as an O_2 analog in other enzymatic activities.[63] Most recently, it was found that HNO can replace O_2 during turnover of quercetinase, a non-heme Mn dioxygenase enzyme. This nitroxygenase activity results in the regioselective incorporation of the N atom derived from HNO within the enzymatic product.[65]

CHAPTER TWO

A Singular Variable Decomposition Approach for Kinetic Analysis of Reactions of HNO with Myoglobin

This chapter published as:
Zapata, A. L.; Kumar, M. R.; Pervitsky, D.; Farmer, P. J. A Singular Value Decomposition Approach for Kinetic Analysis of Reactions of HNO with Myoglobin. *J. Inorg. Biochem.* 2013, *118*, 171–178.

Supplemental Information is found in appendix A.

Abstract

The reactions of various horse heart myoglobin species with nitrosyl hydride, HNO, derived from Angeli's salt (AS) and Piloty's acid (PA) have been followed by UV-visible, ^{1}H NMR and EPR spectroscopies. Spectral analysis of myoglobin-derived speciation during the reactions was obtained by using Single Value Decomposition methods combined with a global fitting program to obtain the rate constants of complex sequential reactions. The analysis also provided spectra for the derived absorbers, which allowed self-consistent calibration to the spectra of known myoglobin species. Using this method, the determined rate for trapping of HNO by metmyoglobin, which produces NO-myoglobin, is found to be 2.7 x 10^5 $M^{-1}s^{-1}$ at pH 7.0 and 1.1 x 10^5 $M^{-1}s^{-1}$ at pH 9.4. The reaction of deoxymyoglobin with HNO generates the adduct HNO-myoglobin directly, but is followed by a secondary reaction of that product with HNO yielding NO-myoglobin; the determined bimolecular rate constants for these reactions are 3.48 x 10^5 $M^{-1}s^{-1}$ and 1.67 x 10^4 $M^{-1}s^{-1}$ respectively, and are independent of pH. The derived spectrum for HNO-myoglobin is characterized by a Soret absorbance maximum at 423 nm with an extinction coefficient of 1.66 x 10^5 $M^{-1}cm^{-1}$. The rate constant for unimolecular loss of HNO from HNO-

myoglobin was determined by competitive trapping with CO at 8.9 x 10^{-5} sec^{-1}, which gives the thermodynamic binding affinity of HNO to deoxymyoglobin as 3.9 x 10^{10} M^{-1}. These results suggest that the formation of HNO-ferrous adducts represent an important consideration in the biological action of HNO-releasing drugs. Pictured below is the graphical abstract of the reaction of deoxy-Mb with excess HNO from Angeli's salt.

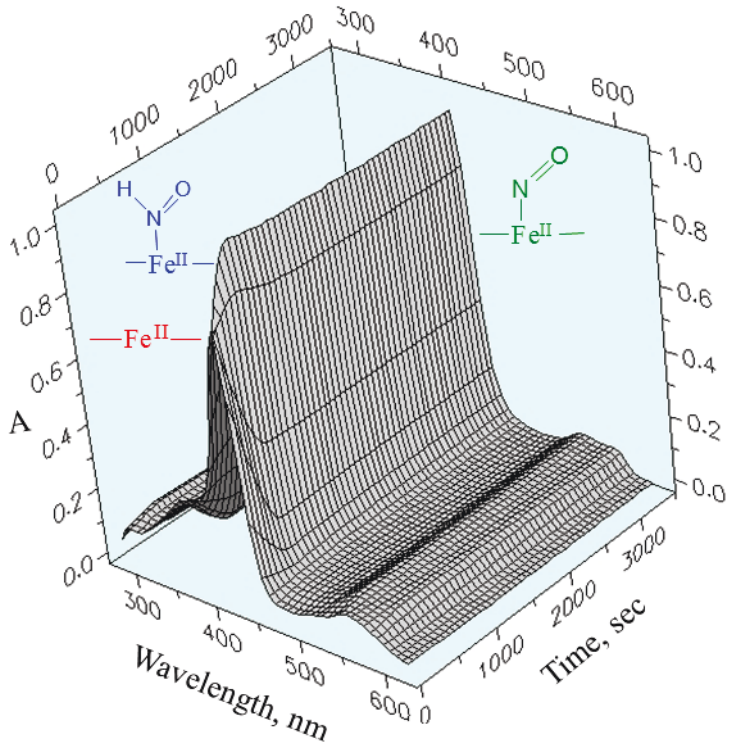

Graphical Abstract

Introduction

A wealth of information on molecular mechanisms that control biological function such as ligand discrimination, allostery and signal transduction have come about as a result of kinetic studies of small molecule (O_2, NO and CO) binding to ferrous heme proteins like myoglobin.[66–69]

The molecular basis for differences in binding affinities between small molecules is most often investigated by a combination of kinetic and mutagenesis experiments, often with theoretical molecular dynamics simulations.[70–72] Key parameters from these studies are the rate constants of association and dissociation of the small molecules to the heme, typically denoted as k_{on} and k_{off}, which allows determination of the thermodynamic binding affinities, denoted by the equilibrium constant K.[73,74] A classic example is of the relative binding affinities of O_2, the native substrate, and CO, a poison, to the oxygen-binding protein myoglobin in comparison with simple ferrous porphyrin like iron tetraphenyporphyrin Fe(TPP).[75] Complexation of a ferrous heme within myoglobin dramatically increases the comparative binding affinities, K_{O2}/K_{CO}, thus increasing our resistance to the noxious gas. A recent addition to the panel of small molecule ligands for such studies is HNO, often termed nitroxyl or nitrosyl hydride, a reduced congener of NO.[57] Free HNO is quite reactive and short-lived in aqueous solution,[76] but we have shown that an HNO adduct of ferrous myoglobin, HNO-Mb can be formed by reduction of NO-Mb,[58,77] by trapping of free HNO by deoxymyoglobin (deoxyMb or Mb-Fe^{II}),[60] or by treatment of metmyoglobin (metMb or Mb-Fe^{III}) with salts of nitrite and borohydride.[61] This stable ferrous heme adduct has been characterized by ^{1}HNMR,[78] ^{1}H-^{15}N *heteronuclear single quantum coherence* (HSQC),[63] as well as resonance Raman and X-ray absorption spectroscopies.[64] As HNO is isoelectronic with $^1O_2$, and forms stable diamagnetic adducts with ferrous hemoglobins from various species, we have suggested its use as an O_2 analog.[63] Most recently, we have shown that HNO may replace O_2 during turnover of a non-heme Mn dioxygenase enzyme, quercetinase; this nitroxygenase activity results in the regioselective incorporation of the N atom derived from HNO within the enzymatic product.[65]

We have long been interested in the kinetic measurements of the trapping of free HNO by deoxyMb, but this reaction is accompanied by side reactions that produce the nitrosyl adduct, NO-Mb. Previous attempts at kinetic analysis have utilized NMR,[60] EPR,[63] flash photolysis,[79] and isosbestic analysis of absorbance spectra,[80] all of which were limited by difficulties in distinguishing all the species present during the complex reaction. NMR studies follow only the diamagnetic HNO-Mb, EPR measures mainly the paramagnetic NO-Mb, and absorbance spectra of the two adduct are quite difficult to separate. The flash photolysis study illustrates a common complication of HNO chemistry - unexpected redox reactivity, as HNO can act as both a reductant and oxidant. For example, photolysis of HNO-Mb produces transient formation of metMb (Mb-Fe^{III}) and presumably HNO^{-}, the aminoxyl radical anion, which recombines on a relatively slow microsecond timescale.[6,80]

In this report, we utilize singular value decomposition (SVD) to analyze these complex reactions. SVD is a mathematical analysis used to separate a complex matrix into simpler, orthogonal component matrices; it is distinctly applicable to deconvolute components of mixed spectra using the evolution of time-based data. For instance, SVD has been used to obtain the spectra of an unisolable intermediate species in the photocycle of bacteriorhodopsin;[81] the separation of individual spectral components then allow modeling to obtain fits of kinetic parameters in complicated systems. Here, we apply SVD methods combined with a global fitting program to obtain the rates of trapping of HNO by met- and deoxyMb, as well as the side reaction forming NO-Mb. Additional investigations of the displacement of the HNO adduct by CO allow us to place our data in the broader context of other small molecule binding by myoglobin. Based on the long-lived stability of purified Mb–HNO, we previously suggested that the affinity of

deoxyMb for HNO is much greater than that of its native substrate O_2, and confirmed by this work as on the same order as that for NO.[57]

Experimental

Materials

Lyophilized horse heart myoglobin was purchased from Sigma. PA and AS were purchased from Cayman Chemical Company. CO gas was purchased from Matheson TriGas, NJ. All other chemicals used were of reagent grade. Inorganic phosphate (iP) buffers (50 mM, pH 7.0) were prepared using monobasic and dibasic sodium phosphate and carbonate buffers (50 mM pH 9.4 and 10) were prepared using sodium carbonate and sodium bicarbonate all from Fisher. All samples were prepared under anaerobic atmosphere in a glovebox, and handled using strictly anaerobic procedures. Nitric oxide (Air Liquid) was purified by passage through a 3 M solution of NaOH.

Instrumentation

Absorption spectra were recorded with a Hewlett Packard 8453 Diode Array spectrophotometer or an Olis RSM 1000 spectrophotometer. ^{1}H NMR experiments were recorded on a Bruker Avance 600. The spectra were acquired by direct saturation of the residual water peak during the relaxation delay. Chemical shifts were referenced to the residual water peak at 4.8 ppm. X-band EPR spectra were recorded with a Bruker EMX spectrometer equipped with a standard TE_{102} (ER 4102ST) or a high sensitivity (ER 4119HS) resonator (Bruker). A built-in frequency counter provided accurate resonant frequency values.

Preparation of Mb Samples

Horse heart metmyoglobin, (metMb or Mb-Fe^{III}) was prepared by reducing commercial Mb sample with 40-fold excess of sodium dithionite followed by purification on G-25 column equilibrated with iP buffer at pH 7.0 to yield oxymyoglobin (oxyMb). An excess of potassium ferricyanide was then added to oxidize oxyMb to metMb; the resulting sample was purified on Sephadex G-25 size exclusion column equilibrated at pH 7.0. Deoxymyoglobin (deoxyMb or Mb-Fe^{II}) was prepared anaerobically by the reduction of metMb with ~ 40-fold excess of sodium dithionite at the appropriate pH for the kinetic experiment (7.0, 9.4 or 10), followed by purification on a Sephadex G-25 size exclusion column equilibrated at the specified pH. Nitrosyl myoglobin, NO-Mb, was generated anaerobically by the addition 20 to 40 fold excess of $NaNO_2$ and $Na_2S_2O_4$ to a freshly prepared solution of metmyoglobin; the resulting NO-Mb solution was purified anaerobically on a Sephadex G25 column. Authentic samples of HNO adduct of myoglobin, HNO-Mb were prepared as previously described,[63] and purified anaerobically on a Sephadex G25 column in a glovebox. All reaction mixtures were generated in an anaerobic glovebox which was maintained with O_2 levels below 5 ppm; under these conditions, solutions of HNO-Mb had a demonstrable lifetime of weeks.

HNO Generation

As free HNO cannot be stored in any practical way, this study employs two widely used precursors to generate HNO in aqueous solution: Angeli's salt, AS or sodium trioxodinitrate, decomposes to release HNO at pH 4 – 9, Equation 2.1;[16] Piloty's acid, PA or benzylsulfohydroxamic acid, generates HNO upon deprotonation at a high pH, Equation 2.2. Once released, HNO does not accumulate due its rapid dimerization producing N_2O between pH 2 to 11,

Equation 2.3.[82] The rate constants of these reactions are known, and will be used in the global fitting program to model the observed speciation changes.

(2.1) $HN_2O_3^- \leftrightarrows HNO + NO_2^-$ $k = 6.75 \times 10^{-4}\ s^{-1}$ *pH 4 to 8*

(2.2) $PhSO_2NHO^- \leftrightarrows PhSO_2^- + HNO$ $k = 3.47 \times 10^{-4}\ s^{-1}$ *pH 10*

(2.3) $2\ HNO \rightarrow [H_2N_2O_2] \rightarrow N_2O(g) + H_2O$

General Protocol for Kinetic Studies Reactions of HNO with Myoglobin Species

The HNO precursor solutions were prepared as concentrated standard solutions buffered to pH that limits decomposition. The PA standard solution (9.0 mM) was prepared in 50 mM iP buffer at pH 7.0; the AS standard solution (12 mM) was in 10 mM NaOH at pH 12. The analyte protein solutions were placed in airtight septa capped UV-Vis cells and the appropriate volume of an HNO precursor reagent (typically 5 to 10 μL of a concentrated solution) was deposited as a drop inside the septa of the cell. The total solution volume in the cell was ca. 2 ml, and thus not affected by the addition of the reagent. The solutions were mixed just before starting the kinetic measurements. All experiments were done at ~22°C and run for 1 to 2 h unless specified.

Reaction of HNO-Mb with CO

A stream of CO gas was scrubbed through a saturated dithionite solution at pH 10 to remove O_2 and other contaminants, and then through a pH 9.4 carbonate buffer to saturation.[83] Samples of this saturated solution were combined with pre-formed HNO-Mb solutions at the same buffer pH and appropriate concentrations. The reaction solution was then placed in the spectrophotometer and spectra acquired over 6 to 24 hour runs.

Kinetic Simulations

The speciation, rate constant parameters and independent verification of species absorbance spectra were obtained by the use of kinetic modeling program JPlus ReactLab Kinetics, a global analysis kinetic modeling program that works in tandem with SVD analysis, which determines the appropriate number of species present during the progression of a reaction. The data is fit by iteratively refining the free parameters according to an adaptation to the Marquardt-Levenberg algorithm, by attempting to minimize the residual square sum, which is a measure of the difference between the real data and that predicted by the current model and prevailing parameters.[84] Model independent factor analysis, in the form of Singular Value Decomposition (SVD) and Evolving Factor Analysis (EFA), was utilized to predict the complexity of the data and was used to estimate the number of colored components to give further insight to the complexity of the reaction independent of residual square sum fitting.

The number of absorbing species, representing different forms of myoglobin present, was directly assessed utilizing SVD, whereas the nitroxyl donors (AS or PA), HNO, and N_2O were modeled as colorless, non-absorbing species. Previously determined rate constants were utilized as initial approximations for the global analysis of reaction rate constants within the proposed sequence of reactions. Similar analysis was done for the spectral data sets obtained at different reaction conditions. All the data sets analyzed reached convergence using 12 or less iterations. The modeled spectra of the absorbing species were analyzed in tandem with speciation to determine the fit. The residual matrix was generated by extrapolating the resulting modeled matrices of absorbing species and speciation plots and analyzed versus the real data. Illustrative residuals and fits are given in the supplemental materials. The parameters were also analyzed by

variance (σr) in the parameters between expected and experimental values, which was on the order of 10^{-3} in all cases.

General Protocol for EPR Experiments.

Aliquots of myoglobin reaction solutions (~350 ml) with HNO donors (PA or AS) in 1 to 4 ratio were frozen in EPR tubes at 10 min intervals over 1 h. Concentration of NO-Mb for each sample was determined by comparing intensities of the observed peak to a calibration curve obtained by authentic NO-Mb.

Results

Reaction of metMb with HNO Donors

Reaction of metMb with AS at pH 7 induced characteristic Soret and Q-band absorbance changes indicating the direct conversion of metMb to NO-Mb, as shown in a and b of Figure 2.1 and described by Equation 2.4.[1] Similar changes were observed in the reaction of metMb with PA at pH 9.4. Because of the relatively slow release of HNO by PA and AS, as well as its rapid dimerization ($8 \times 10^6\ M^{-1}s^{-1}$),[82] rate constants for the HNO reactions can only be obtained by kinetic modeling.

(2.4) $Mb\text{-}Fe^{III} + HNO \rightarrow NO\text{-}Mb + H^+$

Sequential spectra obtained over 1 hour from 280 to 650 nm were loaded into the global fitting program along with initial concentrations of reagents used, a stepwise reaction sequence

[1] The molecularity of these reactions has been tested in range from 0.5 to 40 equivalents of PA to deoxyMb without any observable change in reaction scope. As in previous studies, the rate-limiting step is the release of HNO from the precursors PA or AS, and the overall rate is zero-order in Mb. Likewise, the addition of 20-fold excess concentrations of the metal chelators EDTA and DPTA, which are commonly used to remove extraneous metals, had no effect on the observed rates on the rates or products of reactions described.

with estimated rates, utilizing Equations 2.1, 2.3 and 2.4, and the characteristics (colored, non-absorber) of the species involved. The nitroxyl donors AS and PA, HNO, and N_2O were denoted as colorless species, but their rates of formation and loss were included in the model. The estimated number of colored myoglobin species was assessed utilizing SVD, which was consistent with Equation 2.4. The SVD analysis also generates spectra of the derived colored species, deconvoluted orthogonal components of the total spectrum, which are shown in Figure 2.1c. The close match of the derived spectra and their extinction coefficients with known spectra for metMb and NO-Mb are a secondary verification of the global fit; the concentrations were normalized utilizing the published extinction coefficient for NO-Mb, at 147,000 $M^{-1}cm^{-1}$.[85] Rates constants for Equation 2.4 were obtained from global fitting analysis for pH 7.0 and 9.4, as 2.7 x 10^5 $M^{-1}s^{-1}$ and 1.1 x 10^5 $M^{-1}s^{-1}$ respectively. Independent control experiments showed no further reaction of HNO with the product NO-Mb.

Reaction of DeoxyMb with HNO Donors

Reactions of deoxyMb (Mb-Fe^{II}) with PA generated more complex sequential spectra indicative of an additional following reaction, as shown in Figure 2.2. Following previous work,[63] we modeled the time course absorbance changes using sequential reactions of HNO generation and dimerization, Equations 2.2 and 2.3, and two additional reactions for the trapping of HNO by Mb-Fe^{II} to generate HNO-Mb, HNO-Mb, Equation 2.5, and a subsequent reaction of HNO with HNO-Mb to generate NO-Mb, Equation 2.6.

(2.5) HNO + Mb-Fe^{II} → HNO-Mb

(2.6) HNO + HNO-Mb → NO-Mb + [H_2NO]

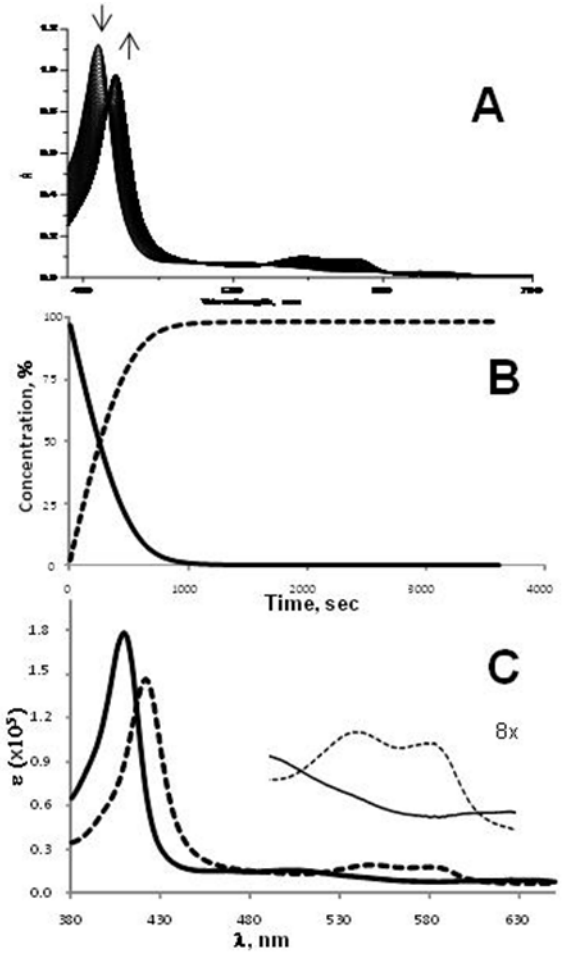

Figure 2.1. Reaction of metMb (6.7 μM) with AS (27 μM) in iP buffer, pH 7. (A) Time course of spectral data over 3600 seconds. 0(B) Modeled speciation of metMb and NO-Mb using ReactLab Kinetics; solid line: metMb; dotted line: NO-Mb. (C) Absorbance spectra extracted from the modeled reaction profile; inset is enlarged Q-band region.

The SVD analysis of the absorbance changes solved for three absorbing species, deoxyMb, HNO-Mb, and NO-Mb. The percentage speciation over the course of reactions are shown in Figures 2.2b and 2.2c for reactions at pH 9.4 and 10, indicating the initial formation of HNO-Mb and its subsequent transformation into NO-Mb within the reaction mixture. HNO-Mb loss correlated directly to generation of NO-Mb, additional confirmation of the secondary reaction of HNO-Mb with HNO as included in the global fitting analysis. The more rapid generation of NO-Mb in reactions at pH 10, Figure 2c, is consistent with a faster release of HNO at this pH.

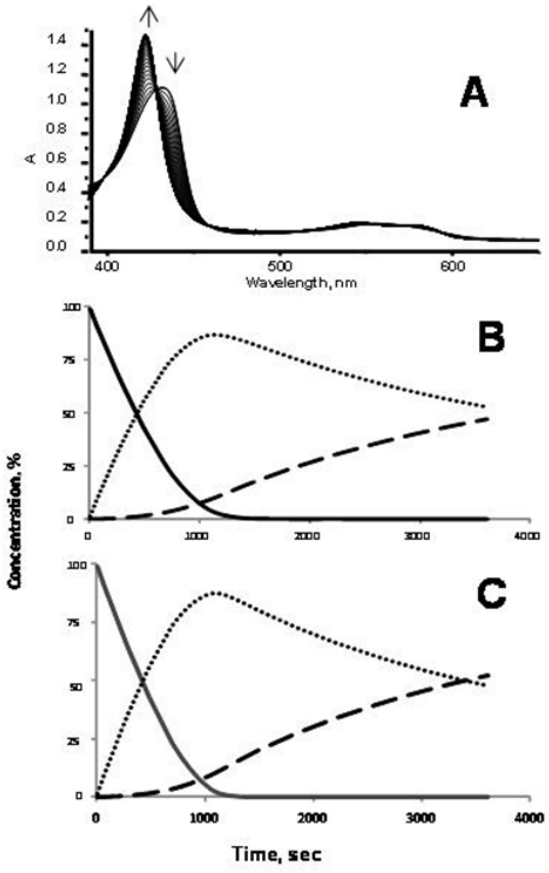

Figure 2.2. Reactions of deoxyMb with PA. (A) Time course spectral data over 3600 sec. at pH 9.4. in iP buffer with [deoxyMb] = 7.2 μM, [PA] = 35 μM. (B) Modeled speciation of deoxyMb, HNO-Mb, and NO-Mb at pH 9.4 using ReactLab Kinetics, solid line: deoxyMb, dotted line: HNO-Mb, and dashed line: NO-Mb. (C) Modeled speciation of similar reaction at pH 10, with [deoxyMb] = 6.4 μM, [PA] = 26 μM, same line formats.

A comparison of the spectra derived from the SVD analysis for the reaction of deoxyMb with PA at pH 9.4 is given in Figure 2.3. As above, these derived spectra were used to calibrate protein concentrations in various reactions, using the extinction coefficient of 1.47 x 10^5 $M^{-1}cm^{-1}$ for the Soret absorbance of NO-Mb at 421 nm as an internal standard.[85] In practice, the experimental concentrations of deoxyMb used in each experiment were altered less than 2% by this correction. The resulting derived extinction coefficients given in Table 2.1, demonstrate the self-consistency of the SVD analysis. The SVD derived Soret extinction coefficients for deoxyMb

from the global fitting analysis match well with the literature value of 1.21 x 10^5 $M^{-1}cm^{-1}$ at 434 nm.[85] This analysis also provides a value of 1.66 x 10^5 $M^{-1}cm^{-1}$ for the extinction coefficient of the Soret absorbance of HNO-Mb at 423 nm.

Table 2.1. Extinction coefficients derived from SVD analysis.*

HNO Donor	Buffer pH	Ɛ, 10^5 $Lmol^{-1}cm^{-1}$ for deoxyMb	Ɛ, 10^5 $Lmol^{-1}cm^{-1}$ for HNOMb
PA	9.4	1.21	1.65
	10	1.20	1.64
AS	7.0	1.22	1.68
	9.4	1.21	1.65
Average Ɛ ($Lmol^{-1}cm^{-1}$)		1.21 ± .008	1.66 ± .017

*All values for horse heart Mb derived species, normalized to NO-Mb absorbance at 421 nm, ε = 1.47 x 10^5 $Lmol^{-1}cm^{-1}$. [83]

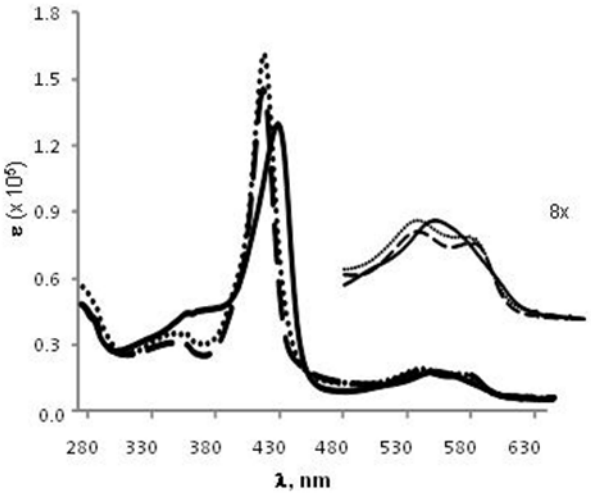

Figure 2.3. Overlay of absorbance spectra derived from SVD analysis of the reaction of deoxyMb with PA in iP buffer at pH 9.4 [deoxyMb] = 7.2 μM with [PA] = 35 μM, program over the time course of 3600 s (solid line: deoxyMb, dotted line: HNO-Mb, dashed line: NO-Mb). Inset: enlarged Q-band region, same line formats.

Analogous reactions of deoxyMb with AS at pH 7 and 9.4 generated similar sequential spectra, as shown in Figure 2.4. These spectra were fit using Equations 2.1, 2.3, 2.5 and 2.6, and

generated similar speciation changes over the course of the reactions as those seen for PA. Table 2.2 gives a comparison of the bimolecular rate constants obtained for Equations 2.5 and 2.6 under different experimental conditions. The rate constant values under each condition are given as the average from three distinct experimental model fits, with standard deviations given in parenthesis. Also given is the standard deviation of the residuals (σr, an estimate of the accuracy of fit) which is less than 1% in all cases. The determined rate constants for Equations 2.5 and 2.6 appear little affected by pH in the measured range; thus we propose the average of these rate constants, 3.48 (± .002) x 10^5 $M^{-1}s^{-1}$ for Equation 2.5 and 1.67 (± 0.27) x 10^4 $M^{-1}s^{-1}$ for Equation 2.6.

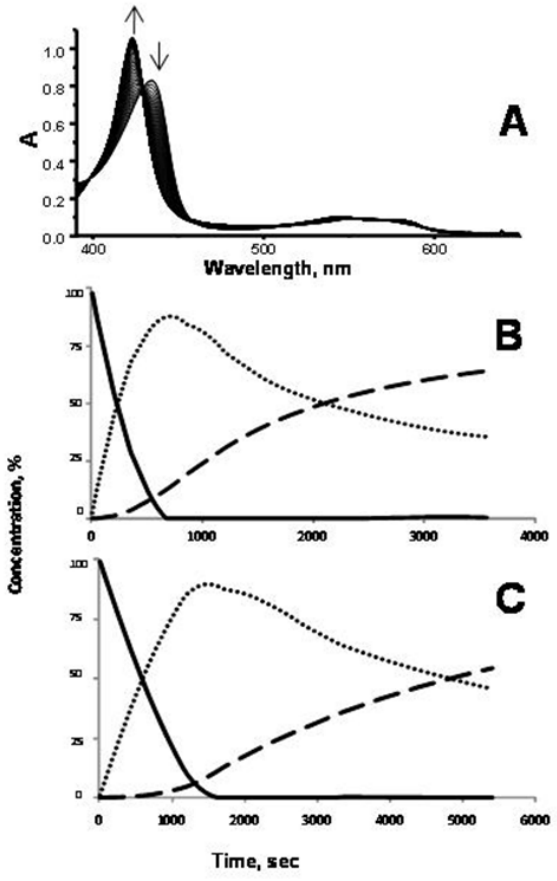

Figure 2.4. Reaction of deoxyMb with AS. (A) Time course (3600 s) of spectral data in iP buffer at pH 7 with [deoxyMb] = 6.7 μM and [AS]= 27 μM. (B) Modeled speciation of deoxyMb, HNO-Mb, and NO-Mb at pH 7, with solid line: deoxyMb, dotted line: HNO-Mb, dashed line: NO-Mb. (C) Modeled speciation of same reaction at pH 9.4, with [deoxyMb]= 8.5 μM with [PA]= μM; same line formats.

Table 2.2. Rate constants for reaction of HNO with Mb-Fe^{II} and HNO-Mb

HNO Donor	Buffer pH	Mb-Fe^{II} k, 10^5 $M^{-1}s^{-1}$	HNO-Mb k, 10^4 $M^{-1}s^{-1}$	σr X 10^{-3}
PA	9.4	3.43 (± .002)	1.60 (± 0.39)	3.53 (± 1.97)
	10	3.37 (± .0009)	1.70 (± 0.27)	8.33 (± 1.65)
AS	7.0	3.61 (± .004)	1.75 (± 0.09)	6.03 (± 1.00)
	9.4	3.50 (± .006)	1.62 (± 0.22)	6.40 (± 0.90)

The global fitting analysis also provides concentration changes over the course of the reaction for the non-absorbing species: the nitroxyl donors PA and AS, HNO, and N_2O. Reactions at pH 9.4 were used for comparison, Figure 2.5, as the unimolecular rates of decomposition of PA and AS are similar at this pH. The speciation time course shows that the concentration of free HNO varies two- to three-fold in the picomolar range over the course of the reactions, ca. three orders of magnitude smaller than that of the donors PA and AS.

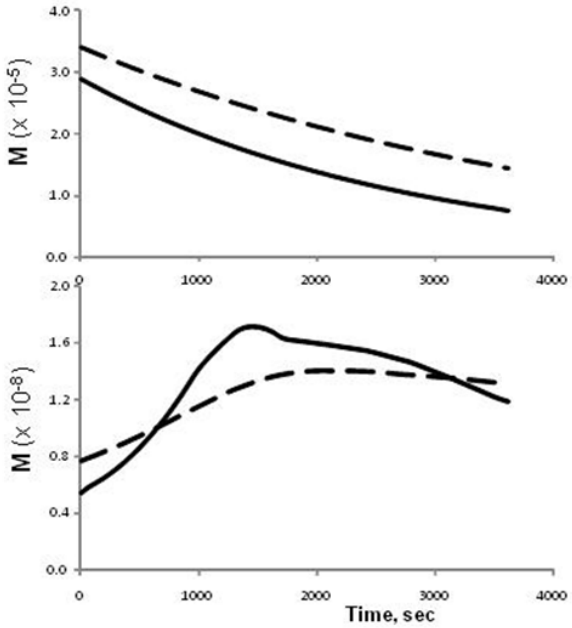

Figure 2.5. Modeled concentration changes for non-absorbing species during reactions in pH 9.4 iP buffer described in Figures 2 and 4. (Top) Concentrations of PA (initially 29 μM, solid line) and AS (initially 35 μM, dashed line). (Bottom) Concentrations of free HNO during the same reactions using HNO donors PA (solid line) and AS (dashed line).

Reaction of HNO-Mb with HNO

As a test of the secondary reaction, Equation 2.6, pre-formed samples of HNO-Mb were reacted with HNO donors and followed by EPR, ^{1}H NMR and SVD analysis. NMR spectra of preformed HNO-Mb samples with AS at pH 7 that show the loss of the nitrosyl hydride peak at 14.8 ppm, Figure 2.6; EPR characterizations show increasing [NO-Mb] formed over the course of reaction of deoxyMb with PA. Absorbance spectra analysis of an analogous reaction of HNO-Mb with PA shows a characteristic but slight loss of intensity of the heme Soret band, Figure 2.7. The rate constant for the formation of NO-Mb from the reaction of HNO-Mb with HNO derived from PA decomposition, Equation 2.6, was calculated to be 1.69 (± 0.10) x 10^{4} $M^{-1}s^{-1}$ ($\sigma r = 2.03 \pm 1.45$ x 10^{-3}), in good agreement with the value derived in the HNO trapping reactions. There is no observable reaction between NO-Mb and AS or PA.

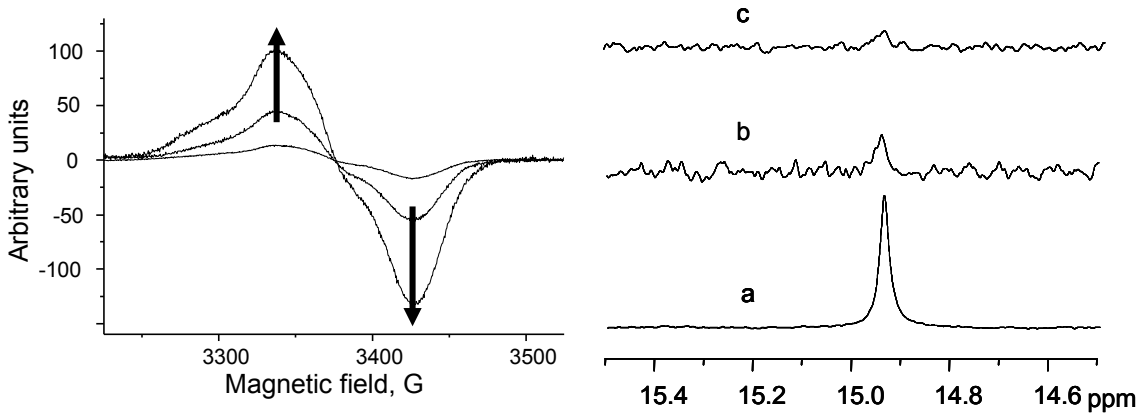

Figure 2.6. (Top) EPR spectra showing increase of NO-Mb during reaction of 72 μM HNO-Mb at pH 9.4 with 280 μM PA. (Bottom) ^{1}H NMR spectra showing disappearance of hydride peak of HNO-Mb (500 mL, 2 mM) during reaction with AS (8 mM) in 50 mM iP buffer at pH 7.0: (a) before the reaction, (b) after 30 min, and (c) after 60 min of reaction.

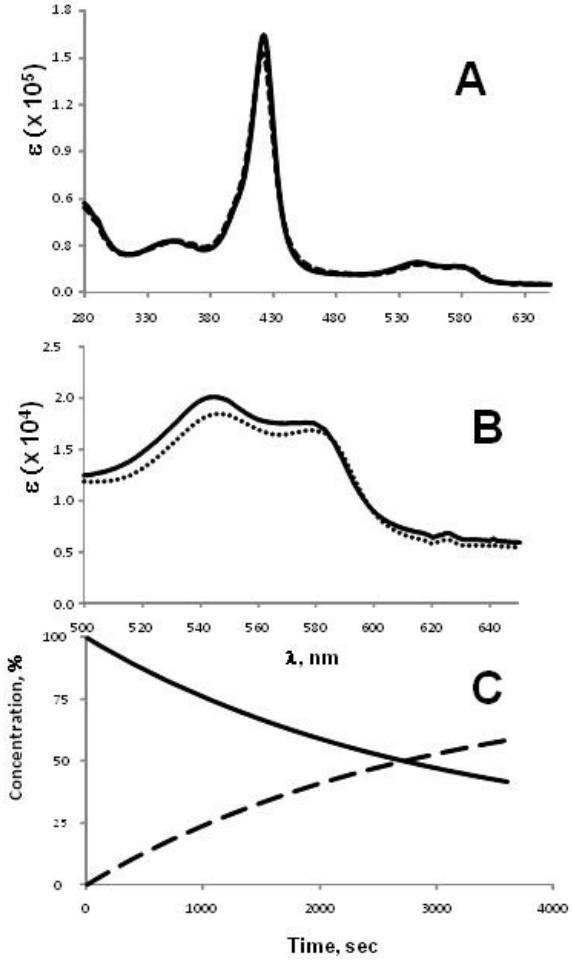

Figure 2.7. Reaction of HNO-Mb (6.8 μM) with PA (27 μM) in pH 9.4 iP buffer and run for 3600 s. (A) Absorbance spectra of HNO-Mb (dashed line) and NO-Mb (solid line) extracted using ReactLab Kinetics program. (B) Enlarged Q-band region of spectra. (C) Speciation of HNO-Mb and NO-Mb.

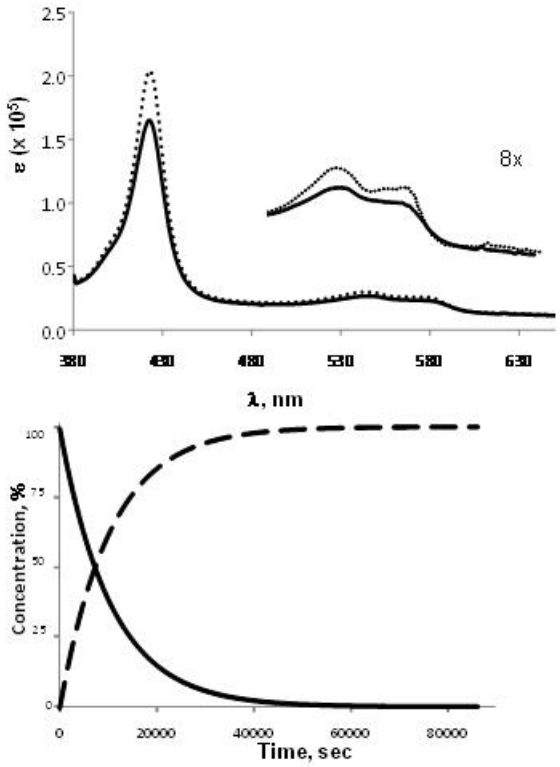

Figure 2.8. Reaction of HNO-Mb (6.8 μM) with CO (920 μM) pH 7 iP buffer over 24 h. (Top) Solid line: initial spectra of HNO-Mb, dashed line: final spectra attributed to CO-Mb. Inset: enlarged Q-band region. (Bottom) Speciation plots of HNO-Mb and CO-Mb over course of reaction, same line formats.

Reaction of HNO-Mb with CO

Contrary to previous reports,[57] samples of HNO-Mb react slowly over a day with excess CO gas to form the ferrous CO-Mb adduct. Although spectrally similar with the starting HNO-Mb, the Soret and Q-band absorbances are observably larger in the product solution, and the spectra of the product solution is unaffected by exposure to air, as is characteristic of CO-Mb. A kinetic analysis of pre-formed HNO-Mb sample reacting with CO (920 μM) over 24 hours is shown in Figure 2.8. The rate of CO-Mb formation appears unchanged at different concentrations of dissolved CO. The slow rate and independence of [CO] suggests that a unimolecular dissociation of HNO from the HNO-Mb complex is rate limiting. Global fitting of the reaction

was performed using a two reaction sequence, Equations 2.7 and 2.8, which invoke the generation of deoxyMb by dissociation of HNO from HNO-Mb, and subsequent binding of CO to generate the observed product; this obtained a rate for Equation 2.7 of 8.9 x 10^{-5} sec^{-1}, many orders of magnitude slower than the bimolecular rate constant for Equation 2.8, 5.1 x 10^5 $M^{-1}s^{-1}$.[73] The SVD derived spectra for CO-Mb obtained from the global fitting analysis gives a value of 2.06 x 10^5 $Lmol^{-1}cm^{-1}$, which compares well with the literature value of 2.07 x 10^5 $M^{-1}cm^{-1}$.[85]

(2.7) HNO-Mb → HNO + deoxyMb

(2.8) CO + deoxyMb → CO-Mb

Discussion

SVD Methodology

Previous attempts at kinetics analysis of HNO reactivity with myoglobins have been problematic. All reported synthetic methods to HNO-Mb potentially generate mixtures of deoxyMb, HNO-Mb and NO-Mb. Typical methods used to characterize these mixtures, such as ^{1}H NMR and EPR, only characterize one of the three species. Absorbance spectroscopy does observe all three, but the similarity of the HNO-Mb and NO-Mb spectra (as well as that of CO-Mb), make differentiation tenuous. An added problem is the combination of relatively fast and slow reactions, many of which relate to species that are not observable, which made modeling and simulations difficult.

The SVD global fitting method has provided self-consistent analysis of these complex sequential reactions, and also generated spectra of the absorbing myoglobin species which match well with known spectra. This work also reports a spectrum for "pure" HNO-Mb which is difficult to attain experimentally. The global-fitting derived spectrum of HNO-Mb, with an extinction

coefficient of 166,000 $Lmol^{-1}cm^{-1}$ for the Soret absorbance at 423 nm, matches well with the estimated extinction coefficient from reductive titration of NO-Mb to HNO-Mb, which predicted a value of 164,000 $M^{-1}cm^{-1}$.[79]

Rate Constants for HNO Trapping and Thermodynamic Binding Affinity

One motivation for this work was to directly compare the relative rates of trapping of the ferric and ferrous forms of Mb, as an indicator of discrimination of HNO and NO reactivity with biological heme proteins. Doyle and Hollocher first investigated the rates of reactivity of AS with Mb and Hb as a test for the formation of HNO from AS decomposition.[7,8,41,85,86] Both groups showed that the reaction of AS with metMb, Equation 4, directly yields NO-Mb. In our hands, such experiments obtained bimolecular rate constants of as 2.7 x 10^5 $M^{-1}s^{-1}$ and 1.1 x 10^5 $M^{-1}s^{-1}$ at pH 7.0 and 9.4, somewhat lower than the value reported by Hollocher of 6.4 x 10^5 $M^{-1}s^{-1}$. The lower rate at pH 9.4 can be attributed to competitive coordination of OH^- to the metMb at this pH. A similar effect was observed during reaction between ferric microperoxidase-11 and HNO donors, which reduced the apparent rate constant half-fold from pH 7.0 to 10.0.[87]

Obtaining the biomolecular rate constant for the trapping of HNO by deoxyMb has been more difficult. The first reports from Hollocher and Doyle suggested deoxyMb reacts stoichiometrically with AS to yield both NO-Mb and metMb, presumably from disproportionation or oxygen contamination.[7,41] Only in the last report on this subject by Doyle, was the possible formation of a transient HNO-Fe(II) adduct considered, but suggested to react with nitrite forming NO-Mb and NO.[7]

We also reported complex product mixtures during attempts to follow the reaction of AS with deoxyMb at millimolar concentrations by NMR; the diamagnetic HNO-Mb adduct was an initial product, but subsequently degraded to NO-Mb during further reaction.[60] Clean time-

dependent ^{1}H NMR data was obtained using methanesulfonylhydroxamic acid, MSHA, which releases HNO at a slow rate. With this reagent, the formation of HNO-Mb due to the trapping of HNO by deoxyMb was given a lower limit of 1.4×10^{4} $M^{-1}s^{-1}$; but its concentration was shown to reach a maximum and decreases at later stages of the reaction, concurrent with buildup of NO-Mb.

Subsequent isosbestic analysis of time-course spectra coupled with kinetic simulations gave values of as 2.0×10^{5} $M^{-1}s^{-1}$ and 4.0×10^{3} $M^{-1}s^{-1}$ for bimolecular rate constants of Equations 2.5 and 2.6;[63–65,79,80] these were used as initial starting points for the global fitting analysis done in this study. The rate constants for the initial trapping of HNO by deoxyMb match well between the two methods, but the value for the secondary reaction of HNO with HNO-Mb is found here to be an order of magnitude higher, at 1.67×10^{4} $M^{-1}s^{-1}$. The differentiation of this secondary reaction was always problematic using the isosbestic method, as the spectral difference between HNO-Mb and NO-Mb was small and not well characterized.

The displacement reaction of HNO-Mb with CO has only recently been observed; the reaction is slow and the change in absorbance small. But the observation of displacement, especially on a timescale much shorter than the decomposition of HNO-Mb, signifies a binding equilibrium. Here we assume that the displacement reaction is rate-limited by the unimolecular dissociation rate constant, k_{off}, for HNO-Mb, Equation 2.7. The binding affinity is simply the ratio of the on- and off-rate constants, both obtained in this work. The determined value is compared with the known binding constants of diatomic gases in Table 2.3.[70,73] The binding affinity of HNO to deoxyMb, at 3.9×10^{9} M^{-1}, is close to that of NO but orders of magnitude greater than those of O_2 or CO. The on-rate for singlet spin-state ^{1}HNO is comparable to that of singlet ^{1}CO, but much smaller than those of radical species ^{2}NO and $^{3}O_2$, which should more readily react with high-spin

(S = 2) deoxyMb. However, the off-rate for ^{1}HNO is very slow, similar to that of ^{2}NO, which results in a binding affinity second only to that of NO. It is likely that hydrogen-bonding interactions of the bound HNO with the distal pocket histidine contributes to the slow off-rate.[31]

Table 2.3. Binding parameters for Mb adducts [a]

Ligand	k_{on} x 10^6 $M^{-1}s^{-1}$	k_{off} s^{-1}	K_{eq} x 10^{-6} M^{-1}
O_2	17	15	1.13
NO	22	1.0×10^{-4}	2.2×10^5
CO	0.51	1.9×10^{-2}	26.8
HNO[b]	0.35	8.9×10^{-5}	3.9×10^4

[a] for sperm whale Mb, reference [85]; [b] determined this work for equine Mb

The Secondary Reaction of HNO-Mb with HNO

An unanswered question is the nature of the byproduct in the secondary reaction of HNO-Mb with HNO. This reactivity has been previously reported,[60,61,63,78] and is the apparent route for the formation of NO-Mb in the reaction of deoxyMb with HNO-releasing compounds. The kinetic analysis clearly matches a simple bimolecular reaction, which therefore suggests the formation of H_2NO, the aminoxyl radical, Equation 2.6. Like HNO itself, H_2NO is known to rapidly dimerize to form N_2 and water, Equation 2.9, with a rate constant of 1.4×10^8 $M^{-1}s^{-1}$.[88] It is also a powerful oxidant, with a standard reduction potential of 0.9 V NHE under acidic conditions.[88] We suggest that this species is responsible for the generation of metMb during the reaction of AS with deoxyMb, in highly concentrated reaction mixtures used for NMR studies as described above.

$$H_2NO + H_2NO \rightarrow N_2 + 2\,H_2O \qquad (2.9)$$

Biological Implications

It has been widely suggested that the pharmaceutical effects of NO and HNO are orthogonal, that NO reacts mainly with ferrous heme enzymes like soluble guanylyl cyclase (sGC) and oxygen-binding globins like Hb and Mb, and that HNO reacts mainly with ferric heme enzymes such as peroxidases and cytochromes P450.[10,89,90] This work, and other reports from our lab clearly show that free HNO reacts with ferrous globins at rates typically faster than with ferric species. As ferrous heme proteins predominate within blood and the cardio-vascular system, we suggest that the formation of HNO-ferrous adducts represent an important consideration in the action of HNO-releasing drugs.

Likewise, the secondary reactivity of HNO-Mb with HNO has been largely ignored by medical researchers, but may play a role in assays determining the physiological effects of HNO donors. The relative rate for this reactivity is highly dependent on the protein; for example, the bimolecular rate constant determined for hemoglobin I from invertebrate clam *Lucina pectinata*, at 8.0 x 10^4 $M^{-1}s^{-1}$, was over an order of magnitude higher than that for equine Mb in the same study.[63]

A recent controversial report found that HNO precursors activate sGC in its native ferrous state.[91] This report was countered by another report suggesting the activation was due to small inherent yields of NO released from the HNO precursors.[92] We suggest that the secondary reaction of ferrous HNO-adduct of sGC with HNO would generate the catalytic NO-bound state, and might account for the reported activation.

Conclusions

The fundamental importance of nitric oxide, NO, in human physiology[93,94] and disease has generated a tremendous interest in the chemistry of heme-nitrosyls.[95] Similarly, HNO precursors

have shown unique pharmaceutical effects, such as a therapeutic effect in damaged hearts.[26] Several reports have described unique physiological responses that occur upon the treatment with HNO precursors,[28,96,97] but the reactivity's that lead to such responses remain poorly understood. Better understanding of HNO reactivity is essential in understanding the pharmacology of HNO releasing drugs. Likewise, the further reactions of HNO-Mb also must be considered in activity assays.

Acknowledgments

We thank Prof. John Olson for stimulating conversations and suggestions on this work, and Mr. Peter King from JPlus Consulting for help and advice. This research was supported by the National Science Foundation (PJF CHE-1057942).

CHAPTER THREE

Global kinetic analysis and singular value decomposition methods applied to complex multicomponent reactions of HNO

This chapter accepted as:
Zapata, A. L.; Kumar, M. R.; Farmer, P. J. Global kinetic analysis and singular value decomposition methods applied to complex multicomponent reactions of HNO. In The Chemistry and Biology of Nitroxyl (HNO) eds. F. Doctorovich, P. Farmer, M. A. Marti, Elsevier , 2015.

Abstract

Global kinetic modeling, using singular value decomposition software, allows the intimate investigation of complex time course spectra. An advantage of the method is that spectra and molar absorptivity's are generated for all absorbing reactants and products, allowing the validation of transient species involved. But analyses of reactions involving HNO are inherently difficult as it must be generated *in situ*, and undergoes several concurrent and competitive reactions; thus its concentration profile is only available via kinetic modeling. In this report, sequential absorbance spectra is used to analyze reactions of HNO with a mixture of met- and deoxy-Mb, which have strongly overlapping spectra, and also to model the flux of HNO over the course of the reaction. The determined trapping rate constants, 2.76 x 10^5 $M^{-1}s^{-1}$ for met-Mb and 3.74 x 10^5 $M^{-1}s^{-1}$ for deoxy-Mb, are qualitatively similar, and thus little kinetic preference is predicted in physiological reactivity of HNO.

Introduction

The physiological effects of NO and its redox congeners NO^+, nitrosonium, and NO^-, nitroxyl, have been largely attributed to reactivity with heme proteins and thiols.[1] The pharmacological activity of nitrosonium donors such as nitrite has garnered much interest, as they seem to play important, but different, biological roles from NO itself.[2] Likewise nitroxyl-releasing compounds have generated much interest in cardiovascular research for showing unique therapeutic effects on damaged hearts.[3] Such physiological investigations typically look for organismal effects that occur in response to treatment with NOx species, but typically cannot define fundamental reaction chemistries that underlie the observed behavior.

The biological targets for all three NO congeners are thought to be reactive thiols and ferric and ferrous hemes. Thus, an understanding the kinetics of individual reactions is essential to interpreting their individual effects within biological systems.[4] In a widely referenced review, the pharmaceutical effects of NO and HNO donor drugs were suggested to be orthogonal, with NO reacting mainly with ferrous hemes and HNO with ferric hemes, leading to distinctive cGMP and cAMP signaling cascades.[4] But the chemical basis for such a distinction is ambiguous and difficult to prove.

Chemical investigations of the reactivity of free HNO are inherently difficult and complex; nitroxyl has a short physiological lifetime due to its rapid reaction with oxygen[5] and thiols,[6] as well as a competitive dimerization reaction which limits its concentration in both aerobic and anaerobic solutions.[7] Since free nitroxyl is short-lived, precursor compounds like Angeli's salt and Piloty's acid are used as HNO sources. Angeli's salt (AS, or trioxodinitrate) decomposes as its monoprotonated form, $HN_2O_3^-$, Scheme 3.1, to give HNO and NO_2^- with half-life of ca. 17 minutes from pH 4 to 8.[8,9] Similarly, Piloty's acid, (PA, or benzenesulfohydroxamic acid) decomposes

via its the monoprotonated form to yield HNO and benzene sulfinate with a half-life of 33 min at pH 10.[10] Both decompositions rates are decreased with addition of byproducts, nitrite or sulfinate, confirming the initial reversibility of these reactions. Under anaerobic conditions both also produce trace amounts of NO, which increases in the presence of air.[11]

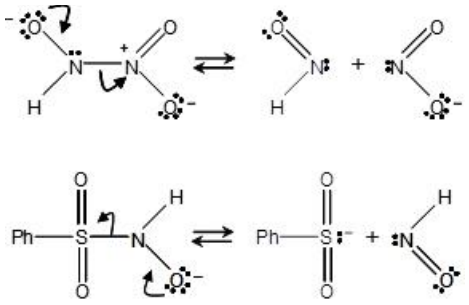

Scheme 3.1. Decomposition of HNO donor's Angeli's salt and Piloty's acid.

Our lab has long sought to define the kinetics of the reaction of HNO with deoxy-Mb which generates a unique HNO adduct, HNO-Mb.[12,13] Like the corresponding O_2 adduct, this species is diamagnetic and characterizable using ^{1}H NMR.[14] The first kinetics measurements of this trapping reaction utilized a relatively long-lived HNO precursor, N-methanesulfonylhydroxyl- amine or MSHA ($t_{1/2}$ ~ 160 m, pH 10) in time course ^{1}H-NMR spectra. These initial experiments demonstrated the loss of paramagnetic deoxy-Mb and concurrent formation of signals indicative of HNO-Mb formation. But midway during such a reaction, the diamagnetic HNO-Mb ^{1}H NMR signal is seen to decrease; EPR experiments correlated this loss of HNO-Mb to the generation of the NO adduct, NO-Mb, via a secondary reaction with HNO. This secondary reactivity was verified independently by reaction of a premade HNO-Mb sample with HNO, which resulted in NO-Mb generation.[15] Because HNO-Mb is both formed and depleted concurrently, and the rate

constant was reported as a lower limit, 1.4 x 10^4 M^{-1} s^{-1}, a value that is still commonly used in recent reviews.[16]

We also investigated flash photolysis of HNO-Mb, a method commonly used to determine the rate constants of association and dissociation, k_{on} and k_{off}, of small molecules like O_2, NO and CO to heme proteins.[17-19] But flash photolysis experiments on samples of HNO-Mb were dominated by redox reactivity. Instead of clean dissociation of HNO-Mb into free HNO and ferrous deoxy-Mb, photolysis instead generates a transient 5-coordinate ferric met-Mb species, and by inference HNO^-, the aminoxyl radical anion.[20] These two photo products were then seen to recombine on the unusually slow microsecond timescale.

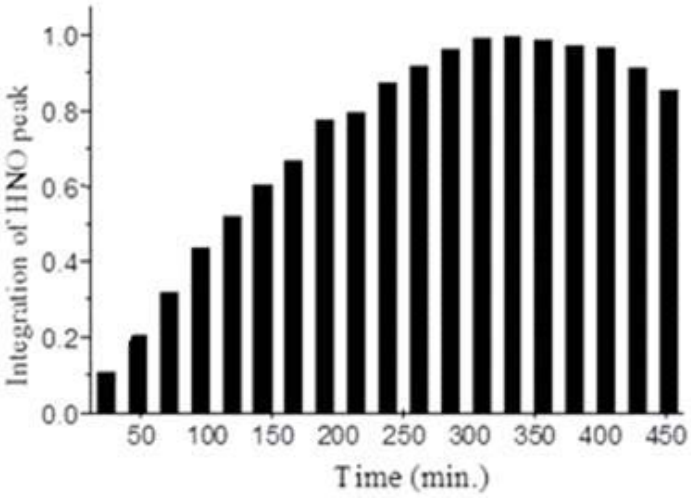

Figure 3.1. Sequential integration areas of HNO-Mb peak at 14.8 ppm over course of 1:1.5 reaction of deoxy Mb with MSHA at 5.7 mM and pH 10. Integration area is represented as relative to maximum value, which corresponds to less than 70% conversion to Mb-HNO.

The secondary reactivity of HNO-Mb with HNO also limits the purity of any HNO-Mb sample obtained in trapping reactions; isolated yields were reported from 60 to 80%, but such

yields were difficult to determine as no single method (^{1}H NMR, EPR, UV-vis) could be used to identify all the Mb species over the course of reaction.

The most readily accessible data for such an analysis is time course absorbance spectra. However, the Soret absorbances of HNO-Mb, at 423 nm, and NO-Mb, at 421 nm, overlap and are difficult to resolve in mixtures. Initial attempts utilized pseudo-isosbestic points in the Q band region that correlated to concentration changes in NO-Mb (460 nm), deoxy-Mb (492 nm) and HNO-Mb (517 nm).[16] The resulting concentration profiles over the course of the reaction, at top of Figure 3.2, suggested a much faster trapping rate constant, ca. $k = 8 \times 10^5\ M^{-1}\ s^{-1}$, and gave an initial estimate for the secondary reaction of $k = 3 \times 10^4\ M^{-1}s^{-1}$ at pH 7.[16] But these analyses were flawed, as the two sequential reactions are too close in rate to distinguish by apparent isosbestic analysis.

Recently, such shortcomings were overcome by use of global kinetic modeling methods to analyze these reactions. A critical component in applying this method to complex systems is singular value decomposition or SVD, a mathematical analysis used to separate a complex matrix into simpler, orthogonal component matrices. This analysis is used in combination with global kinetic modeling to deconvolute components of mixed spectra using the evolution of time-based data.

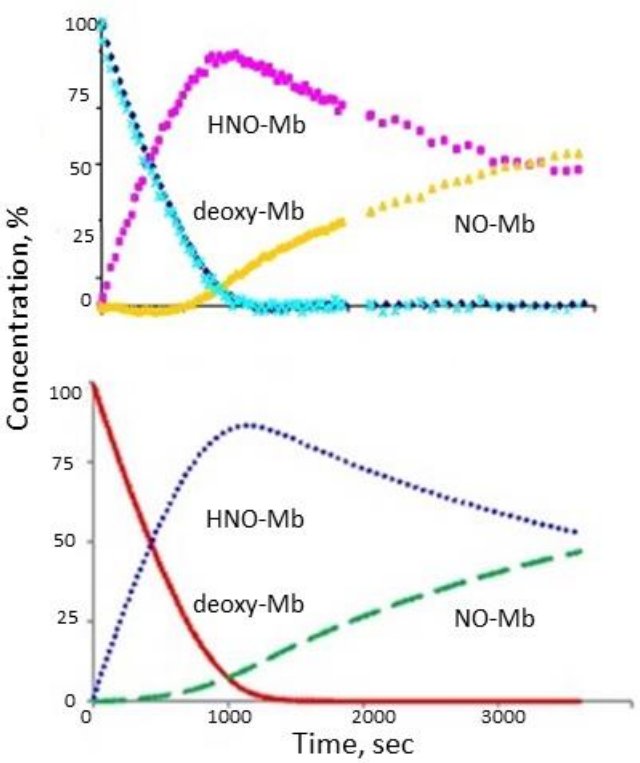

Figure 3.2. Top) Concentration profiles derived from isosbestic spectral analysis of the absorbance spectra of the reaction of Mb-Fe^{II} with PA in 1:4 ratio at pH 10.[15] Bottom) Concentration profiles from spectral global analysis of the reaction of Mb-Fe^{II} with PA in 1:4 ratio at pH 9.4.[21]

By this method, time course spectra of the HNO trapping reactions were modeled, and the resulting speciation plots gave independent verification of the secondary reactivity producing NO-Mb, shown at the bottom of Figure 3.2.[21] The determined bimolecular rate constant for the trapping of HNO by deoxy-Mb determined was 3.48 x 10^5 $M^{-1}s^{-1}$, and a constant of 1.67 x 10^4 $M^{-1}s^{-1}$ was found for the secondary reaction that generates NO-Mb; both rate constants were independent of pH and HNO donor (AS and PA). Importantly these methods also produce model-generated spectra for all colored species involved, which provided a derived spectrum for pure HNO-myoglobin, with a Soret maximum at 423 nm at an absorptivity of 1.66 x 10^5 $M^{-1}cm^{-1}$. This work also determined the unimolecular HNO dissociation rate, found by competitive trapping with

CO, which allowed calculation of the overall binding affinity, K_{eq}, of HNO to deoxy-Mb. At 3.9 x 10^9 M^{-1}, this affinity constant is less than that of NO to deoxy-Mb, but orders of magnitude greater than those of O_2 or CO, Table 3.1.

Table 3.1. Binding parameters for deoxy-Mb adducts.[21]

Ligand	k_{on} x 10^6 $M^{-1}s^{-1}$	k_{off} s^{-1}	K_{eq} M^{-1}
NO [a]	22	1.0 x 10^{-4}	2.20 x 10^{11}
CO [a]	0.51	1.90 x 10^{-2}	26.80
O_2 [a]	17	15	1.13
HNO [b]	0.35	8.90 x 10^{-5}	3.93 x 10^9

[a] for sperm whale Mb; [b] for equine Mb.

In this report, we will demonstrate the application of this methodology step by step, in a more complex spectral analysis of the competitive trapping of HNO by mixtures of deoxy- and met-Mb, i.e., in a direct comparison of HNO trapping between ferrous (Fe^{II}) and ferric (Fe^{III}) hemes.

Experimental

Materials

Lyophilized myoglobin was purchased from Sigma. Angeli's Salt ($Na_2N_2O_3$, AS) was purchased from Cayman Chemical Company. All other chemicals used were of reagent grade and purchased from Sigma. Phosphate buffers (50 mM, pH 7.0) were prepared using monobasic and dibasic sodium phosphate salts purchased from Fisher.

Preparation of Mb Samples

Samples of met-Mb were purified using a size exclusion filter as previously described.[22] Deoxy-Mb was prepared by the reduction with sodium dithionite, [13] and subsequent anaerobic purification on a Sephadex G25 column in a glovebox. All reaction mixtures were generated in an anaerobic glovebox which was maintained with O_2 levels below 5 ppm, and handled using strictly anaerobic procedures. Concentrations of Mb species were determined based on the protein band of Mb at 280 nm, with a molar absorptivity of 13,980 L $mol^{-1}cm^{-1}$.[23]

General Protocol for Reactions of HNO with Mb Samples

The protein samples were diluted in 2 mL of pH 7 phosphate buffer to give solutions in the micromolar range, and transferred into airtight septa capped UV-vis cells in the glovebox. A standard solution of AS was dissolved in pH 9.4 carbonate buffer at a concentration of 0.1 mM and maintained anaerobically in the glovebox. A four-fold excess of the AS standard solution at pH 9.4 was placed as a drop in the cap of a sealed UV-vis cell above the mixture of deoxy-Mb and met-Mb. This cell was then carefully moved from the glovebox to the spectrometer, the sample shaken to initiate the reaction, and the spectra collected on a Hewlett Packard 8453 Diode Array spectrophotometer in the range of 280 to 650 nm, on the time scale of 3600 secs at 27° C.

Kinetic Simulations and Data Fitting

Time course absorbance data files were transferred as comma delimited files to a modeling computer. The Jplus ReactLab Kinetics modeling program was used, which utilizes Excel and Matlab operating procedures. The number of Mb species, their concentration profiles, and fitted rate constant values for the modeled reaction sequence were determined as described below.

Results

Competitive Trapping of HNO by met-Mb and deoxy-Mb

The reaction of AS with a mixture of deoxy-Mb and met-Mb induced characteristic heme Soret and Q band absorbance, as shown in Figure 3.3. The initial spectrum shows two distinct Soret peaks corresponding to the two heme oxidation states, ferrous deoxy-Mb and ferric met-Mb. These spectra can be deconvoluted using authentic spectra to confirm the concentrations used; the total protein concentration is given by absorbance at the protein band at 280 nm. The final spectra shows one broad Soret peak at 422 nm, due to the mixture of NO-Mb and HNO-Mb products; this spectra can also be deconvoluted by similar methods. The mixtures seen in before and after spectra give evidence that the rate of HNO trapping by the two different heme oxidation states are of the same order of magnitude.

Free HNO cannot be stored in any practical way, therefore we utilize a commonly used precursor Angeli's salt, AS or sodium trioxodinitrate, which decomposes to release HNO within the range of pH 4 to 8, Equation 3.1.[10] Once released, HNO does not accumulate due its rapid dimerization producing N_2O between pH 2 to 11, Equation 3.2. The rate constants of these reactions are known, and will remain constant in the global fitting analysis. Previous reports for the rate constants of trapping of free HNO by deoxy-Mb and met-Mb are also available in the literature, Equations 3.3 and 3.4. In this work, these two constants as well as the secondary reaction, Equation 3.5, will be solved independently in competitive reactions.

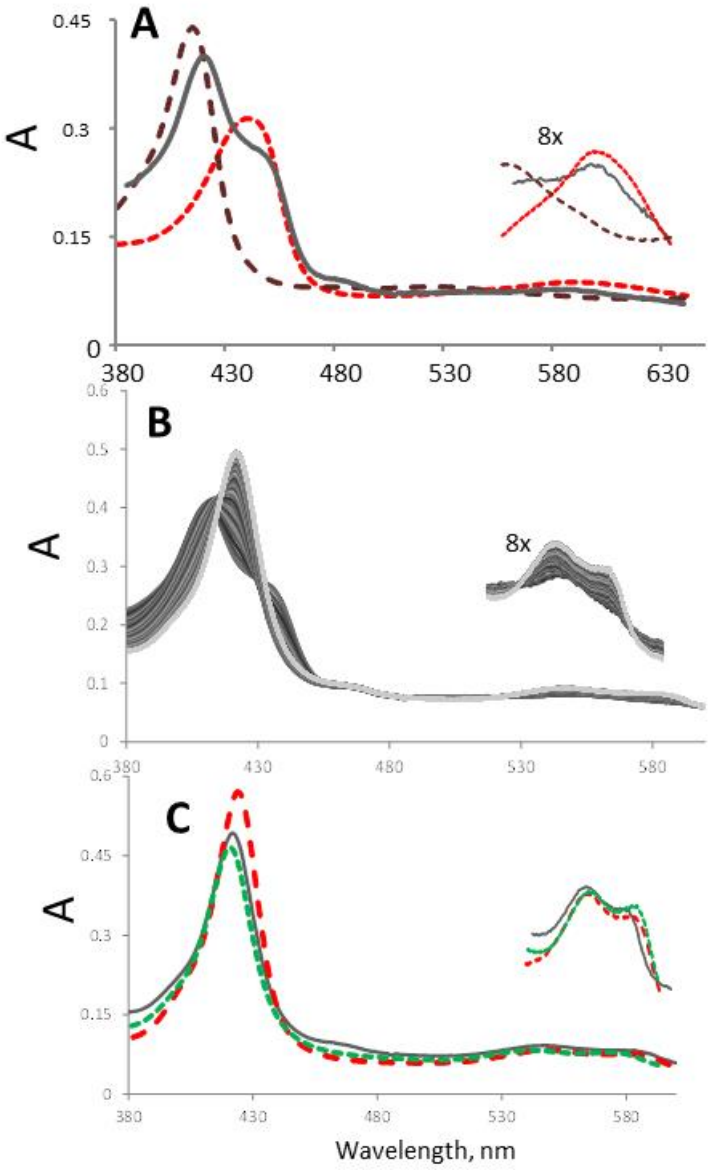

Figure 3.3. Reaction of met- and deoxy-Mb mixture (each at 8.4 μM) with AS (33 μM) in iP buffer, pH 7. A) Initial spectra of met- and deoxy-Mb mixture (solid line), overlaid with the deconvoluted spectra of met-Mb (long dash) and deoxy-Mb (dash); inset: Q band region expanded 8 fold. B) Time course spectral data of reaction over 3600 sec. C) Final spectra of reaction (solid line), overlaid with deconvoluted spectra of HNO-Mb (long dash) and NO-Mb (dash); inset: Q band region expanded 8 fold.

(3.1) AS → HNO $k = 6.75 \times 10^{-4}\ s^{-1}$ *pH 4 to 8*

(3.2) HNO + HNO → N_2O $k = 8.00 \times 10^{6}\ M^{-1}s^{-1}$

(3.3) HNO + deoxy-Mb → HNO-Mb $k = ?$

(3.4) HNO + Met-Mb → NO-Mb k = ?

(3.5) HNO + HNO-Mb → NO-Mb k = ?

Global Model Fitting

The global kinetic fitting method applies matrix algebra to actual time course data using the Beer Lambert law, using a matrix of sequential time course absorbance data by wavelength over time. This collection of spectra should then match the matrix equation, Y = CA, where the rows of the matrix Y are the measured spectra over time, the columns of C are the concentration profiles of the reacting species changing over time and the rows of A are the molar absorptivities of each species.[24] The matrix C representing the concentration profiles of all components over time, derives from the sequential reaction mechanism, which includes the rate constants and the initial concentration for all reacting species. The computation is explicit only for a relatively small number of simple reaction Scheme; for more complex reaction sequences the computations involve numerical integration.[25] Non-linear fitting is then applied to find the best set of rate constants for a proposed mechanism and the given data. Establishing the correct mechanism is more difficult, and requires the researcher to apply independent chemical knowledge of the system under investigation. There is no general algorithm for the determination of the correct mechanism, other than chemical plausibility.

The actual data used in the non-linear fitting only accounts for the colored species, i.e. in this case only the Mb derivatives in Equations 3.3, 3.4 and 3.5. All other species are considered colorless, which include AS, HNO and N_2O, in Equations 3.1 and 3.2. The first iterations of fitting utilized previously determined rate constants for the independent reactions of deoxy-Mb and met-Mb with HNO, Equations 3.3 and 3.4. The data was plotted in dimensions of time, absorbance, and wavelength to generate a working 3D matrix which was used for the decomposition analysis.

Factor analysis is a multivariate statistical method for extracting informational content from a data set. In this case we have a large matrix consisting of many sequential absorbance spectra as functions of both wavelength and time. SVD reduces these spectra to smaller matrices that contain all the information present in the data.[26] The kinetic information is contained in a kinetic eigenvector matrix.[24] Typically, only a small number of eigenvectors are needed to describe such data sets. The various rate processes are solved over a small number of eigenvectors and to which a kinetic model may be fit and the rate constants extracted. Similarly the spectral information is stored as a set of eigenvectors, which are derived from summations of the individual absorbances of species present.[24] Finally a vector of singular values is produced, which are listed from highest value (greatest likelihood) and fall off rapidly to zero. The initial analysis generates a table of possible eigenvalue solutions consistent with the time course absorbance changes. The number of high singular values is an indication of the number of colored species present and therefor useful for testing the chemical plausibility of various proposed reaction sequences.

In practice, the program generates a listing of eigenvector solutions ranked by their distance from zero, top of Figure 3.4, and a plot of variation from the initial spectrum attributable to this possible eigensolution. The most positive eigenvectors represent viable colored species present during the reaction, but chemical intuition must be used. In this reaction, the eigenvectors should represent four colored species: met-, deoxy-, NO- and HNO-Mb but only 3 are observed. The initial SVD deconvolution defined the final products as NO-Mb and HNO-Mb as shown below in the Figure 3.5. But examination of the dominant eigenvector spectra showed that it represents a mixture of both met- and deoxy-Mb absorbances as a single species; this was corrected in the kinetic model sequence used.

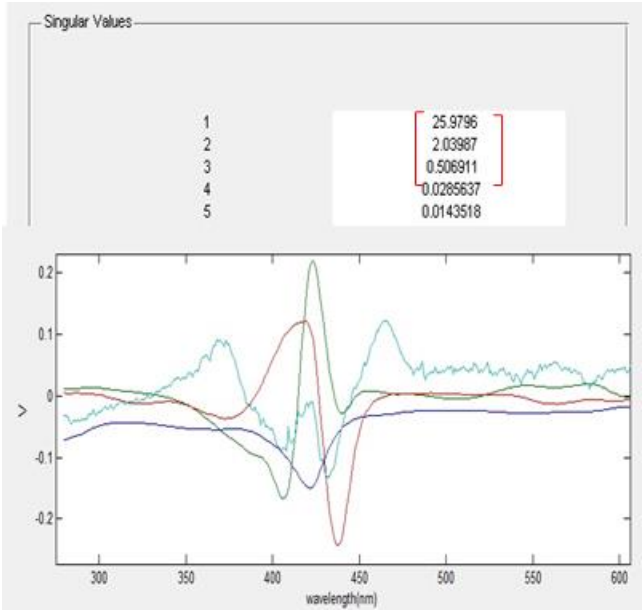

Figure 3.4. Screen shot from ReactLab program displaying at top, the table of possible SVD eigenvectors for absorbing species. At bottom are plots of spectral variations associated with the obtained individual SVD eigenvectors.

A preliminary modeled solution was obtained using only Equations 3.1-3.4, i.e., disregarding the secondary reaction of Equation 3.5. The spectral combination of met- and deoxy-Mb was corrected by listing them as separate species within the working kinetic model, and defining their absorptivities and concentrations. To be sure of initial concentrations, known spectra of both met- and deoxy-Mb were subtracted from the starting spectra to generate the difference spectra which matched with known spectra and absorptivities of the other component. The starting concentrations of both met- and deoxy-Mb were then introduced into the stepwise reaction model as well as the concentration of colorless AS used. All the products generated during the reaction, HNO, N_2O, NO-Mb and HNO-Mb were included, were included, thus giving a total of 7 species whose concentrations would be solved within the multistep reaction mechanism. In agreement with our chemical intuition, the determined concentration profiles tracked initial met-

and deoxy-Mb concentrations individually as two separate reactions occurring at distinctive rates and generating distinctive products.

Table 3.2. Reported bimolecular rate constants, k_{on}, for reactions of ferrous and ferric Mb with HNO.

Previous report	deoxy-Mb x 10^5 $M^{-1}s^{-1}$	met-Mb x 10^5 $M^{-1}s^{-1}$
Miranda 2003[a]		8.00
Sulc 2004[b]	0.140	
Zapata 2013[c]	3.71	2.73
This work	3.74	2.76

From references: [a] (4), from absorbance data at 37^0C; [b] (13), lower limit from NMR data at room temperature; [c] (21), from absorbance data at room temperature.

From this point on, the Marquardt-Levenberg algorithm (MLA) is used to minimize least squares curve fitting errors, a softer method that allows variation in rate constants. With this method, all the data sets analyzed reached convergence using 12 or less iterations. The determined rate constants for the trapping reactions were close to previous modeled values, Table 3.2 but did not include the secondary reaction, Equation 3.5. The generated spectra of the absorbing species were analyzed in tandem with speciation to determine the fit; in all cases they matched well with literature values for Soret wavelength and molar absorptivity.

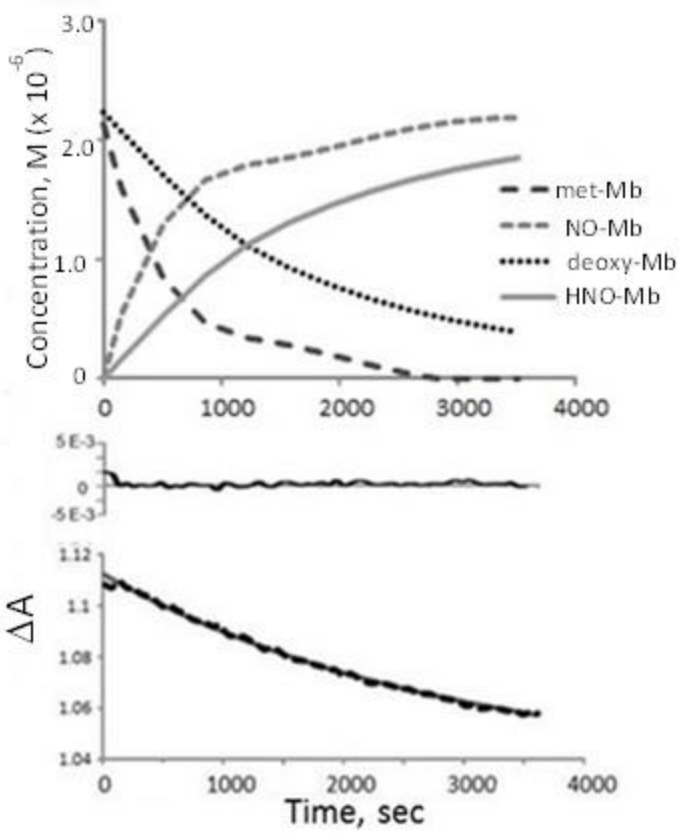

Figure 3.5. Initial data fitting without inclusion of Equation 3.5. Top) Concentration profile of the absorbing species as indicated. Bottom) Plots of model and real data absorbance at 434 nm, corresponding to the loss of deoxy-Mb loss; the residual plot is shown at top, on a finer scale.

The fitting error is determined using the matrices of the model generated spectra and concentration profile, as seen at top of Figure 3.5. First, the best fit spectra profile matrix is transposed onto a new spreadsheet along with the concentration profile matrix. Then the matrices are multiplied (e.g. using the Excel MMULT formula) to obtain the residual matrix, which contains model-generated UV-vis spectra of the entire reaction. The fit was evaluated by variance between expected and experimental total absorbances over time, σr, shown at bottom of Figure 3.5, which was on the order of 10^{-3} for all three independent reaction data sets. Even though the fitting converged with low variance, the resulting concentration profile curves show unusual deviations

around 1000 sec, at the point where the effects of the secondary reaction, Equation 3.5, would be apparent.

At the bottom of Figure 3.5, the residual matrix data at 434 nm, which corresponds to deoxy-Mb loss, is plotted against the real data. Here the model and data values at this wavelength were subtracted to get a residual plot resembling a time course spectra. In this work, hand mixing was used to initiate the reactions; therefore scattering noise is seen in the initial spectra of each reaction, as seen in Figure 3.5, but rapidly falls within expected error. In previous work, initial spectra were omitted from the analysis if the final residual deviation exceeds +/- 3 x 10^{-3} absorbance; a rule of thumb is omit less than 1% of time course spectra used in the analysis. But in this initial solution, no omissions were necessary to obtain sufficient overall residual parameters

The Secondary Reaction of HNO-Mb with HNO

Including the secondary reactivity of HNO-Mb with HNO, Equation 5, within the global fitting presented several difficulties. The rate constant for this reaction is an order of magnitude slower than the trapping reactions in Equations 3.3 and 3.4, and thus the data fit reasonably well in its absence, even though examination of the speciation curves shows that the secondary reactivity is evident. When Equation 3.5 was added to the global fitting model, the convergent solutions were obtained, but with fitting errors $\sigma r >> 0.001$. Alternative attempts were made using the previously determined rate constant for Equation 3.5 and solving for the constant for Equations 3.3 or 3.4, but also resulted in large fitting errors, as well as giving concentration profiles inconsistent with known product yields.

Because the rates of all the reactions were determined independently, they were all input into the fitting program and a predicted spectral matrix for the reaction course was calculated. The resulting data is shown in Figure 3.6, and does indeed fit the initial characteristics of the reaction

speciation, up to ca. 1500 sec, but deviates unrealistically afterward. The fitting error was allowable, at σr = 0.003, but the apparent regeneration of deoxy- and met-Mb seen at latter stages of the reaction is counter to chemical plausibility.

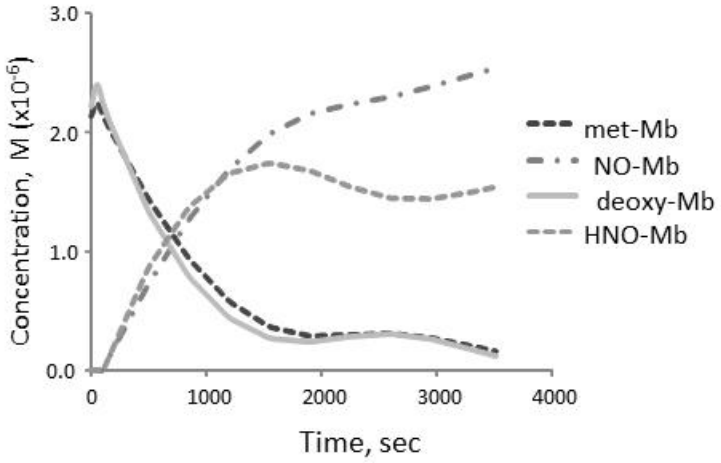

Figure 3.6. Concentration profile data calculated with inclusion of Equation 5, using reported rates of Equations 1-5.

The difficulty with the inclusion of Equation 3.5 may be attributed to the linear dependence of the generation and loss of HNO-Mb to colorless HNO, as well as the generation of NO-Mb from two different sources, Equations 3.4 & 3.5. To circumvent this difficulty, the absorbance tolerance within the algorithm was decreased two orders of magnitude, from 10^{-6} to 10^{-8}, stiffening the MLA variation during fitting of non-linear least squares. This resulted in a significantly better fit, shown in Figure 3.7, with results that are self-consistent with the chemical transformations , e.g., at the end of the reaction [NO-Mb] is 25% larger than the initial [met-Mb], the difference being NO-Mb generated by the secondary reactivity. The residual error modeled at 409 nm is shown to have a +/- 1.7 x 10^{-3} difference in deviation, much better than previous fittings. As a

final verification, the model-derived spectra for the individual species, also shown in Figure 3.7, matched the known shapes and molar absorptivities of the colored Mb species.

The final global fitting analysis also provides concentration profiles for the non-absorbing species: the nitroxyl donor AS, HNO, and N_2O over the course of the reaction, shown in Figure 3.8. As illustrated, ca. 20% of HNO generated by AS decomposition is lost in dimerization to N_2O. There is currently no definitive experimental method to measure the flux of HNO over time within a reaction mixture; but the global modeling solution shows a variance in HNO concentration of from 4 to 9 nM during the reaction. Note that at no time over the course of the reaction can the concentration of HNO be considered steady-state.

Discussion

In many reports on SVD modeling, a simple linear reaction model has been used, in synchronous order;[27] this is likely due to the limitations of commercial modeling packages as well as difficulties in handling concurrent reactivities. However, such a simplified approach is not viable for reactions involving HNO, which rely on the relatively slow generation of HNO from its precursor and its rapid loss to dimerization. These two reactions have rate constants separated by 11 orders of magnitude, and thus are impossible to model as sequential reactions.

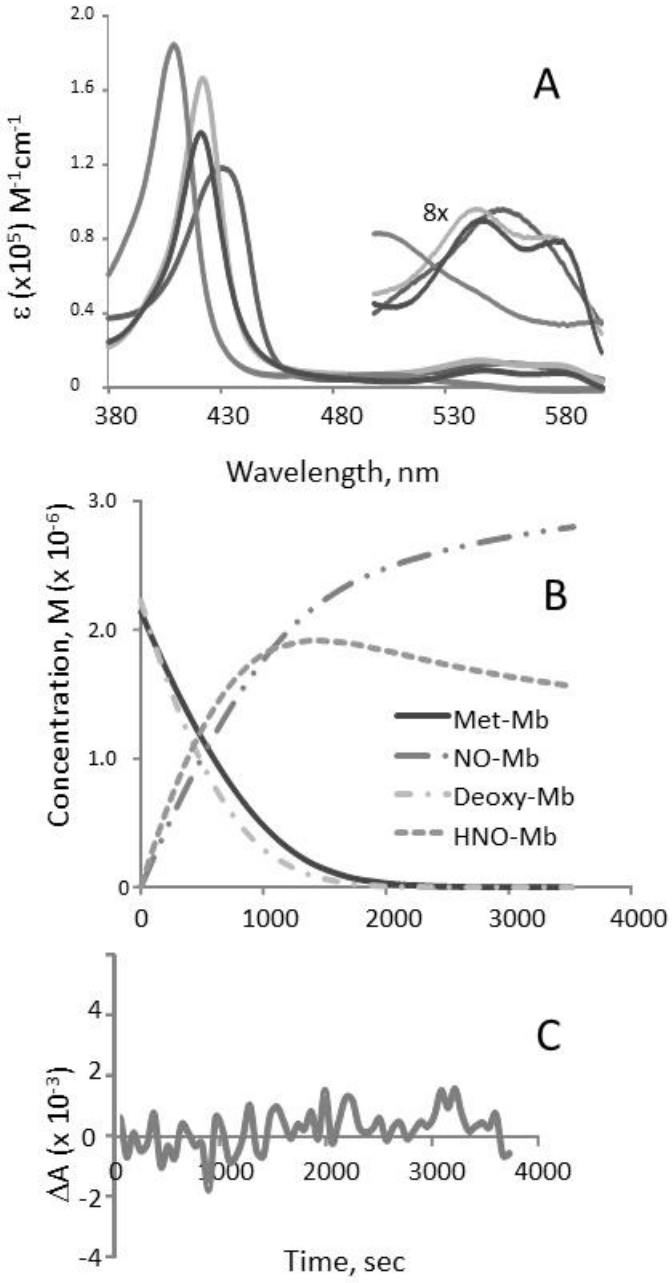

Figure 3.7. Final data fitting with inclusion of Equation 3.5. A) Plots of model-generated spectra of individual absorbing species (λ_{max}, absorptivity $M^{-1}cm^{-1}$): met-Mb (409 nm, 1.8 x 10^5), NO-Mb (421 nm, 1.4 x 10^5), deoxy-Mb (434 nm, 1.2 x 10^5), HNO-Mb (423 nm, 1.68 x 10^5); inset: Q band region expanded 8 fold. B) Concentration profiles of modeled species. C) A residual plot of model vs. data variance, showing a less than 2 x 10^{-3} deviation over the course of the reaction.

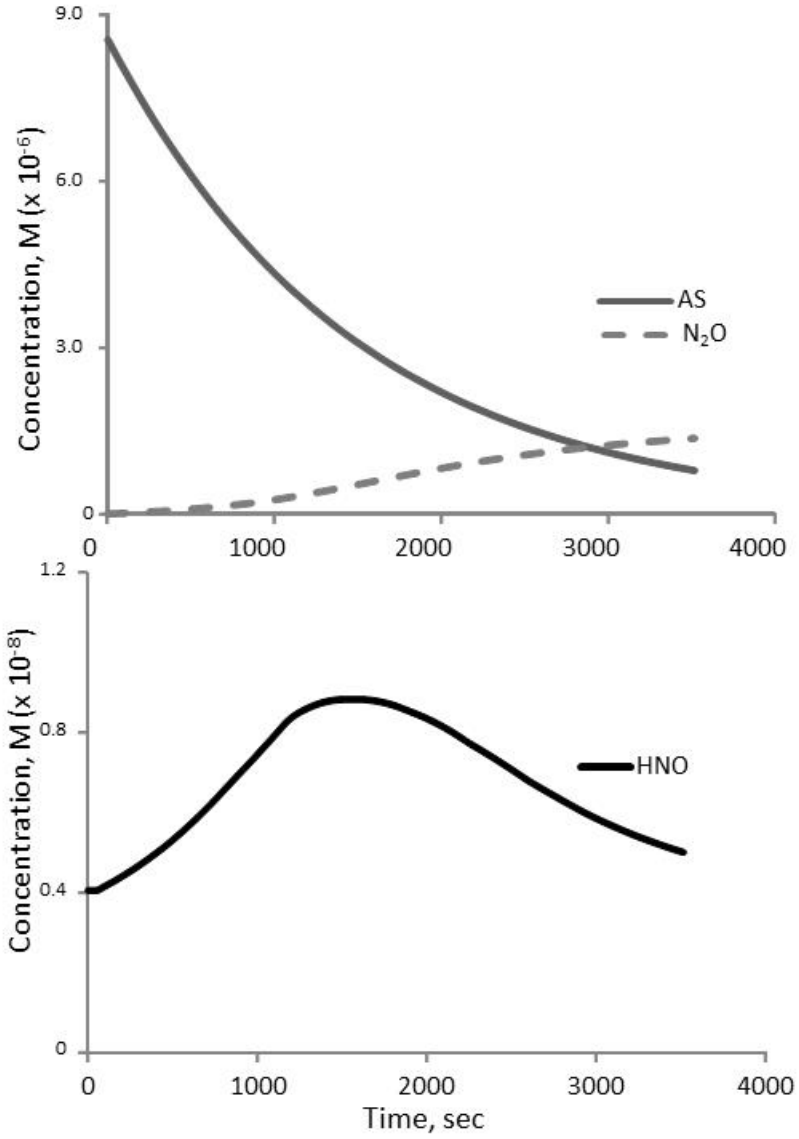

Figure 3.8. Plots of predicted concentration profiles for non-colored species. Top) Concentration variation of AS (initially 33 μM at 100%) and byproduct N_2O. Bottom) Predicted transient concentrations of free HNO during the reaction.

.....Because of this, HNO trapping must be solved holistically with all reactions assumed to be occurring simultaneously. Here we have demonstrated how the global fitting methods provide self-consistent analysis of complex concurrent reactions. The analysis is verified by generation of modeled spectra of the absorbing species which match well with known myoglobin spectra. At each step, the results must be evaluated by and consistent with chemical intuition.

Physiological important reactivity is inherently complex due to the number and variability of such concurrent reactivity. In one recent paper on the nitric oxide dioxygenase reactivity of globins, SVD analysis was used to disprove a leading mechanistic hypothesis suggesting the generation of a ferryl heme intermediate.[28] The authors used the Runge-Kutta integration (RKI) method, which utilizes an adaptive step size that allows spectra to be viewed in steps along its time course. The sequential spectra were analyzed by comparison with known spectra of the proposed ferryl intermediate, which was but one of several species that might be present at any stage of the reaction. The authors were thus able to discount such an intermediate due to the lack of its buildup, using known rate constants to model several proposed reaction paths. Thus chemical intuition must be used to assess the modeling results throughout the process.

The competitive physiological trapping of HNO by different heme proteins has obvious importance to the proposed pharmacological use of HNO-releasing compounds. Of the various heme proteins in our bodies, the native states of hemoglobin, deoxy and oxy-Hb, dominate; they compose some 95% of the physiological Fe content. By contrast, normal individuals have less than 1% of Hb in the ferric met-Hb state,[29] thus the reactions of HNO with ferrous hemes should be of interest. Some 25 years ago, Doyle described the reaction of oxy-Hb with HNO to generate met-Hb, but the mechanism remains obscure.[30] More recently, HNO has been shown to accelerate the oxidation of oxy-Hb by nitrite, both being produced by the commonly used precursor AS.[31] A recent controversial report found that HNO precursors activate sGC in its native ferrous state.[32] Our results suggest that the formation of HNO adducts and their secondary reactivity with HNO, which have been largely ignored, may play a role in assays determining the physiological effects of HNO donors.

Acknowledgements

We thank Mr. Peter King from JPlus Consulting for help and advice. This research was supported by the National Science Foundation (PJF CHE-1057942).

*CHAPTER FOUR

The Reaction of HNO-Mb with Dioxygen: a Model for the Nitric Oxide Dioxygenase Reactivity

Introduction

The utilization of dioxygen is the defining characteristic of aerobic life on earth. However, its side effect is oxidative stress, characterized by formation of reduced oxygen species (ROS) such as superoxide, peroxide and hydroxy radical, schematically illustrated in Equation 4.1. Oxidative stress is a common occurrence in all aerobic organisms, but is typically kept in check by enzymes and proteins that inhibit ROS, the most common being super oxide dismutase (SOD).[98–100] Dysfunction of these ROS neutralizers can cause life-threatening problems like neurodegenerative disease,[101] and can also affect systems such as cardiovascular integrity and macrophage response.[102]

Nitric oxide, NO, is another small gaseous molecule of widespread importance in human physiology and disease.[92–94] Generated enzymatically by the several isoforms of nitric oxide synthases, NO plays important roles in a wide variety of biologically processes including vascular tension, immune response, and long term memory.[92–94] Its production also results in analogous toxins termed nitrosative stress, typically initiated from the reaction of nitric oxide with superoxide to form peroxynitrite, Equation 4.2. Peroxynitrite is a reactive nitrogen species (RNS) implicated in diseases such as heart disease, diabetes, shock and inflammation.[103]

(4.1) O_2 (dioxygen) → HO_2 (superoxide) → H_2O_2 (peroxide) → $HO^{\cdot}$ (hydroxy radical)

(4.2) $NO + O_2^- \rightarrow ONOO^-$ (peroxynitrite) → NO_3^- (nitrate)

(4.3) $NO + O_2\text{-}Fe^{II}globin \rightarrow NO_3^- + Fe^{III}$ globin

Neither superoxide or NO are particularly toxic *in vivo* due to efficient means to minimize their accumulation.[36] Importantly, the ferrous O_2 adducts of the ferrous globins, hemoglobin (Hb) and myoglobin (Mb), have been shown to react with NO to form relatively harmless nitrate (NO_3^-) and oxidized ferric heme protein, Equation 4.3, termed the nitric oxide dioxygenase (NOD) reactivity.[37] Because NO diffuses rapidly through tissue and blood, the NOD reactivity catalyzed by oxy-globins represents the major mechanism of NO detoxification.[38]

The detailed mechanism of NOD reactivity has been somewhat controversial. The reaction was initially observed by Doyle in competitive trapping of NO and O_2 by deoxy-Hb, and by Skibsted in the aging of cured meat. [39, 41,42] In 1986, Olson proposed that the reaction proceeded through a ferric peroxynitrite adduct, followed by a rapid isomerization of the adduct to nitrate.[43] In the late 1990s, Gardner characterized true NOD flavohemoglobin enzymes in *E. Coli* which detoxify high levels of nitric oxide; he later proposed that mammalian myoglobin's true function is as an NOD, not an O_2 storage protein. [37, 104, 44–49] Subsequently, Herold identified an apparent intermediate in the NOD reaction at high pH, suggested to be a ferric peroxynitrite adduct, which was seen as a transient absorbance in the heme q-band region at 634 nm. [5]

Herold's observation inspired several attempts to characterize this species, in both heme proteins and non-physiological porphyrin model complexes.[51,52] A team led by Moennes-Loccoz used resonance Raman spectroscopy on samples generated using Herold's alkaline reaction conditions paired with rapid-freeze-quenching at millisecond timescales.[53] Analysis of the vibrational data obtained implied that the intermediate was of a transient ferric nitrate adduct, not peroxynitrite adduct. As ferric hemes have no affinity for nitrate, no authentic sample of such a ferric nitrate complex can be made to verify the characterization.

Groves investigated the direct reaction of ferric myoglobin with pre-formed peroxynitrite, which resulted in the formation of a transient ferryl heme, Fe^{IV}=O, and nitrogen dioxide gas, NO_2.[54] These geminate species may then recombine to form nitrate as the major product by a so-called rebound mechanism; alternatively, NO_2 escape results in nitrosation of nearby tyrosine residues. The formation of such a ferryl intermediate in the native NOD reaction was disputed in a subsequent report by Pacheco, who studied the native NOD reaction of oxy-Mb with NO using time resolved spectra with SVD and global kinetic modeling. Their analysis showed no evidence of a ferryl intermediate on the millisecond timescale under alkaline conditions.[56] Thus the chemical character of the alkaline intermediate and the reaction path followed in NOD reactivity remain contentious.

(4.4) $HNO + O_2 \rightarrow ONOOH$

(4.5) $HNO\text{-}Mb + O_2 \rightarrow ?$

An alternative path to peroxynitrite is by reaction of HNO, termed nitroxyl or nitrosyl hydride, with O_2, Equation 4.4.[9,76,82] In this work, the reaction of O_2 with the stable HNO adduct of myoglobin, HNO-Mb, is used to model NOD type reactivity, Equation 4.5. Nitroxyl or HNO, the single electron reduced form of NO, forms stable ferrous protein adducts at a rate and stability that is only second to that of nitrosyl.[18] We have shown that the HNO adduct of ferrous myoglobin, HNO-Mb, is stable and long-lived. NMR, resonance Raman and X-ray absorption spectroscopy have characterized this species. HNO-Mb is slow to react with CO, forming CO-Mb at rate of 8.9×10^{-5} s^{-1}, with a $t_{1/2} \sim 6$ hrs under 1 atm CO. The determined binding affinity of HNO to deoxyMb, at 3.9×10^{9} M^{-1}, is close to that of NO but orders of magnitude greater than those of O_2 or CO. In this work we investigate the reaction of HNO-Mb with O_2 with and

without the presence CO, which generates transient intermediates with absorbance bands similar to that seen by Herold in native NOD reactivity.

Experimental

Materials

Lyophilized myoglobin was purchased from Sigma-Aldrich. Purified sodium nitrite, sodium dithionite and sodium borohydride were purchased through Cayman Chemical. Carbon monoxide (CO) and dioxygen (O_2) gas were purchased from Matheson TriGas, NJ. All other chemicals used were of reagent grade. Phosphate buffers (50 mM, pH 7.0 and 9.4) were prepared using monobasic and dibasic sodium phosphate and carbonate buffers (50 mM pH 9.4) were prepared using sodium carbonate and sodium bicarbonate all from Fisher. Borate buffers were made using sodium borate (50 mM pH 10.4) All samples were prepared in a low water and oxygen atmosphere in a wet glove box, and handled using anaerobic procedures.

Preparation of HNO-Mb Samples

Authentic samples of HNO adduct of myoglobin, HNO-Mb were prepared as previously described and purified in a wet-box on a Sephadex G25 column.[63] The reaction mixtures were also generated in the wet-box which. The box O_2 levels were kept below 5 ppm; under wetbox conditions, the HNO-Mb samples demonstrated a lifetime on the order of weeks.

Reactions of HNO-Mb with O_2

In a typical experiment, the anaerobic HNO-Mb sample was transferred to an airtight quartz Starna UV-vis cell with 2 mL of pH 9.4 carbonate buffer or pH 10.4 borax buffer. Oxygen gas was bubbled into a separate airtight vial containing the same buffer until saturated, estimated as 1.2 mMol.[105] The concentration of HNO-Mb was determined using the protein band at 280 nm

which has a molar absorptivity at 13,980 $Lmol^{-1}cm^{-1}$. After the reagent concentrations were calculated, a stoichiometric amount of the oxygen-saturated buffer was added via syringe, the cell shaken to initiate the reaction, and spectra collected on a Hewlett Packard 8453 Diode Array spectrophotometer at room temperature, ca. 22°C.

Reaction of HNO-Mb with O_2 in the Presence of CO

In a typical experiment, the protein solutions were placed in airtight septa capped UV-vis cells prepared in the glovebox and concentrations were kept in the micromolar range. The protein was placed in 2 mL of pH 9.4 carbonate buffer. CO gas was then bubbled through the cell to create an excess CO atmosphere within the cell. After CO saturation the UV-vis cell was immediately placed in the spectrophotometer and reacted stoichiometrically with oxygen saturated pH 9.4 carbonate buffer. The analysis was run at 22 °C.

^{1}H NMR Experiments

HNO-Mb was concentrated to reflect a concentration of 1-5 mM. The solution was then reacted with a 1:0.25 (HNO-Mb:O_2) ratio and allowed to react for 10 minutes in the case of the CO absent reaction before data acquisition was started, in order to run the experiment in the presence of excess CO. The CO gas was bubble into a sealed NMR tube for 5 minutes, then the O_2 was added using a 1:0.25 (HNO-Mb:O_2) ratio to start the reaction. Data was acquired after 10 minutes and then later acquired at 30 minutes after reaction was mixed. The pH of the experiments were conducted at pH 7 as an iP buffer and at pH 9.4 as a carbonate buffer. ^{1}H NMR spectra were recorded on a Varian 500 MHz NMR equipped with an HCN probe that utilized the Bio NMR package, which uses pulse program excitation sculpting (dpfgse_water, Agilent) water suppression program. Data analysis was done using the Mestrenova NMR analysis program (Mestrelab Research S.L.).

Liquid Chromatography-High Resolution Mass Spectrometry (LC/HRMS)

Reaction solutions were analyzed on an Accela liquid chromatograph coupled to an LTQ Orbitrap Discovery mass spectrometer (Thermo Electron, Bremen, Germany) using positive electrospray ionization (+ESI/-ESI). The reaction samples were diluted 100 fold into mobile phase and then injected (10 μL) into the LC system consisting of a 15 cm x 2.1 mm (5 μm, 80 Å) Extended-C18 column (Agilent Technologies, Palo Alto, CA). A binary mobile phase gradient containing 0.1 % (v/v) formic acid in water (A) and acetonitrile (B) was applied as follows 99% A for 1 min, to 99% B in 7 min, held for 1 min, back to 99% A in 1 min, and equilibrated for 3 min at 99% A. The mass spectra data were processed using Xcalibur v.2.0.7 software.

Ion Chromatography (IC)

Analysis was carried out on a Dionex ICS-3000 series liquid chromatography system equipped with an EG eluent generator, DP gradient pump, AS autoinjector (10 μL sample loop), DC chromatography oven, and DC electrochemical detector. Chromatographic separation was carried out at 40 °C using a 50 mm x 4 mm IonPac AS11-HC guard column and 250 mm x mm IonPac AS11-HC analytical column connected in series and gradient elution (1-38.4 mM aqueous NaOH at 1.5 mL/min). A non-normalized external calibration curve was utilized to determine a final concentration of nitrate in each sample.

Resonance Raman Studies

HNO-Mb was concentrated to 1 to 5 mM. The solution was then reacted with a 1:0.25 (HNO-Mb:O_2) ratio and allowed to react for 30 seconds in the case of the CO absent reaction before freeze quenching. The ^{15}N-labeled samples were reacted in the same manner. In order to run the experiment in the presence of excess CO, CO gas was bubble into a sealed NMR tube for 5 minutes, then the O_2 was added using a 1:0.25 (HNO-Mb:O_2) ratio to start the reaction, and then

freeze-quenched the reaction after 30 seconds. The pH of the experiments were conducted at pH 9.4 as a carbonate buffer. The rR measurements were done at 77 K using 415 nm excitation line and laser power on the sample was 1.0 mW; slit 150 μm, total collection time for each spectrum was 90 min. In order to identify CO-Mb as the final product the samples were allowed to thaw and remain at room temperature for an additional 15 minutes. The samples were then freeze quenched after the layover to analyze at 77 K using 423 nm excitation line and laser power on the sample was 1.0 mW; slit 150 μm, total collection time for each spectrum was 90 min.

EPR Studies

The pH of all EPR experiments were conducted at pH 9.4, carbonate buffer. Natural abundance and ^{15}N-labeled HNO-Mb samples were concentrated to 1 to 5 mM, analogous to those used in NMR and rR studies, and placed anaerobically into quartz EPR tubes. The natural abundance sample was then reacted with oxygen at a 1:0.25 (HNO-Mb:O_2) ratio and allowed to react for 30 seconds before freeze quenching in an EPR tube. The ^{15}N-labeled sample was reacted in the same manner. In some experiments, CO gas was bubbled into a sealed EPR tube containing concentrated HNO-Mb solution for 5 minutes, then the O_2 was added using a 1:0.25 (HNO-Mb:O_2) ratio to start the reaction; the reaction mixture was freeze-quenched after 30 seconds. The frozen samples were then analyzed by EPR spectroscopy. EPR spectra were obtained using a EMX Plus Spectrometer (Billerica, MA) equipped with a EMX Plus spectrometer equipped with a EMX Plus and EMX micro standard resonator (Bruker model ER 4102ST). Low-temperature measurements were taken using an Oxford ESR900 cryostat and an Oxford ITC 503 temperature controller. A modulation frequency of 100 kHz was used for all EPR spectra. This instrument was purchased from NSF major research instrumentation grant funding.

Kinetic Simulations

The speciation rate constant parameters and modeled absorbance spectra were obtained by the use of kinetic modeling program JPlus ReactLab Kinetics, a global analysis kinetic modeling program that utilizes SVD analysis to determine the appropriate number of species present during the progression of a reaction. The number of absorbing species was directly assessed utilizing SVD. Previously reported rate constants were utilized as initial parameters for the global analysis simulation. All the data sets analyzed reached convergence using 12 or less iterations. The modeled spectra of the absorbing species were analyzed in tandem with speciation to determine the fit. The parameters were also analyzed by variance (σr) in the parameters between expected and experimental values, and only models that showed residuals on the order of 10^{-3} were considered. The equation sequence that is used in the model is a generic reaction Scheme that does not account for everything but can account for what is observed at a very basic level (Equations 4.4 and 4.5).

(4.6) HNO-Mb + O_2 → intermediate

(4.7) intermediate → oxyMb + NO_3^-

This Scheme allows for direct analysis using the Marquardt-Levenberg algorithm. The pH and O_2 were excluded from the modeling Scheme to reduce the amount of artifacts present because the reaction intermediates are not previously characterized.

Results

Oxygenation of HNO-Mb at pH 7

At pH 7, addition of oxygenated buffer in a 1:10 stoichiometric ratio to HNO-Mb causes rapid absorbance changes, Figure 1. The Soret band undergoes a hypochromic shift towards 418 nm, consistent with the loss of HNO-Mb and the production of O_2-Mb, followed by a slower

conversion to ferric metMb over an hour. Confirmation of the initial generation of O_2-Mb was obtained by ^{1}H NMR, as both the HNO-Mb and O_2-Mb are diamagnetic, with characteristic resonances below 0 ppm due to heme pocket valine methyl groups.[64] ESI-MS of the product solution shows no change to porphyrin or protein. Ion chromatographic analysis of the reaction solution showed nitrate as the major N-based product, Table 1, under all conditions tested (*vide supra*); no nitrite was observed under any condition.

Table 4.1. Nitrate analysis of reaction mixtures after reaction of HNO-Mb with O_2 in a 1:1 ratio.

[HNO-Mb] mM	pH, atmosphere	[NO_3^-] mM, %
3.0	pH 7.0, anaerobic	2.5, 83%
2.7	pH 7.0, excess CO	2.2, 81%
2.8	pH 9.4, anaerobic	2.3, 81%
2.8	pH 9.4 , excess CO	2.2, 78%

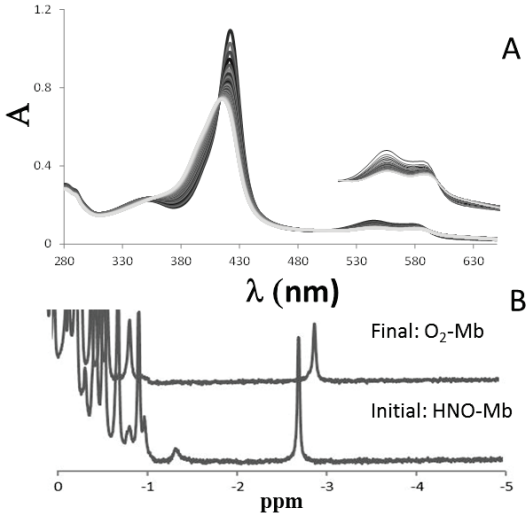

Figure 4.1. A) Reaction of HNO-Mb (6.9 uM) with O_2, in a 1:3 ratio at pH 7.0 for 500 secs. Time course of spectral data; inset, 8 x expanded q-band region. Final spectra represents a mixture of O_2-Mb and met-Mb. B) ^{1}H NMR (10% D_2O, 500 MHz, 256 scans); of HNO-Mb (1.1 mM) before and after reaction with O_2, in a 1:20 ratio at pH 7.0, showing Val68 methyl peaks for HNO-Mb at δ -2.7 (s, 3H) and oxy-Mb at σ -2.9 (s, 3H).

Oxygenation of HNO-Mb at High pH

At pH 9.4, after addition of oxygenated buffer to a sample of HNO-Mb, a transient intermediate absorbance is immediately observed in the q-band region at 611 nm, illustrated by Figure 2. A similar shift of the Soret band towards 418 nm is seen, the reaction goes to completion in ca. 400 secs. The formation of oxy-Mb as main product was also confirmed by NMR, Figure 4.3, and shown to be dependent on excess O_2. A side product is also observed with resonances at δ -1.65, -2.27, -3.54, and -4.01 ppm, and observed as sole diamagnetic product in 1:1 [HNO-Mb]:[O_2] reactions.

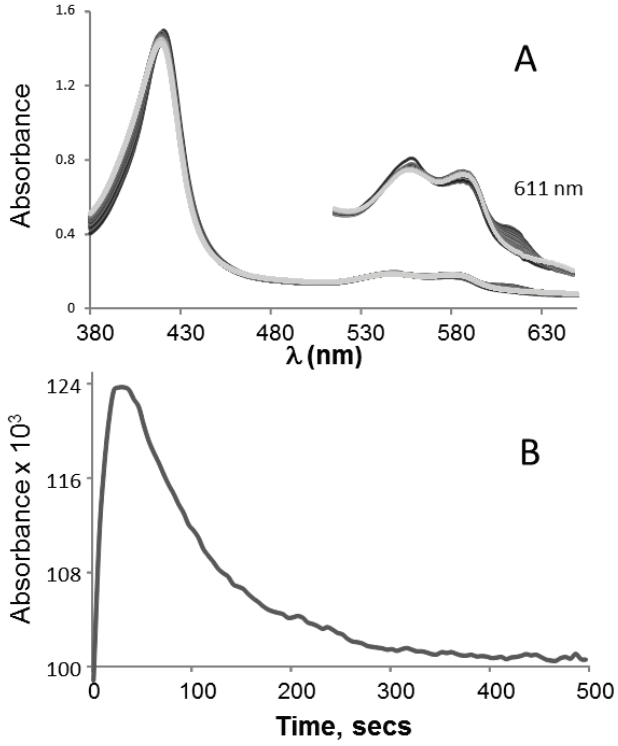

Figure 4.2. Reaction of HNO-Mb [8.3 uM] with O_2 in a 1:3 ratio at pH 9.4 for 500 secs. A) Time course of spectral data, highlighting the intermediate absorbance at 611 nm; inset shows 8x expanded q-band region. B) Kinetic trace of the 611 nm absorbance.

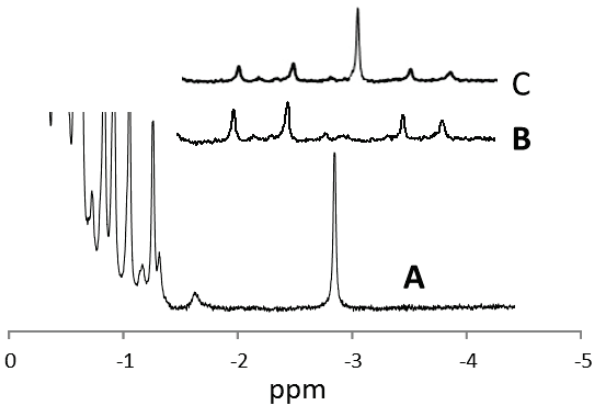

Figure 4.3. ^{1}H NMR spectra (10% D_2O, 500 MHz, 256 scans) in Val68 region of reactions of HNO-Mb [0.9 mM] with O_2 at pH 9.4: A) before reaction. B) Reaction product mixture for 1:1 [HNO-Mb]:[O_2] ratio reaction after 30 minutes. C) Reaction product mixture for 1:10 ratio after 30 minutes*H*

The rates of formation and loss of the 611 nm intermediate are unaffected by buffer (tris, borate, carbonate), but highly dependent on the pH, Figure 4.4. As previously shown, the 611 nm is not seen at pH 7; at pH 10.4 its decay is dramatically slowed. At this pH, metMb undergoes an alkaline denaturation.[106] While no protein degradation was observed by MS at the higher pH, denaturation cannot be ruled out. The dependence on [O_2] was also investigated. As seen in Figure 4.4, both the formation and decomposition of intermediate are dependent on O_2. These results suggest the stepwise formation and decomposition of the intermediate, Equations 8 and 9.

(4.8) $\text{HNO-Mb} + O_2 + H^+ \rightarrow X$

(4.9) $X + H^+ + O_2 \rightarrow O_2\text{-Mb} + HNO_3$

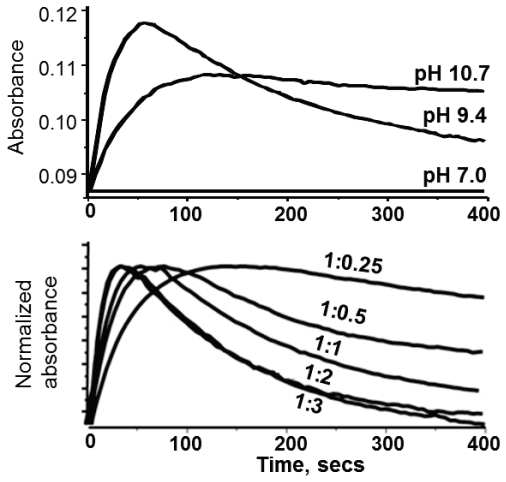

Figure 4.4. Kinetic absorbance traces of the 611 nm intermediate in reactions of HNO-Mb with O_2 in 50 mM iP buffers. A) Varying pH of 1:1 ratio of [HNO-Mb]:[O_2] reactions. B) Varying [HNO-Mb]:[O_2] ratios as indicated at pH 9.4.

Reaction of HNO-Mb with O_2 in a CO Environment

As there appeared no change in heme oxidation state in the overall oxygenation, i.e. Eq. 8 and 9, analogous reactions were run under excess CO atmosphere in the hope of trapping a ferrous heme intermediate. At neutral pH the reaction proceeds rapidly, with conversion of HNO-Mb to CO-Mb upon exposure to O_2.

At high pH, the presence of CO slows the reaction progression substantially and a new intermediate absorbance in the q-band region at 600 nm is observed, Figure 4.5. Examination of sequential absorbance spectra indicate that this new 600 nm species, formed rapidly upon addition of O_2, decays into the 611 nm species over 100 sec, which then decays at approximately the same rate as in the absence of CO, Figure 4.6. Likewise, the Soret absorbance rapidly shifts to 416 nm, then to 423 nm, with continued growth over hours, Figure 4.5

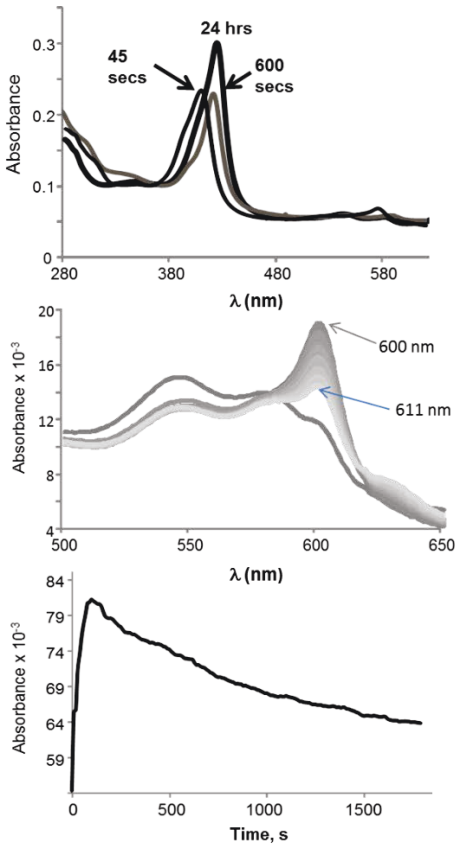

Figure 4.5. Reaction of a 1:1 ratio of HNO-Mb (6.8 uM) with O_2 under excess CO at pH 9.4. Top) selected spectra showing Soret maxima shift from 416 nm after 45 secs to 423 nm after 600 secs, and continuing to grow at 423 nm after 24 hrs. Middle) overlay of spectra in q-band region showing two characteristic peaks at 600 and 611 nm. Bottom) Kinetics trace of absorbance at 600 nm.

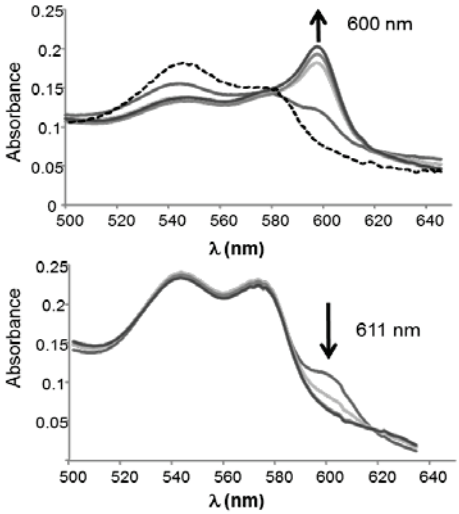

Figure 4.6. Distinct phases of reaction of a 1:1 ratio of HNO-Mb (6.8 uM) with O_2 under excess CO at pH 9.4. A.) Initial growth of 600 nm intermediate over first 20 secs. B.) Final loss of the 611 nm intermediate between 100 - 300 secs.

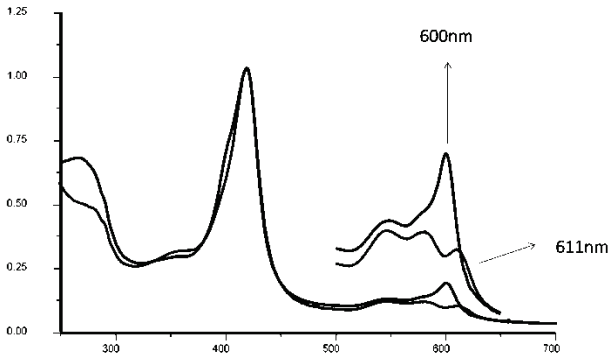

Figure 4.7. Comparison of the 611 and 600 nm with enlarged q-band region.

Kinetic traces for formation and loss of absorbance at 600 nm are shown in Figure 4.8. Interpretation of these are complicated by the apparent conversion to the absorbance at 611 nm, but some the formation is dependent on pH and [O_2]; but the conversion to the 611 nm absorbance is relatively independent of both. In certain runs, metMb contamination of the starting sample was observed, seen as a shoulder on the Soret band and ca. 630 nm in the q-band region, but spectral analysis showed that its concentration did not change during the course of the reaction.

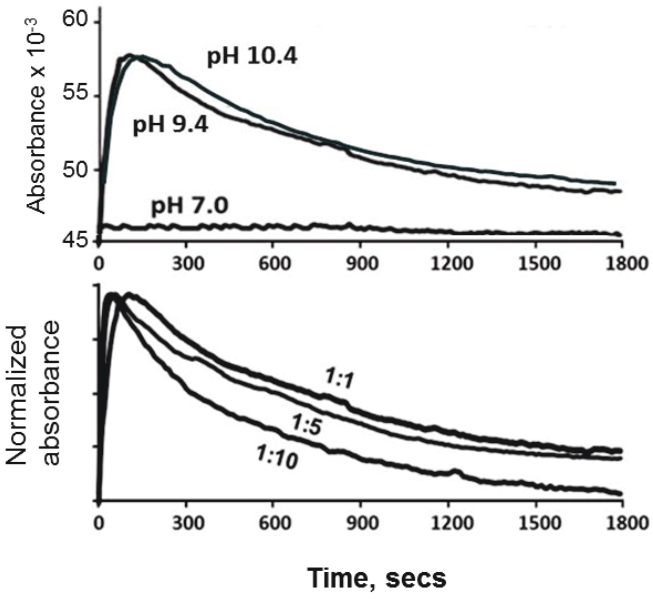

Figure 4.8. Kinetic traces of 600 nm intermediate at 1800 secs showing pH and [O_2] dependence of reaction of HNO-Mb (6.8 uM) with O_2 under CO atm. A) At 1:1 [HNO-Mb]:[O_2] ratio in 50 mM buffer at pH 7.0, 9.4 and 10.4. B.) At [O_2] from 1:1 to 1:10.

Under these conditions, ^{1}H NMR of the reaction solution confirms the production of CO-Mb as well as a substantial amount of the identical byproduct previously identified, as well as other unidentified peaks, Figure 4.9. All byproduct peaks are lost upon addition of excess dithionite under CO, suggesting these species are ferric hemes. Subsequent exposure of the reduced samples to air over a day, under which condition CO-Mb is stable, regained small amounts of byproduct, Figure 4.10.

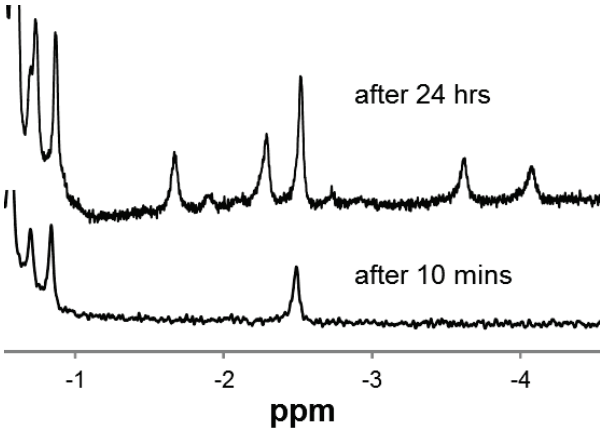

Figure 4.9. ^{1}H NMR of the reaction of HNO-Mb (1.4 mM) at pH 9.4 with 1:1 O_2 under CO. Bottom) spectra after 10 mins reaction. Top) same solution after 24 hrs under CO.

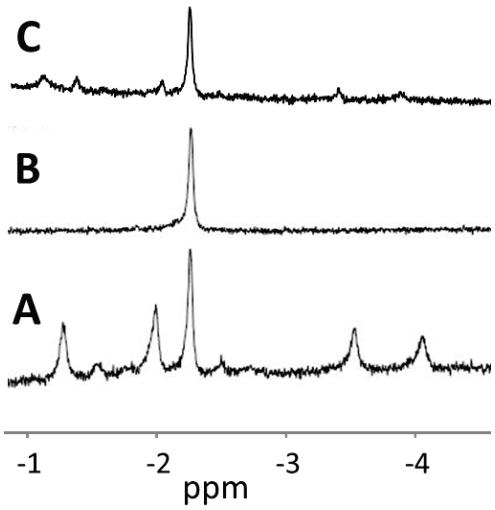

Figure 4.10. Normalized ^{1}H NMR spectra (10% D_2O, 500 MHz, 256 scans) in Val68 region of the reaction of HNO-Mb (1.4 mM) with 1:1 O_2 under CO. A) The product mixture 30 mins after reaction initialized; B) Same after addition of excess dithionite under CO purge. C) Same solution after 24 hrs exposure to air.

Kinetic Simulation

For the reaction of HNO-Mb with O_2 in the absence of CO, a reaction Scheme was generated that accounts for observed data, Scheme 4.2. As seen in Scheme 4.1, both the formation and decomposition of the 611 nm intermediate are dependent on O_2.

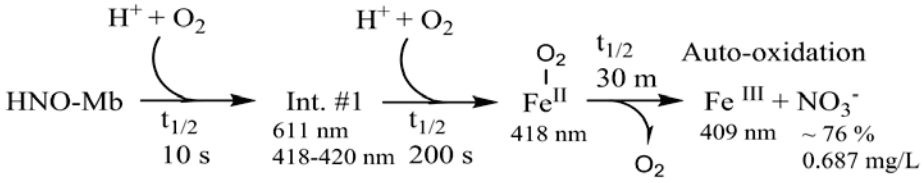

pH and [O_2] dependence on both formation and loss of intermediate

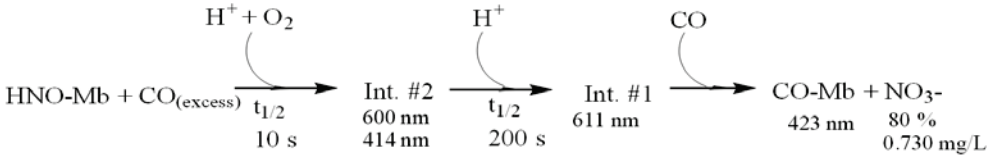

pH and [O_2] dependence on formation of first intermediate, only pH on second

Scheme 4.1 Top) Reaction Scheme of proposed mechanism for addition of oxygen to HNO-Mb. Bottom) same reaction carried out in CO environment.

This Scheme allowed for direct analysis of the time course absorbance spectra using the Marquardt-Levenberg algorithm. In fitting the data, the pH dependence was excluded from the modeling Scheme to reduce the complexity. The modeling results for the 1:5 [HNO-Mb]:[O_2] reactions at pH 9.4 are shown, but similar results were obtained for other ratios. Our goal in this modeling was to identify the speciation of different species over the course of reaction and to obtain a modeled spectra of the intermediate species seen.

Both of these results are shown in Figure 4.11. As seen in the speciation plot, the consumption of HNO-Mb is tied to the generation of the intermediate, which rapidly converts to oxy-Mb under excess O_2. The bimolecular rate constants determined under these conditions are

$k1 = 0.998 \pm 0.15 \times 10^3$ and $k_2 = 6.44 \pm 0.23 \times 10^{-3}\ M^{-1}sec^{-1}$. The fit of the modeled reaction was tested against the kinetic trace of the 611 nm intermediate.

Of interest is the modeled spectra of the intermediate, with a molar extinction coefficient at 611 nm of $8.7 \times 10^5\ M^{-1}cm^{-1}$. The position and intensity of these intermediate absorbances resemble those of altered hemes, such as chlorins or porphyrin cation radicals, in which the symmetry of the porphyrin has been altered, as described by Gouterman's theoretical analysis of porphyrin absorbances.[107] Specifically, the dramatically increased absorbance in the Q-band region resembles that of an $^2A_{1u}$ cation radical, with localized radical density on a pyrole ring.[108] This suggests the reaction initiates via electron transfer, and that the intermediate species contain a porphyrin radical cation. As well characterized in flash quench studies, oxidations at the heme porphyrin are kinetically much faster than at the Fe center.[109–113]

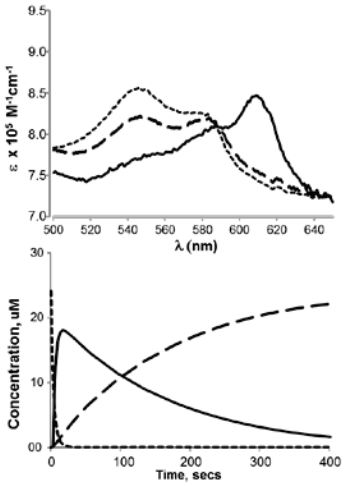

Figure 4.11. Modeled reaction of HNO-Mb with O_2 in a 1:3 ratio at pH 9.4 for 400 secs. Top: Modeled q-band region showing the starting material (small dash line), modeled intermediate at 611 nm (solid line) and the final product of O_2-Mb (long dash line). Bottom: Concentration profile of the modeled reaction, after 5 sec delay, using same line designations.

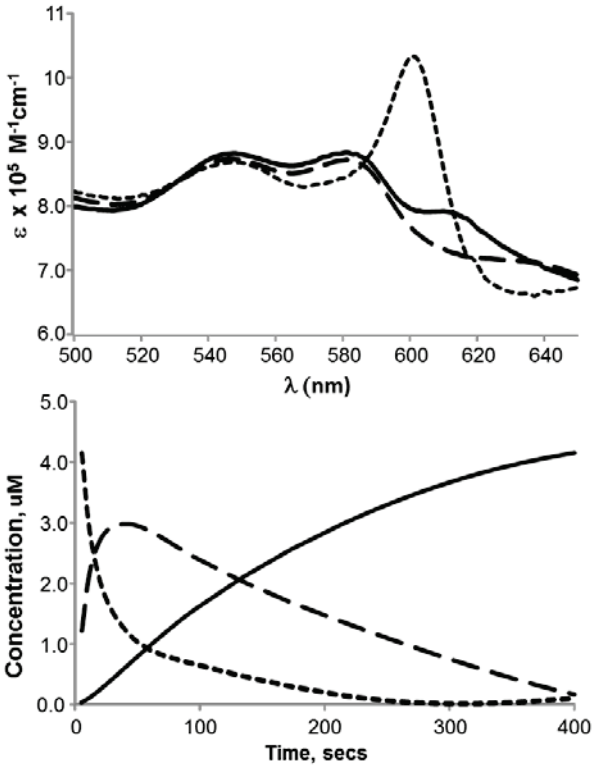

Figure 4.12. Modeled reaction of HNO-Mb with a 1:5 ratio O_2 under excess CO at pH 9.4 for 400 secs. Top: Modeled q-band region showing 600 nm intermediate (small dash line), intermediate at 611 nm (solid line) and the final product of CO-Mb (long dash line). Bottom: Concentration profile of the modeled reaction 600 nm intermediate (small dash line), final product of CO-Mb (solid line) and the intermediate at 611 nm (long dash line)

Modeling time course absorbance studies of reactions under CO atmosphere were difficult as they are much more complex, Figure 4.12. Under CO, only the formation of the 600 nm intermediate showed definitive dependence on pH and [O_2], the loss of the absorbance at 600 nm showed diminished dependence, but it is difficult to deconvolute from the generation and loss of the 611 nm intermediate. The best-fit model used a sequential reaction Scheme, HNO-Mb forming the 600 nm intermediate, which then forms the 611 nm intermediate. As shown in Equations 4.10 - 4.12 below. The formation of the 600 nm intermediate was too rapid to solve using the SVD decomposition method;. therefore the modeling was done assuming that the intermediate was fully

formed at its maximum absorbance, seen after 20 seconds. Results of global anlysis modeling can be observed in Table 4.2.

$HNO\text{-}Mb + O_2 + H^+ + CO \rightarrow$ 600 nm intermediate not modeled (4.10)

600 nm intermediate $\rightarrow$ 611 nm intermediate (4.11)

611 nm intermediate $+ H^+ + CO \rightarrow CO\text{-}Mb + HNO_3$ (4.12)

Table 4.2. Rates of elementary reaction steps as determined by kinetic modeling.

Ratio HNOMb : O_2 : CO	600 nm Int. k_d , x 10^4 $M^{-1}sec^{-1}$	611 nm Int. k_f , x 10^3 $M^{-1}sec^{-1}$	611 nm Int. k_d, x 10^{-3} $M^{-1}sec^{-1}$	σr x 10^{-3}
1:3		0.998 ($^+$/- 0.15)	6.44 ($^+$/- 0.23)	6 ($^+$/- 0.30)
1 : 5 : excess	2.11 ($^+$/- 0.40)	1.25 ($^+$/- 0.37)	5.68 ($^+$/- 0.62)	5 ($^+$/- 0.11)

Assessment of Heme Modification by Mass Spectrometry

LCMS analysis of the final Mb-based products were carried out to assess possible heme modifications. Analysis of reaction mixtures at pH 7 or 9.4, with or without CO are all-similar, with the major heme product as unmodified ferric heme with a ~100% peak at 616 m/z, Figure 4.13. Small peaks were observed in all reactions at high pH values that correspond to the addition of an O atom (632 m/z) and/or H_2O (634 m/z); these peaks have distinct Single Ion Chromatographs indicating they are individual species in the reaction mixture, Figure 4.14. Similarly, comparison of spectra from reactions of $^{14/15}$N-labelled HNO-Mb identified a peak at 663 m/z corresponding to the addition of NO to the heme, Figure 4.15. But the relative mass spectral intensities of 632, 634 & 663 species with respect to 616 is very small, at 0.88, 0.53 and 0.25 % respectively.

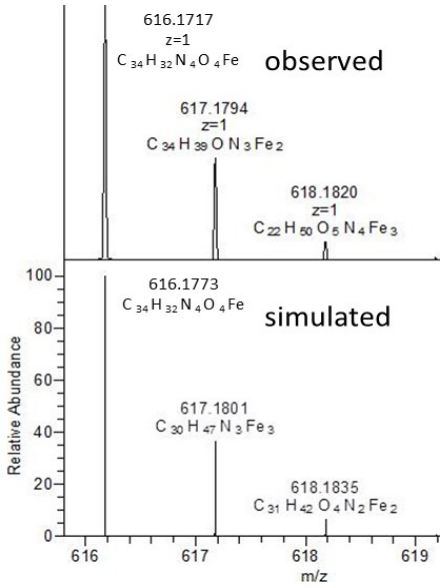

Figure 4.13. Mass spectra of unmodified heme derived from oxygenation reactions at pH 9.4. Real data on top, isotopic model on the bottom.

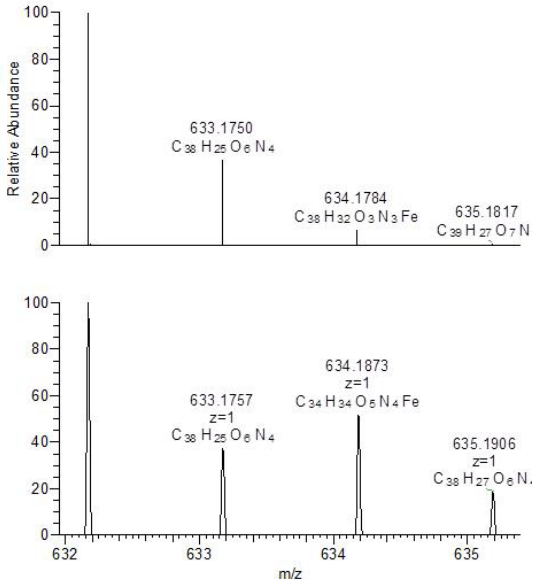

Figure 4.14. Heme product corresponding to the addition of oxygen or water to the heme, observed by LCMS for all reactions. Real data on the bottom, isotopic model on top.

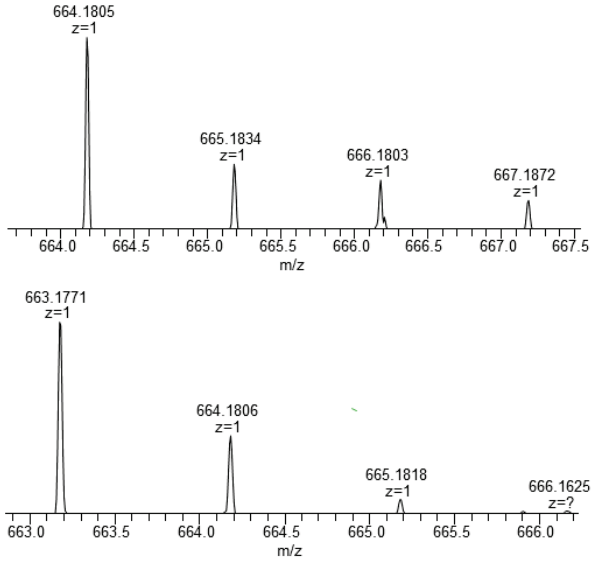

Figure 4.15. LC/HRMS of N isotope sensitive species, at 663 in natural abundance HNO-Mb (bottom) and 664 in ^{15}N-labelled HNO-Mb reactions (top).

Additional large scale reactions were run to identify possible heme-based sideproducts. Acid cleavage of the heme group was carried out by using 0.1 M HCl to lower the pH to 2. Then ice cold dichloromethane was added to the acidic solution in a seperatory funnel to remove the organic heme group. After the heme was removed, a concentrated solution of the heme was analyzed using MS and was shown to contain no modified heme group.

Characterizations of Initial Intermediates

A series of characterizations were used to better understand the intermediates formed at the beginning and end of reactions of HNO-Mb and O_2. As the reaction is substantially slower under CO, time course ^{1}H NMR spectra were obtained and shown in Figure 4.16. Under the conditions used, the loss of HNO-Mb Val68 peak is clearly completed well before the growth of that corresponding resonance of CO-Mb. Thus the initial 600 and 611 nm intermediates are not observed by NMR in this region (and likely not diamagnetic).

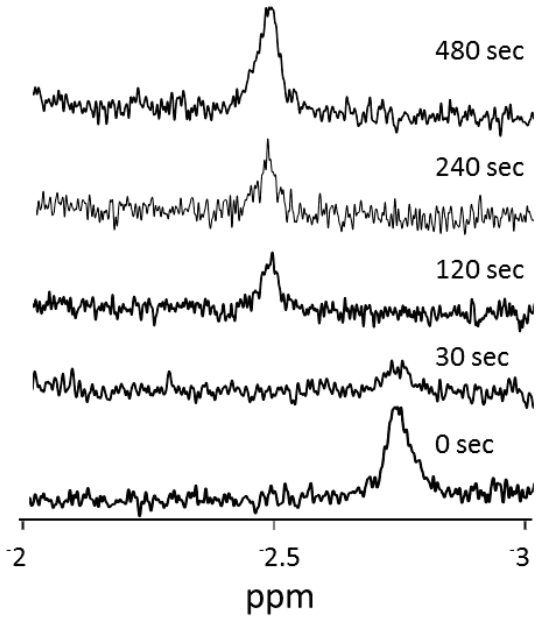

Figure 4.13. Time course ^{1}H NMR of the reaction of 1:1 reaction of HNO-Mb (1.2 mM) with O_2 under CO atmosphere.

Additional resonance Raman experiments were performed in collaboration with the Kincaid lab at Marquette University. For these experiments, reactions were freeze quenched 30 seconds after the introduction of sub-stoichiometric O_2, with and without CO head gas and ^{15}N-labeling of the nitrosyl hydride. The low frequency rR spectra, shown in Figure 4.17, covers the region associated with Fe-N bond stretches, e.g. the spectrum of Mb-H^{14}NO exhibits a band at 648 cm^{-1} that shifts to 635 cm^{-1} upon H^{15}NO substitution, assigned to the ν(Fe-N) stretching frequency of the Fe^{II}-HNO adduct.

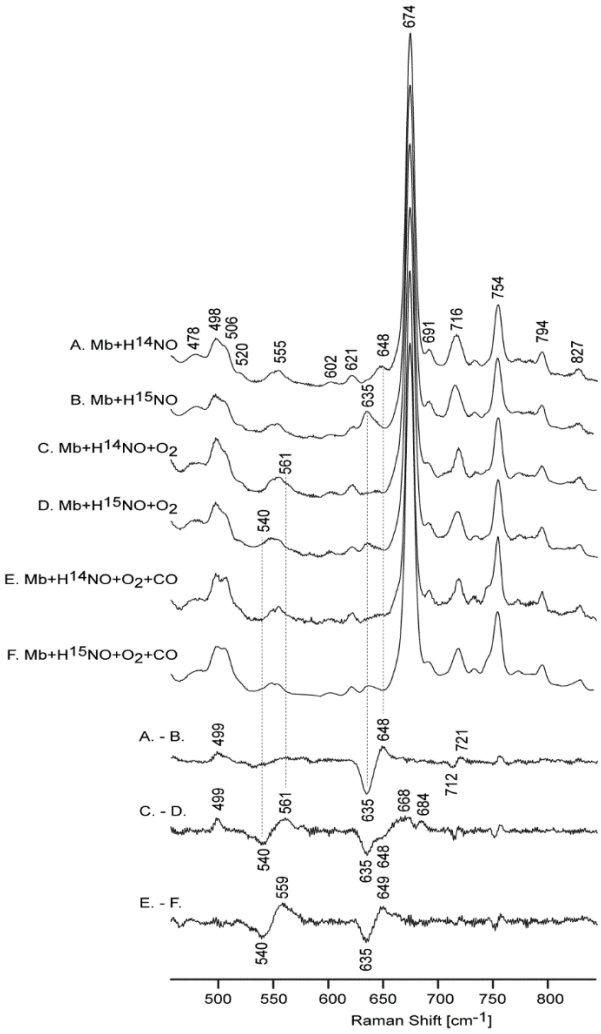

Figure 4.17 The low frequency rR spectra of Mb-$H^{14}NO$ (A), Mb-$H^{15}NO$ (B), Mb-$H^{14}NO$ +O_2 (C), Mb-$H^{15}NO$ +O_2 (D), Mb-$H^{14}NO$ +O_2+CO (E) and Mb-$H^{15}NO$ +O_2+CO (F) and their difference traces. Spectra are normalized to the ν_7 mode at 674 cm^{-1}.

Upon reaction with O_2, a new mode is seen in the spectrum of Mb-$H^{14}NO$ sample at 561 cm^{-1}, that shifts to 540 cm^{-1} in the Mb-$H^{15}NO$ sample. This mode is most reasonably assigned to a ν(Fe-N) of a ferrous NO adduct, though significantly shifted from the stable NO-Mb at 558 cm^{-1}. Additionally, this mode undergoes a smaller isotopic shift (21 cm^{-1} vs 26 cm^{-1}) than NO-Mb, which may indicate a different geometry of Fe-N-O fragment. Very similar changes are seen in samples under CO (spectra E and F, Figure 4.17). Additionally, new features are seen at 668 cm^{-1} that shifts to

635 cm^{-1} (33 cm^{-1}) and at 684 cm^{-1} that shifts to 648 cm^{-1} (36 cm^{-1}) upon ^{15}N substitution, the origin of which have to be yet established. Further investigations are needed using $^{18}O_2$ to better characterize possible peroxynitrite species. Another consideration is to use ^{13}CO gas to understand the role that CO plays in the formation of these transient intermediates.

Table 4.3. Literature values of stretching and bending modes of NO, O_2 and CO adducts of myoglobin. In parenthesis are values of ^{14}N-^{15}N isotopic shifts.[114,115]

	δ(Fe-X-Y)	**ν(Fe-X)**	**ν(X-Y)**
Fe^{II}-NO	454 (12)	558 (26)	1613 (27)
Fe^{III}-NO	573	595	1922 (38)
Fe^{II}-HNO		647 (19)	
Fe^{II}-O_2		572	
Fe^{II}-CO		509	1941

Importantly, the high frequency data of all samples exhibit ν_4 mode at 1377 cm^{-1} and ν_3 mode at 1505 cm^{-1}, indicative of low-spin ferrous heme, Figure 4.18. No modes associated with the ν(CO) stretching modes were found in freeze quenched samples from reactions under CO. After initial analysis, the samples were allowed to thaw and react for an additional 15 minutes in a CO atmosphere; spectra of the resulting species match closely to that for ferrous CO-Mb, suggesting it to be the only heme species resulting from the reaction, Figure 4.19.

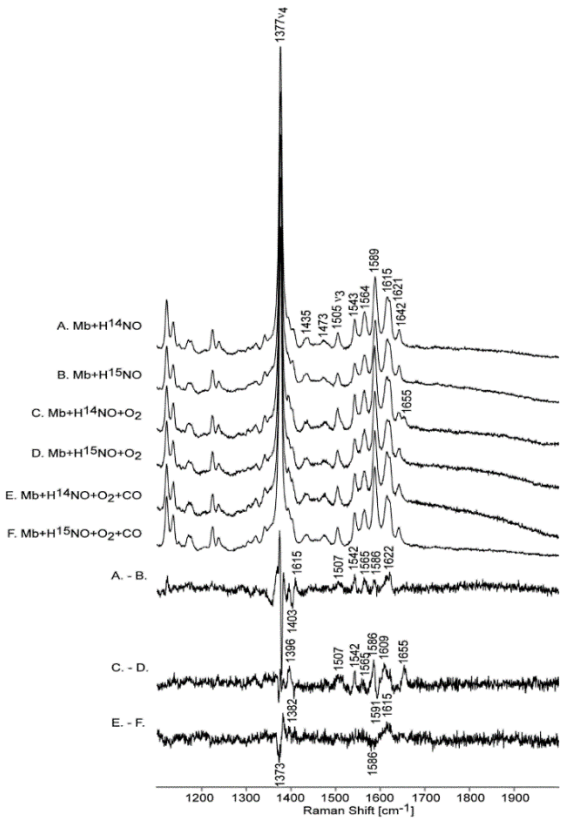

Figure 4.18. The high frequency rR spectra of Mb-H^{14}NO (A), Mb-H^{15}NO (B), Mb-H^{14}NO +O_2 (C), Mb-H^{15}NO +O_2 (D), Mb-H^{14}NO +O_2+CO (E) and Mb-H^{15}NO +O_2+CO (F) and their difference traces. Spectra are normalized to the ν_4 mode at 1377 cm^{-1}.

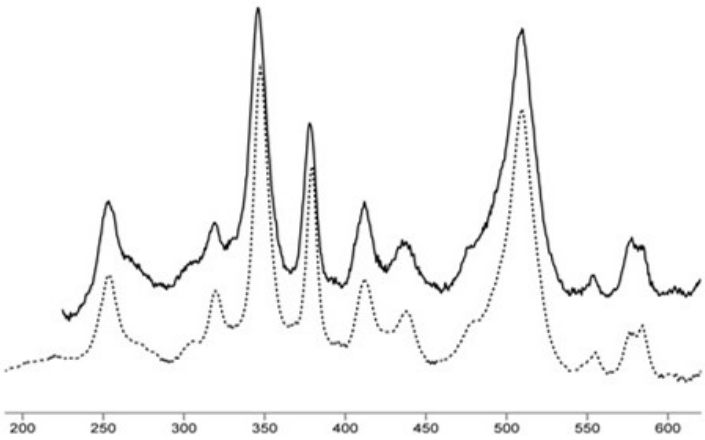

Figure 4.19. Top) The low frequency rR spectra of Mb-H^{14}NO with excess CO after 15 min and their referenced traces. Spectra are normalized to the ν_4 mode at 1377 cm^{-1}. Bottom) The high frequency rR spectra of Mb-H^{14}NO with excess CO after 15 mins and their referenced traces. Spectra are normalized to the ν_4 mode at 1377 cm^{-1}.

For EPR experiments, samples were prepared analogous to those for rR; i.e., reactions were freeze quenched 30 seconds after the introduction of sub-stoichiometric O_2, with and without CO head gas and ^{15}N-labeling of the nitrosyl hydride. In these experiments, a small contamination of NO-Mb is seen in certain HNO-Mb batches,[64] but is unchanged during the oxygenation reactions, as determined by EPR; no ferric Mb signals were observed.

Discussion

The reaction of HNO-Mb with O_2 produces nitrate and O_2-Mb, or CO-Mb if run under a CO atmosphere. At basic pH intermediates are seen, whose formation and loss are dependent on pH and [O_2]; at pH 9.4 the reaction is slow enough to be modeled by global kinetic analysis using electronic absorbance spectra. Time course NMR experiments show conversion from HNO-Mb to O_2-Mb, or to CO-Mb under CO, but no indentifiable species apparent during the life span of the intermediates, implying that these species are not NMR active (e.g. paramagnetic). The rR analysis conclusively showed that no CO adduct was formed during the lifespan of the intermediates. What was observed was a ferrous NO stretch is observed, somewhat different than that of standard NO-Mb. Ultimately, the final products are similar to what is observed by previously studied NOD reactions, only differing in the final oxidation state of the heme iron, and its related adducts. At this time, rR experiments are in the preliminary stages and further experiments need to be conducted to validate the rR analysis that was conducted by the Kincaid laboratory.

The NMR studies also suggest a long-lived sideproduct is generated, which we hypothesized to be generated by reaction of the "peroxynitrite-like" intermediates with the heme porphyrin. Analysis of the final heme-based products to determine heme modification were carried

out using LCMS. Identifiable products totaled less than 1% of the intensity of the normal unmodified heme group, suggesting that the modification is not a relevant factor in the formation of the intermediates at 600 and 611 nm, or that the technique and procedure used to seperate the porphyrin group causes the modified heme group to revert back to its native form.

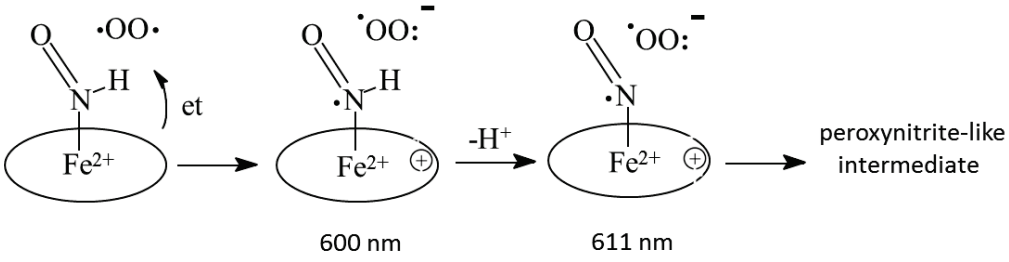

Scheme 4.2. Proposed mechanism for addition of O_2 to HNO-Mb in and out of a CO environment.

Without conclusive structural characterization of the intermediates with absorbances at 600 and 611 nm, we have accumulated data that suggests a possible sequential reaction pathway as detailed in Scheme 4.1. Initiation of this proposed reaction pathway is triggered when O_2 accesses the distal heme pocket of HNO-Mb. CO, most likely, blocks access of O_2, thereby reducing reactivity without changing the nature of the initial intermediates formed. An initial electron transfer generates superoxide and a porphyrin cation radical. Subsequently, a ferrous nitrosyl is formed, which is marginally perturbed by the close proximity of superoxide. The coupling of these two radical species forms a permutation of N-bound peroxynitrite-like species, which spontaneously rearranges to release nitrate from the ferrous heme. Subsequent binding of O_2 or CO to generate the observed protein products.

Conclusion

In this work, we take an unusual look at NOD reactivity from a decidedly different starting point, but which generates analogous products via spectroscopically similar intermediates. Although the nature of the intermediates formed in this reactivity remain enigmatic; the possible involvement of porphyrin-based radicals may help define the native NOD reactivity, a very potent detoxification mechanism of an important biochemical-signaling agent.

An important aspect of this study is the use of global kinetic modeling to deconvolute complicated spectral data. The power of this statistical analysis is seen in its ability to handle complex chemical reactivity, allowing the user to identify and characterize short-lived intermediates and determine the kinetics of their formation and loss. When coupled with other chemical characterizations, this can provide critical insight into the chemical mechanisms involved in complex reactions. I hope that this method will be used to deconvolute the sub millisecond spectral data of the physiologically important NOR reaction.

At this time, much care needs to be taken in the applying this method to the analysis of complex reactions for several reasons. First, the method does not handle equilibria well, and so sequential reactivity sequence were used. In addition, much chemical intuition is needed during the SVD analysis, to distinguish important species from statistical noise. It has been my observation in the current literature that global analysis is often used improperly; the scientific community would benefit greatly from a better understanding of the inherent limitations of computer modeling.

APPENDICES

APPENDIX A

Supplemental Information for Chapter Two

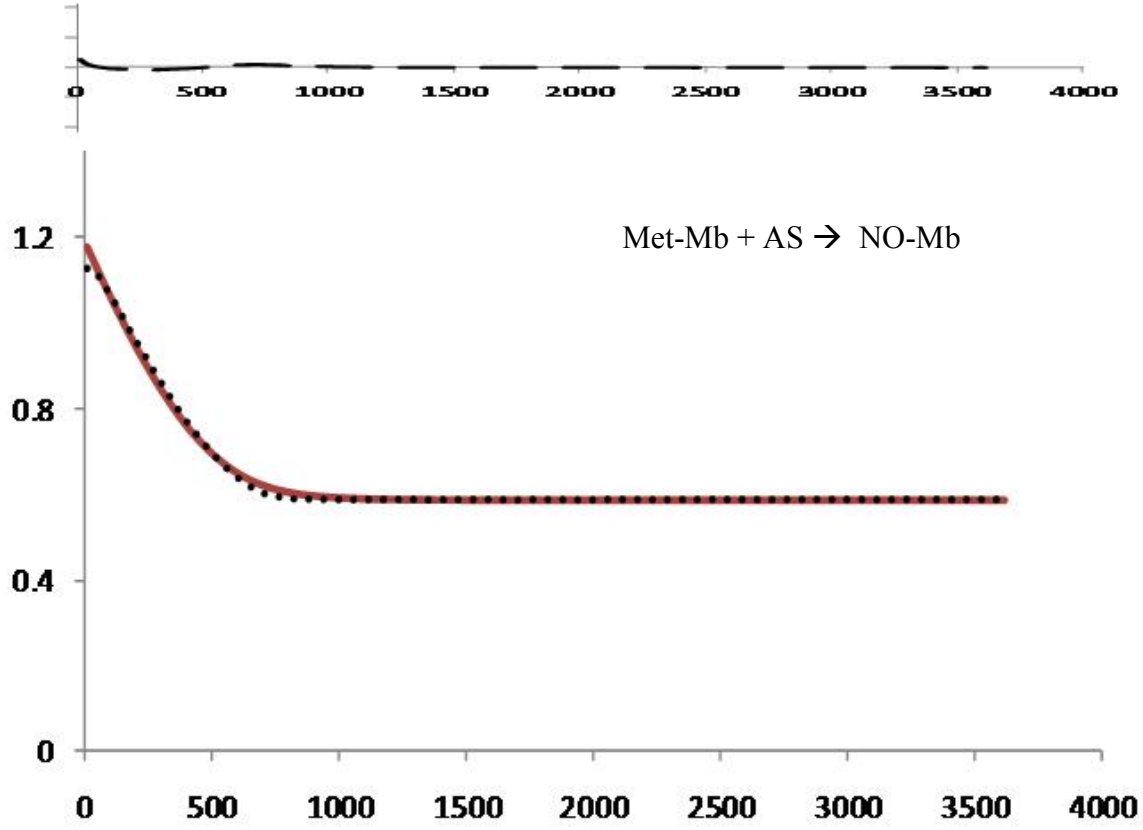

Figure A.1. Plots of reaction of metMb (6.7 μM) with AS (27 μM) in iP buffer at pH 7, corresponding to Figure 1 in the text, showing the time course of absorbance at 409 nm over 3600 seconds. Solid red line: model generated residual matrix; dotted line: real data. Residual plotted on top on the same scale of absorbance.

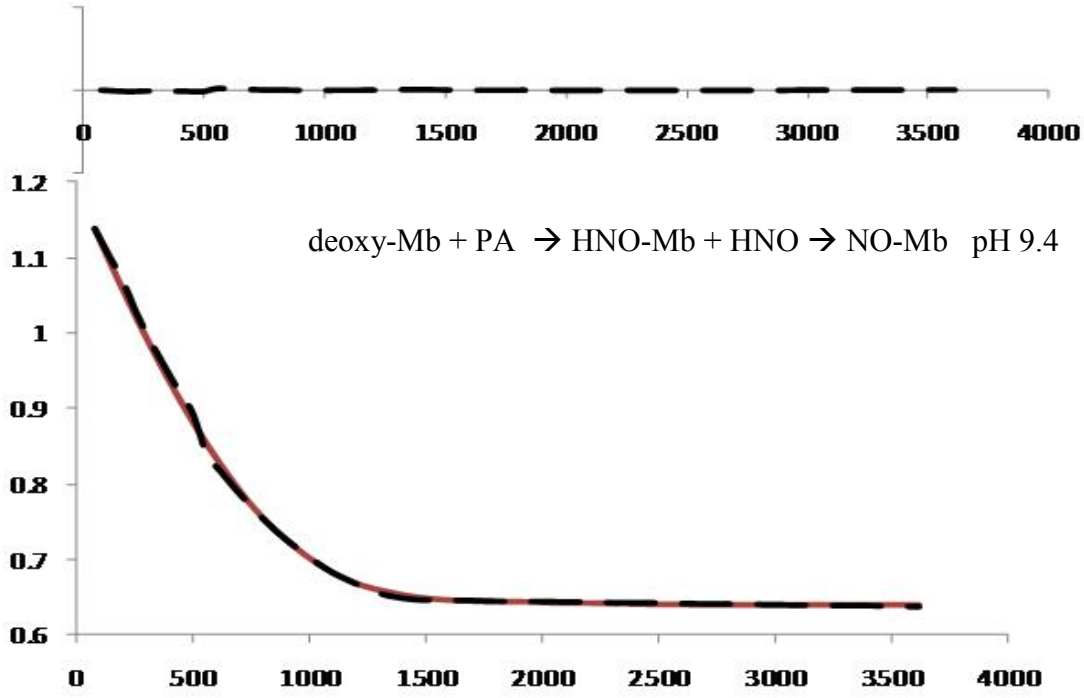

Figure A.2. Plots of the reaction of deoxyMb with PA at pH 9.4, from Figure 2B, with time course of absorbance at 434 nm over 3600 sec. in iP buffer with [deoxyMb] = 7.2 μM, [PA] = 35 μM. Solid red line: model generated residual matrix; dashed line: real data. Residual plotted on top on the same scale of absorbance.

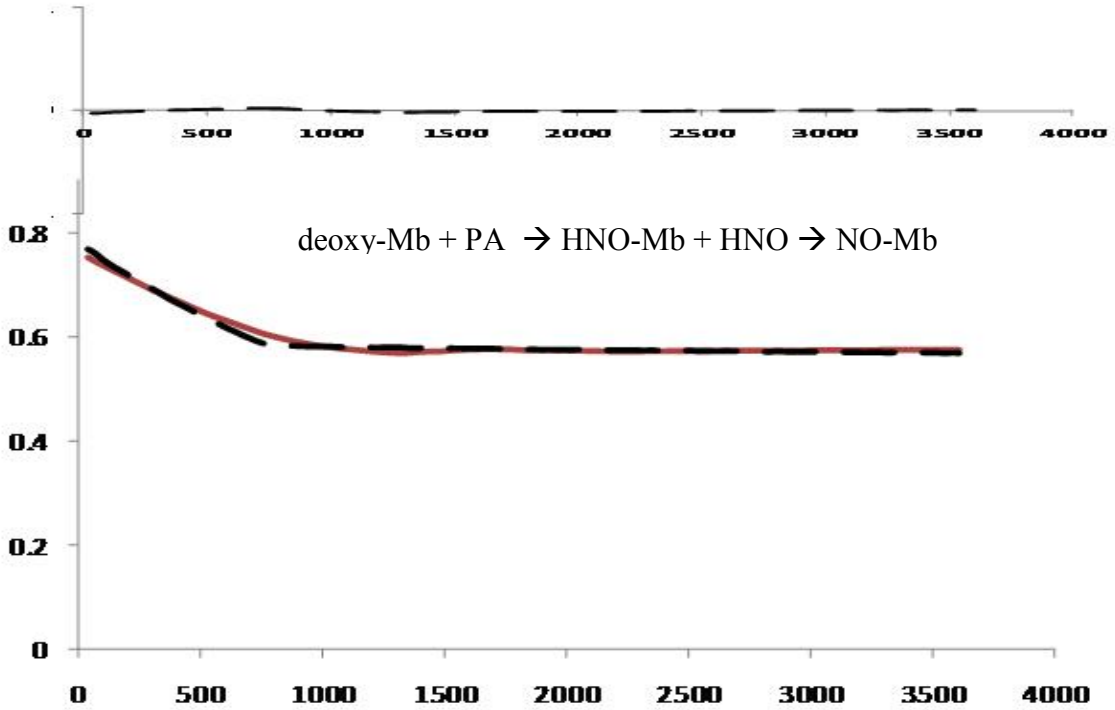

Figure A.3. Plots of reaction of deoxyMb with PA at pH 10 showing time course of absorbance at 434 nm over 3600 sec., from Figure 2C, with [deoxyMb] = 6.4 μM, [PA] = 26 μM, in iP buffer with [deoxyMb] = 7.2 μM, [PA] = 35 μM. Solid red line: model generated residual matrix ; dashed line: real data. Residual plotted on top on the same scale of absorbance.

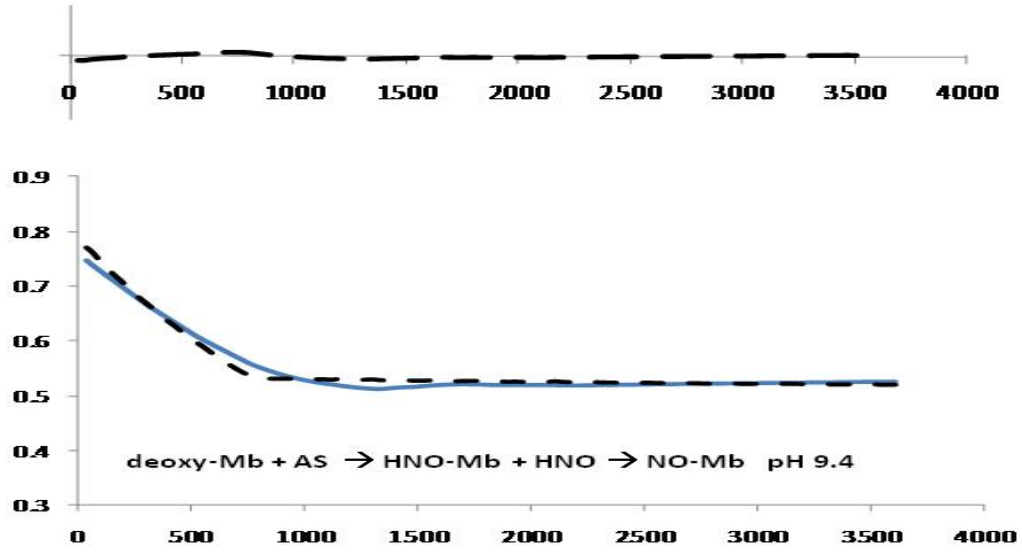

Figure A.4. Plots of the reaction of metMb (6.7 μM) with AS (27 μM) in iP buffer, pH 9.4 showing time course of absorbance at 434 nm over 3600 seconds. Solid blue line: model generated residual matrix; dashed line: real data. Residual plotted on top on the same scale of absorbance. (Figure 2.4B in text)

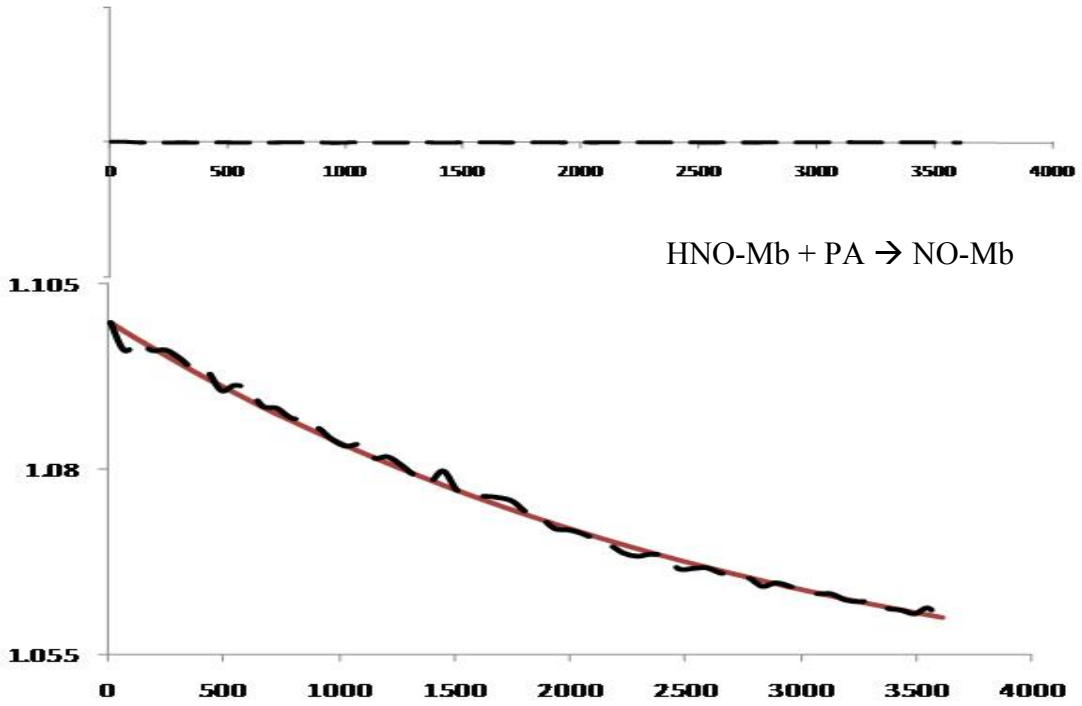

Figure A.5. Plots of reaction of HNO-Mb (6.8 μM) with PA (27 μM) in pH 9.4 iP buffer and run for 3600 sec., from Figure 7, showing time course of absorbance at 423 nm over 3600 seconds. Solid red line: model generated residual matrix; dashed line: real data. Residual plotted on top on the same scale of absorbance.

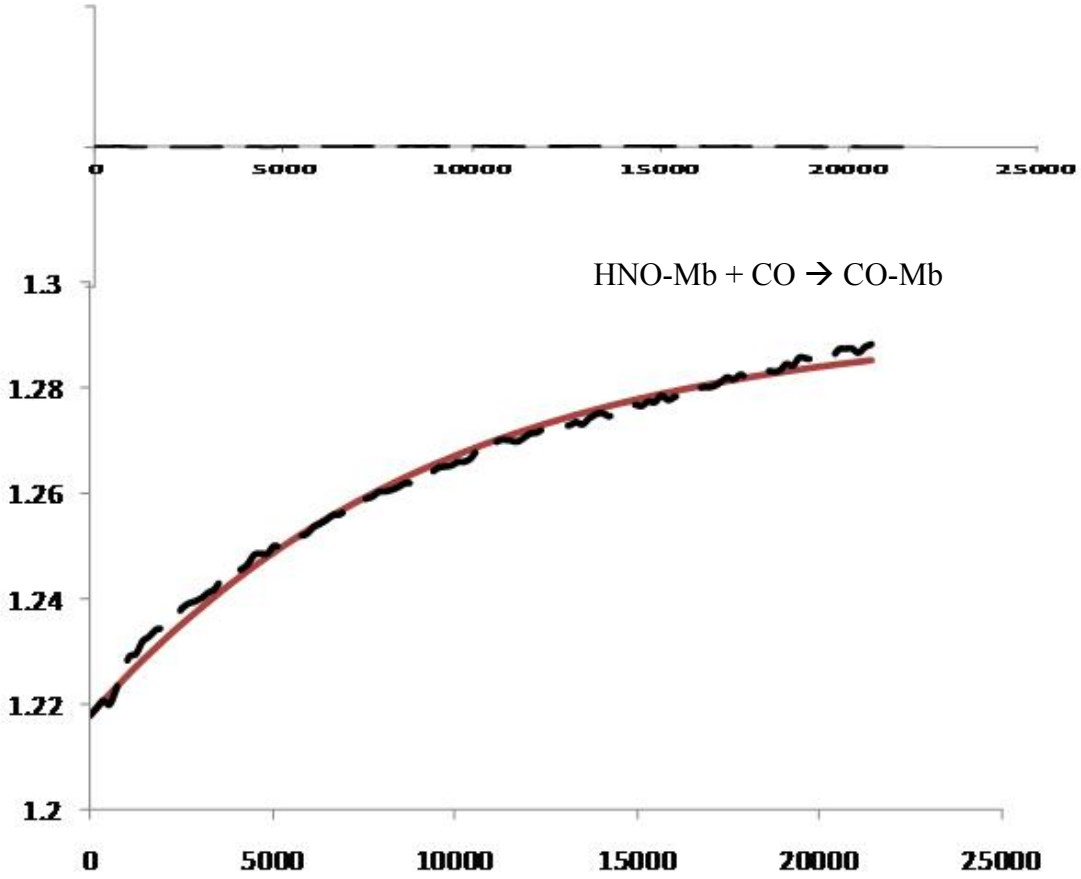

Figure A.6. Plots of reaction of HNO-Mb (6.8 μM) with CO (920 μM) at pH 7 showing time course of absorbance at 423 nm over 6 hrs, from Figure 8. Solid red line: model generated residual matrix; dashed line: real data. Residual plotted on top on the same scale of absorbance.

REFERENCES

(1) Culotta, E.; Koshland, D. E. NO News Is Good News. *Science* **1992**, *258* (5090), 1862–1865.

(2) Gibaldi, M. What Is Nitric Oxide and Why Are so Many People Studying It? *J. Clin. Pharmacol.* **1993**, *33* (6), 488–496.

(3) Fontijn, A.; Sabadell, A. J.; Ronco, R. J. Homogeneous Chemiluminescent Measurement of Nitric Oxide with Ozone. Implications for Continuous Selective Monitoring of Gaseous Air Pollutants. *Anal. Chem.* **1970**, *42* (6), 575–579.

(4) Ignarro, L. J.; Buga, G. M.; Wood, K. S.; Byrns, R. E.; Chaudhuri, G. Endothelium-Derived Relaxing Factor Produced and Released from Artery and Vein Is Nitric Oxide. *Proc. Natl. Acad. Sci. U. S. A.* **1987**, *84* (24), 9265–9269.

(5) Palmer, R. M.; Ferrige, A. G.; Moncada, S. Nitric Oxide Release Accounts for the Biological Activity of Endothelium-Derived Relaxing Factor. *Nature* **1987**, *327* (6122), 524–526.

(6) Sulc, F. University of California at Irvine: Irvine, CA, 2006.

(7) Bazylinski, D. A.; Hollocher, T. C. Evidence from the Reaction between trioxodinitrate(II) and Nitrogen-15-Labeled Nitric Oxide That trioxodinitrate(II) Decomposes into Nitrosyl Hydride and Nitrite in Neutral Aqueous Solution. *Inorg. Chem.* **1985**, *24* (25), 4285–4288.

(8) Bazylinski, D. A.; Hollocher, T. C. Metmyoglobin and Methemoglobin as Efficient Traps for Nitrosyl Hydride (Nitroxyl) in Neutral Aqueous Solution. *J. Am. Chem. Soc.* **1985**, *107* (26), 7982–7986.

(9) Shafirovich, V.; Lymar, S. V. Nitroxyl and Its Anion in Aqueous Solutions: Spin States, Protic Equilibria, and Reactivities toward Oxygen and Nitric Oxide. *Proc. Natl. Acad. Sci. U. S. A.* **2002**, *99* (11), 7340–7345.

(10) Miranda, K. M.; Paolocci, N.; Katori, T.; Thomas, D. D.; Ford, E.; Bartberger, M. D.; Espey, M. G.; Kass, D. A.; Feelisch, M.; Fukuto, J. M.; Wink, D. A. A Biochemical Rationale for the Discrete Behavior of Nitroxyl and Nitric Oxide in the Cardiovascular System. *Proc. Natl. Acad. Sci. U. S. A.* **2003**, *100* (16), 9196–9201.

(11) Ledo, A.; Frade, J.; Barbosa, R. M.; Laranjinha, J. Nitric Oxide in Brain: Diffusion, Targets and Concentration Dynamics in Hippocampal Subregions. *Mol. Aspects Med.* **2004**, *25* (1–2), 75–89.

(12) Santos, R. M.; Lourenço, C. F.; Ledo, A.; Barbosa, R. M.; Laranjinha, J. Nitric Oxide Inactivation Mechanisms in the Brain: Role in Bioenergetics and Neurodegeneration. *Int. J. Cell Biol.* **2012**, *2012*, e391914.

(13) Gardner, P. R. Hemoglobin: A Nitric-Oxide Dioxygenase. *Scientifica* **2012**, *2012*, e683729.

(14) Stamler, J. S.; Singel, D. J.; Loscalzo, J. Biochemistry of Nitric Oxide and Its Redox-Activated Forms. *Science* **1992**, *258* (5090), 1898–1902.

(15) Bonner, F. T.; Stedman, G. The Chemistry of Nitric Oxide and Redox-Related Species. *ChemInform.* **1997**, *28* (15).

(16) Hughes, M. N. Relationships between Nitric Oxide, Nitroxyl Ion, Nitrosonium Cation and Peroxynitrite. *Biochim. Biophys. Acta BBA - Bioenerg.* **1999**, *1411* (2–3), 263–272.

(17) King, S. B.; Nagasawa, H. T. Chemical Approaches toward Generation of Nitroxyl. *Methods Enzymol.* **1999**, *301*, 211–220.

(18) Zapata, A. L.; Kumar, M. R.; Pervitsky, D.; Farmer, P. J. A Singular Value Decomposition Approach for Kinetic Analysis of Reactions of HNO with Myoglobin. *J. Inorg. Biochem.* **2013**, *118*, 171–178.

(19) Suarez, S. A.; Bikiel, D. E.; Wetzler, D. E.; Marti, M. A.; Doctorovich, F. Time-Resolved Electrochemical Quantification of Azanone (HNO) at Low Nanomolar Level. *Anal. Chem.* **2013**, *85* (21), 10262–10269.

(20) Wrobel, A. T.; Johnstone, T. C.; Liang, A. D.; Lippard, S.; Rivera-Fuentes, P. A Fast and Selective Near-Infrared Fluorescent Sensor for Multicolor Imaging of Biological Nitroxyl (HNO). *J. Am. Chem. Soc.* **2014**, *136* (12), 4697–4705.

(21) Miao, Z.; Reisz, J. A.; Mitroka, S. N.; Pan, J.; Xiam, M.; King, S. B. A Selective Phosphine-Based Fluorescent Probe for Nitroxyl in Living Cells. *Bioorg. Med. Chem. Lett.* **2015**, *25* (1), 16–19.

(22) Wink, D. A; Feelisch, M. Formation and Detection of Nitroxyl and Nitrous Oxide. In *Methods Nitric oxide*; Wiley: Chinchester, UK, 1996; pp 403–412.

(23) Gratzel, V. M.; Taniguchi, S.; Henglein, A. Pulsradiolytische Untersuchung Kurzlebigerzwischenprodukte Der NO-Reduktionin Wassriger Losung. *Ber. Bunsen-Ges. Phys. Chem.* **1970**, *74*, 1003–1010.

(24) Bartberger, M. D.; Fukuto, J. M.; Houk, K. N. On the Acidity and Reactivity of HNO in Aqueous Solution and Biological Systems. *Proc. Natl. Acad. Sci. U. S. A.* **2001**, *98* (5), 2194–2198.

(25) Paolocci, N.; Saavedra, W. F.; Miranda, K. M.; Martignani, C.; Isoda, T.; Hare, J. M.; Espey, M. G.; Fukuto, J. M.; Feelisch, M.; Wink, D. A.; Kass, D. A. Nitroxyl Anion Exerts Redox-Sensitive Positive Cardiac Inotropy in Vivo by Calcitonin Gene-Related Peptide Signaling. *Proc. Natl. Acad. Sci. U. S. A.* **2001**, *98* (18), 10463–10468.

(26) Pagliaro, P.; Mancardi, D.; Rastaldo, R.; Penna, C.; Gattullo, D.; Miranda, K. M.; Feelisch, M.; Wink, D. A.; Kass, D. A.; Paolocci, N. Nitroxyl Affords Thiol-Sensitive Myocardial Protective Effects Akin to Early Preconditioning. *Free Radic. Biol. Med.* **2003**, *34* (1), 33–43.

(27) Norris, A. J.; Sartippour, M. R.; Lu, M.; Park, T.; Rao, J. Y.; Jackson, M. I.; Fukuto, J. M.; Brooks, M. N. Nitroxyl Inhibits Breast Tumor Growth and Angiogenesis. *Int. J. Cancer J. Int. Cancer* **2008**, *122* (8), 1905–1910.

(28) Nagasawa, H. T.; DeMaster, E. G.; Redfern, B.; Shirota, F. N.; Goon, D. J. W. Evidence for Nitroxyl in the Catalase-Mediated Bioactivation of the Alcohol Deterrent Agent Cyanamide. *J. Med. Chem.* **1990**, *33* (12), 3120–3122.

(29) Nagasawa, H. T.; Kawle, S. P.; Elberling, J. A.; DeMaster, E. G.; Fukuto, J. M. Prodrugs of Nitroxyl as Potential Aldehyde Dehydrogenase Inhibitors Vis-a-Vis Vascular Smooth Muscle Relaxants. *J. Med. Chem.* **1995**, *38* (11), 1865–1871.

(30) DeMaster, E. G.; Redfern, B.; Nagasawa, H. T. Mechanisms of Inhibition of Aldehyde Dehydrogenase by Nitroxyl, the Active Metabolite of the Alcohol Deterrent Agent Cyanamide. *Biochem. Pharmacol.* **1998**, *55* (12), 2007–2015.

(31) Staurengo-Ferrari, L.; Zarpelon, A. C.; Longhi-Balbinot, D. T.; Marchesi, M.; Cunha, T. M.; Alves-Filho, J. C.; Cunha, F. Q.; Ferreira, S. H.; Casagrande, R.; Miranda, K. M.; Verri, W. A. Nitroxyl Inhibits Overt Pain-like Behavior in Mice: Role of cGMP/PKG/ATP-Sensitive Potassium Channel Signaling Pathway. *Pharmacol. Rep. PR* **2014**, *66* (4), 691–698.

(32) Sabbah, H. N.; Tocchetti, C. G.; Wang, M.; Daya, S.; Gupta, R. C.; Tunin, R. S.; Mazhari, R.; Takimoto, E.; Paolocci, N.; Cowart, D.; Colucci, W. S.; Kass, D. A. Nitroxyl (HNO) a Novel Approach for the Acute Treatment of Heart Failure. *Circ. Heart Fail.* **2013**, *6* (6), 1250–1258.

(33) Dai, T.; Tian, Y.; Tocchetti, C. G.; Katori, T.; Murphy, A. M.; Kass, D. A.; Paolocci, N.; Gao, W. D. Nitroxyl Increases Force Development in Rat Cardiac Muscle. *J. Physiol.* **2007**, *580* (3), 951–960.

(34) Irvine, J. C.; Favaloro, J. L.; Widdop, R. E.; Kemp-Harper, B. K. Nitroxyl Anion Donor, Angeli's Salt, Does Not Develop Tolerance in Rat Isolated Aortae. *Hypertension* **2007**, *49* (4), 885–892.

(35) Kerwin, J. F.; Lancaster, J. R.; Feldman, P. L. Nitric Oxide: A New Paradigm for Second Messengers. *J. Med. Chem.* **1995**, *38* (22), 4343–4362.

(36) Beckman, J. S. Oxidative Damage and Tyrosine Nitration from Peroxynitrite. *Chem. Res. Toxicol.* **1996**, *9* (5), 836–844.

(37) Gardner, P. R.; Gardner, A. M.; Martin, L. A.; Salzman, A. L. Nitric Oxide Dioxygenase: An Enzymic Function for Flavohemoglobin. *Proc. Natl. Acad. Sci. U. S. A.* **1998**, *95* (18), 10378–10383.

(38) Butler, A. R.; Megson, I. L.; Wright, P. G. Diffusion of Nitric Oxide and Scavenging by Blood in the Vasculature. *Biochim. Biophys. Acta* **1998**, *1425* (1), 168–176.

(39) Doyle, M. P.; Pickering, R. A.; DeWeert, T. M.; Hoekstra, J. W.; Pater, D. Kinetics and Mechanism of the Oxidation of Human Deoxyhemoglobin by Nitrites. *J. Biol. Chem.* **1981**, *256* (23), 12393–12398.

(40) Doyle, M. P.; Pickering, R. A.; Cook, B. R. Oxidation of Oxymyoglobin by Nitric Oxide through Dissociation from Cobalt Nitrosyls. *J. Inorg. Biochem.* **1983**, *19* (4), 329–338.

(41) Doyle, M. P.; Mahapatro, S. N. Nitric Oxide Dissociation from trioxodinitrate(II) in Aqueous Solution. *J. Am. Chem. Soc.* **1984**, *106* (12), 3678–3679.

(42) Andersen, H. J.; Skibsted, L. H. Kinetics and Mechanism of Thermal Oxidation and Photooxidation of Nitrosylmyoglobin in Aqueous Solution. *J. Agric. Food Chem.* **1992**, *40* (10), 1741–1750.

(43) Eich, R. F.; Li, T.; Lemon, D. D.; Doherty, D. H.; Curry, S. R.; Aitken, J. F.; Mathews, A. J.; Johnson, K. A.; Smith, R. D.; Phillips, G. N.; Olson, J. S. Mechanism of NO-Induced Oxidation of Myoglobin and Hemoglobin. *Biochemistry (Mosc.)* **1996**, *35* (22), 6976–6983.

(44) Herold, S. Kinetic and Spectroscopic Characterization of an Intermediate Peroxynitrite Complex in the Nitrogen Monoxide Induced Oxidation of Oxyhemoglobin. *FEBS Lett.* **1999**, *443* (1), 81–84.

(45) Gardner, P. R. Assay and Characterization of the NO Dioxygenase Activity of Flavohemoglobins. *Meth. Enzymolo.* **2008**, *436*, 217-237.

(46) Gardner, P. R. Hemoglobins Dioxygenate Nitric Oxide with High Fidelity. *J. Inorg. Biochem.* **2006**, *100* (4), 542-550

.

(47) Gardner, P. R. Nitric Oxide Dioxygenase Function and Mechanism of Flavohemoglobin, Hemoglobin, Myoglobin and their Associated Reductases. *J. Inorg. Biochem.* **2005**, *99* (1), 247-266.

(48) Gardner, P. R.; Gardner, A. M.; Martin, L. A.; Salzman, A. L. Nitric Oxide Dioxygenase: An Enzymic Function for Flavohemoglobin. *Proc. Natl. Acad. Sci. U. S. A.* **1998**, *95* (18), 10378–10383.

(49) Gardner, A. M. Steady-State and Transient Kinetics of Escherichia Coli Nitric-Oxide Dioxygenase (Flavohemoglobin). The B10 Tyrosine Hydroxyl is Essential for Dioxygen Binding and Catalysis. *J. Biol. Chem.* **2000**, *275* (17), 12581–12589.

(50) Herold, S. Kinetic and Spectroscopic Characterization of an Intermediate Peroxynitrite Complex in the Nitrogen Monoxide Induced Oxidation of Oxyhemoglobin. *FEBS Lett.* **1998**, *439* (1), 85–88.

(51) Su, J.; Groves, J. T. Mechanisms of Peroxynitrite Interactions with Heme Proteins. *Inorg. Chem.* **2010**, *49* (14), 6317–6329.

(52) Herold, S.; Koppenol, W. H. Peroxynitritometal Complexes. *Coord. Chem. Rev.* **2005**, *249* (3), 499–506.

(53) Yukl, E. T.; de Vries, S.; Moënne-Loccoz, P. The Millisecond Intermediate in the Reaction of Nitric Oxide with Oxymyoglobin Is an iron(III)--Nitrato Complex, Not a Peroxynitrite. *J. Am. Chem. Soc.* **2009**, *131* (21), 7234–7235.

(54) Su, J.; Groves, J. T. Direct Detection of the Oxygen Rebound Intermediates, Ferryl Mb and NO2, in the Reaction of Metmyoglobin with Peroxynitrite. *J. Am. Chem. Soc.* **2009**, *131* (36), 12979–12988.

(55) Ortiz de Montellano, P. Substrate Oxidation by Cytochrome P450 Enzymes. In *Cytochrome P-450: Structure, Mechanism, and Biochemistry.* 3rd Edition.; Ortiz de Montellano, P., Ed. Springer, 1986, 183-245.

(56) Koebke, K. J.; Pauly, D. J.; Lerner, L.; Liu, X.; Pacheco, A. A. Does the Oxidation of Nitric Oxide by oxyMyoglobin Share an Intermediate with the metMyoglobin-Catalyzed Isomerization of Peroxynitrite? *Inorg. Chem.* **2013**, *52* (13), 7623–7632.

(57) Farmer, P. J.; Sulc, F. Coordination Chemistry of the HNO Ligand with Hemes and Synthetic Coordination Complexes. *J. Inorg. Biochem.* **2005**, *99* (1), 166–184.

(58) Bayachou, M.; Lin, R.; Cho, W.; Farmer, P. J. Electrochemical Reduction of NO by Myoglobin in Surfactant Film: Characterization and Reactivity of the Nitroxyl (NO-) Adduct. *J. Am. Chem. Soc.* **1998**, *120* (38), 9888–9893.

(59) Lin, R.; Farmer, P. J. The HNO Adduct of Myoglobin: Synthesis and Characterization. *J. Am. Chem. Soc.* **2000**, *122* (10), 2393–2394.

(60) Sulc, F.; Immoos, C. E.; Pervitsky, D.; Farmer, P. J. Efficient Trapping of HNO by Deoxymyoglobin. *J. Am. Chem. Soc.* **2004**, *126* (4), 1096–1101.

(61) Kumar, M. R.; Fukuto, J. M.; Miranda, K. M.; Farmer, P. J. Reactions of HNO with Heme Proteins: New Routes to HNO−Heme Complexes and Insight into Physiological Effects. *Inorg. Chem.* **2010**, *49* (14), 6283–6292.

(62) Sulc, F.; Fleischer, E.; Farmer, P. J.; Ma, D.; Mar, G. N. L. 1H NMR Structure of the Heme Pocket of HNO-Myoglobin. *J. Biol. Inorg. Chem.* **2003**, *8* (3), 348–352.

(63) Kumar, M. R.; Pervitsky, D.; Chen, L.; Poulos, T.; Kundu, S.; Hargrove, M. S.; Rivera, E. J.; Diaz, A.; Colón, J. L.; Farmer, P. J. Nitrosyl Hydride (HNO) as an O2 Analogue: Long-Lived HNO Adducts of Ferrous Globins. *Biochemistry (Mosc.)* **2009**, *48* (22), 5018–5025.

(64) Immoos, C. E.; Sulc, F.; Farmer, P. J.; Czarnecki, K.; Bocian, D. F.; Levina, A.; Aitken, J. B.; Armstrong, R. S.; Lay, P. A. Bonding in HNO-Myoglobin as Characterized by X-Ray Absorption and Resonance Raman Spectroscopies. *J. Am. Chem. Soc.* **2005**, *127* (3), 814–815.

(65) Kumar, M. R.; Zapata, A.; Ramirez, A. J.; Bowen, S. K.; Francisco, W. A.; Farmer, P. J. Nitrosyl Hydride (HNO) Replaces Dioxygen in Nitroxygenase Activity of Manganese Quercetin Dioxygenase. *Proc. Natl. Acad. Sci. U. S. A.* **2011**, *108* (47), 18926–18931.

(66) Olson, J. S.; Phillips, G. N. Kinetic Pathways and Barriers for Ligand Binding to Myoglobin. *J. Biol. Chem.* **1996**, *271* (30), 17593–17596.

(67) Harvey, J. N. Spin-Forbidden CO Ligand Recombination in Myoglobin. *Faraday Discuss.* **2004**, *127*, 165–177.

(68) Olson, J. S.; A. Ghosh. Mammalian myoglobin as a model for understanding ligand affinities and discrimination in heme proteins. In *The Smallest Biomolecules: Perspectives on Heme-Diatomic Interactions.*; Elsevier: Amsterdam, 2007.

(69) Frauenfelder, H.; Wolynes, P. G. Rate Theories and Puzzles of Hemeprotein Kinetics. *Science* **1985**, *229* (4711), 337–345.

(70) Tsai, A.-L.; Berka, V.; Martin, E.; Olson, J. S. A "Sliding Scale Rule" for Selectivity among NO, CO, and O $_2$ by Heme Protein Sensors. *Biochemistry (Mosc.)* **2012**, *51* (1), 172–186.

(71) Draghi, F.; Miele, A. E.; Travaglini-Allocatelli, C.; Vallone, B.; Brunori, M.; Gibson, Q. H.; Olson, J. S. Controlling Ligand Binding in Myoglobin by Mutagenesis. *J. Biol. Chem.* **2002**, *277* (9), 7509–7519.

(72) Kundu, S.; Snyder, B.; Das, K.; Chowdhury, P.; Park, J.; Petrich, J. W.; Hargrove, M. S. The Leghemoglobin Proximal Heme Pocket Directs Oxygen Dissociation and Stabilizes Bound Heme. *Proteins Struct. Funct. Genet.* **2002**, *46* (3), 268–277.

(73) Gibson, Q. H.; Olson, J. S.; McKinnie, R. E.; Rohlfs, R. J. A Kinetic Description of Ligand Binding to Sperm Whale Myoglobin. *J. Biol. Chem.* **1986**, *261* (22), 10228–10239.

(74) Walda, K. N.; Liu, X. Y.; Sharma, V. S.; Magde, D. Geminate Recombination of Diatomic Ligands CO, O2, and NO with Myoglobin. *Biochemistry (Mosc.)* **1994**, *33* (8), 2198–2209.

(75) Spiro, T. G.; Kozlowski, P. M. Is the CO Adduct of Myoglobin Bent, and Does It Matter? *Acc. Chem. Res.* **2001**, *34* (2), 137–144.

(76) Lymar, S. V.; Shafirovich, V.; Poskrebyshev, G. A. One-Electron Reduction of Aqueous Nitric Oxide: A Mechanistic Revision. *Inorg. Chem.* **2005**, *44* (15), 5212–5221.

(77) Lin, R.; Farmer, P. J. The HNO Adduct of Myoglobin: Synthesis and Characterization. *J. Am. Chem. Soc.* **2000**, *122* (10), 2393–2394.

(78) Sulc, F.; Fleischer, E.; Farmer, P. J.; Ma, D.; La Mar, G. N. 1H NMR Structure of the Heme Pocket of HNO-Myoglobin. *J. Biol. Inorg. Chem.* **2003**, *8* (3), 348–352.

(79) Pervitsky, D.; Immoos, C.; van der Veer, W.; Farmer, P. J. Photolysis of the HNO Adduct of Myoglobin: Transient Generation of the Aminoxyl Radical. *J. Am. Chem. Soc.* **2007**, *129* (31), 9590–9591.

(80) Dmitry Pervitsky. HNO Reactivity, University of California at Irvine: Irvine, CA, 2008.

(81) Zimanyi, L.; Kulcsar, A.; Lanyi, J. K.; Sears, D. F.; Saltiel, J. Singular Value Decomposition with Self-Modeling Applied to Determine Bacteriorhodopsin Intermediate Spectra: Analysis of Simulated Data. *Proc. Natl. Acad. Sci. U. S. A.* **1999**, *96* (8), 4408–4413.

(82) Shafirovich, V.; Lymar, S. V. Spin-Forbidden Deprotonation of Aqueous Nitroxyl (HNO). *J. Am. Chem. Soc.* **2003**, *125* (21), 6547–6552.

(83) Kozma, F.; Johnson, R. A.; Zhang, F.; Yu, C.; Tong, X.; Nasjletti, A. Contribution of Endogenous Carbon Monoxide to Regulation of Diameter in Resistance Vessels. *Am. J. Physiol.* **1999**, *276* (4), R1087-1094.

(84) ReactLab Kinetics. http://jplusconsulting.com/files/ReactLab_Kinetics_Manual.pdf

(85) Romberg, R. W.; Kassner, R. J. Nitric Oxide and Carbon Monoxide Equilibriums of Horse Myoglobin and (N-Methylimidazole)protoheme. Evidence for Steric Interaction with the Distal Residues. *Biochemistry (Mosc.)* **1979**, *18* (24), 5387–5392.

(86) Doyle, M. P.; Mahapatro, S. N.; Broene, R. D.; Guy, J. K. Oxidation and Reduction of Hemoproteins by trioxodinitrate(II). The Role of Nitrosyl Hydride and Nitrite. *J. Am. Chem. Soc.* **1988**, *110* (2), 593–599.

(87) Suarez, S. A.; Neuman, N. I.; Muñoz, M.; Álvarez, L.; Bikiel, D. E.; Brondino, C. D.; Ivanović-Burmazović, I.; Miljkovic, J. L.; Filipovic, M. R.; Martí, M. A.; Doctorovich, F. Nitric Oxide Is Reduced to HNO by Proton-Coupled Nucleophilic Attack by Ascorbate, Tyrosine, and Other Alcohols. A New Route to HNO in Biological Media? *J. Am. Chem. Soc.* **2015**, *137* (14), 4720–4727.

(88) Lind, J.; Merényi, G. Kinetic and Thermodynamic Properties of the Aminoxyl ($NH_2O^{\bullet}$) Radical. *J. Phys. Chem. A* **2006**, *110* (1), 192–197.

(89) Wink, D. A.; Miranda, K. M.; Katori, T.; Mancardi, D.; Thomas, D. D.; Ridnour, L.; Espey, M. G.; Feelisch, M.; Colton, C. A.; Fukuto, J. M.; Pagliaro, P.; Kass, D. A.; Paolocci, N. Orthogonal Properties of the Redox Siblings Nitroxyl and Nitric Oxide in the Cardiovascular System: A Novel Redox Paradigm. *Am. J. Physiol. Heart Circ. Physiol.* **2003**, *285* (6), H2264-2276.

(90) Miranda, K. M.; Dutton, A. S.; Ridnour, L. A.; Foreman, C. A.; Ford, E.; Paolocci, N.; Katori, T.; Tocchetti, C. G.; Mancardi, D.; Thomas, D. D.; Espey, M. G.; Houk, K. N.; Fukuto, J. M.; Wink, D. A. Mechanism of Aerobic Decomposition of Angeli's Salt (Sodium Trioxodinitrate) at Physiological pH. *J. Am. Chem. Soc.* **2005**, *127* (2), 722–731.

(91) Miller, T. W.; Cherney, M. M.; Lee, A. J.; Francoleon, N. E.; Farmer, P. J.; King, S. B.; Hobbs, A. J.; Miranda, K. M.; Burstyn, J. N.; Fukuto, J. M. The Effects of Nitroxyl (HNO) on Soluble Guanylate Cyclase Activity: Interactions at Ferrous Heme and Cysteine Thiols. *J. Biol. Chem.* **2009**, *284* (33), 21788–21796.

(92) Zeller, A.; Wenzl, M. V.; Beretta, M.; Stessel, H.; Russwurm, M.; Koesling, D.; Schmidt, K.; Mayer, B. Mechanisms Underlying Activation of Soluble Guanylate Cyclase by the Nitroxyl Donor Angeli's Salt. *Mol. Pharmacol.* **2009**, *76* (5), 1115–1122.

(93) Marletta, M. A. Nitric Oxide Synthase: Aspects Concerning Structure and Catalysis. *Cell* **1994**, *78* (6), 927–930.

(94) Denninger, J. W.; Marletta, M. A. Guanylate Cyclase and the .NO/cGMP Signaling Pathway. *Biochim. Biophys. Acta* **1999**, *1411* (2), 334–350.

(95) Cannon, R. O. Role of Nitric Oxide in Cardiovascular Disease: Focus on the Endothelium. *Clin. Chem.* **1998**, *44* (8), 1809–1819.

(96) Fukuto, J. M.; Bartberger, M. D.; Dutton, A. S.; Paolocci, N.; Wink, D. A.; Houk, K. N. The Physiological Chemistry and Biological Activity of Nitroxyl (HNO): The Neglected, Misunderstood, and Enigmatic Nitrogen Oxide. *Chem. Res. Toxicol.* **2005**, *18* (5), 790–801.

(97) Foresti, R. The Interaction of Nitric Oxide with Distinct Hemoglobins Differentially Amplifies Endothelial Heme Uptake and Heme Oxygenase-1 Expression. *J. Pharmacol. Exp. Ther.* **2006**, *317* (3), 1125–1133.

(98) Rahal, A.; Kumar, A.; Singh, V.; Yadav, B.; Tiwari, R.; Chakraborty, S.; Dhama, K. Oxidative Stress, Prooxidants, and Antioxidants: The Interplay. *BioMed. Res. Int.* **2014**, *2014*, e761264.

(99) Schaap, A. P.; Thayer, A. L.; Faler, G. R.; Goda, K.; Kimura, T. Singlet Molecular Oxygen and Superoxide Dismutase. *J. Am. Chem. Soc.* **1974**, *96* (12), 4025–4026.

(100) Lee, J.; Koo, N.; Min, D. B. Reactive Oxygen Species, Aging, and Antioxidative Nutraceuticals. *Compr. Rev. Food Sci. Food Saf.* **2004**, *3* (1), 21–33.

(101) Patel, V. P.; Chu, C. T. Nuclear Transport, Oxidative Stress, and Neurodegeneration. *Int. J. Clin. Exp. Pathol.* **2011**, *4* (3), 215–229.

(102) Nijs, J.; Meeus, M.; De Meirleir, K. Chronic Musculoskeletal Pain in Chronic Fatigue Syndrome: Recent Developments and Therapeutic Implications. *Man. Ther.* **2006**, *11* (3), 187–191.

(103) Pacher, P.; Beckman, J. S.; Liaudet, L. Nitric Oxide and Peroxynitrite in Health and Disease. *Physiol. Rev.* **2007**, *87* (1), 315–424.

(104) Eich, R. F.; Li, T.; Lemon, D. D.; Doherty, D. H.; Curry, S. R.; Aitken, J. F.; Mathews, A. J.; Johnson, K. A.; Smith, R. D.; Phillips, George N.; Olson, J. S. Mechanism of NO-Induced Oxidation of Myoglobin and Hemoglobin†. *Biochemistry (Mosc.)* **1996**, *35* (22), 6976–6983.

(105) Puhl, H. Solubility of Gases in Liquids. *Von* P. G. T. Fogg *und* W. Gerrard. John Wiley & Sons Ltd., Chichester, New York 1990. XII, 332 S., zahlr. Abb. u. Tab., geb., £ 75,–. *Chemie. Ingenieur. Technik.* **1991**, *63*, 1272.

(106) Rossi-Fanelli, A.; Azzone, G. F.; Mondovi, B. Alkali Denaturation of Myoglobin and Hemoglobin. *Stud. Kinet. React.* **1955**, *58* (1), 119–123.

(107) Weiss, C.; Kobayashi, H.; Gouterman, M. Spectra of Porphyrins: Part III. Self-Consistent Molecular Orbital Calculations of Porphyrin and Related Ring Systems. *J. Mol. Spectrosc.* **1965**, *16*, 415.

(108) Fajer, J.; Borg, D. C.; Forman, A.; Dolphin, D.; Felton, R. H. N-Cation Radicals and Dications of Metalloporphyrins. *J. Am. Chem. Soc.* **1970**, *92*, 3452–3459.

(109) Hamachi, I.; Tsukiji, S.; Shinkai, S.; Oishi, S. *J. Am. Chem. Soc.* **1999**, *121*, 5500–5506.

(110) Hamachi, I.; Takashima, H.; Hu, Y. Z.; Shinkai, S.; Oishi, S. *Chem. Commun.* **2000**, *13*, 1127–1128.

(111) Berglund, J.; Pascher, T.; Winkler, J. R.; Gray, H. B. *J. Am. Chem. Soc.* **1997**, *119*, 2464–2469.

(112) Low, D. W.; Winkler, J. R.; Gray, H. B. Photoinduced Oxidation of Microperoxidase-8: Generation of Ferryl and Cation-Radical Porphyrins. *J. Am. Chem. Soc.* **1996**, *118*, 117–120.

(113) Immoos, C. E.; Di Bilio, A. J.; Cohen, M. S.; Van der Veer, W.; Gray, H. B.; Farmer, P. J. Electron Transfer Chemistry of Ru-Linker-(Heme)-Modified Myoglobin: Rapid Intraprotein Reduction of a Photogenerated Porphyrin Cation Radical. *Inorg. Chem.* **2004**, *43*, 3593–3596.

(114) Kim-Shapiro, D. B.; Schechter, A. N.; Gladwin, M. T. Unraveling the Reactions of Nitric Oxide, Nitrite, and Hemoglobin in Physiology and Therapeutics. *Arter. Thromb. Vasc. Biol.* **2006**, *4* (26), 697–705.

(115) Kim-Shapiro, D. B.; Gladwin, M. T.; Patel, R. P.; Hogg, N. The Role of Nitrite in Hemoglobin-Mediated Hypoxic Vasodilation. *J. Inorg. Biochem.* **2005**, *1* (99), 237–246.